NASA TN D-435

TECHNICAL NOTE
D-435

TRANSONIC AND SUPERSONIC WIND-TUNNEL TESTS OF WING-BODY COMBINATIONS DESIGNED FOR HIGH EFFICIENCY AT A MACH NUMBER OF 1.41

By Frederick C. Grant and John R. Sevier, Jr.

Langley Research Center
Langley Field, Va.

NATIONAL AERONAUTICS AND SPACE ADMINISTRATION
WASHINGTON
October 1960

NATIONAL AERONAUTICS AND SPACE ADMINISTRATION

TECHNICAL NOTE D-435

TRANSONIC AND SUPERSONIC WIND-TUNNEL TESTS OF WING-BODY COMBINATIONS DESIGNED FOR HIGH EFFICIENCY AT A MACH NUMBER OF 1.41

By Frederick C. Grant and John R. Sevier, Jr.

SUMMARY

Wind-tunnel force tests of a number of wing-body combinations designed for high lift-drag ratio at a Mach number of 1.41 are reported. Five wings and six bodies were used in making up the various wing-body combinations investigated. All the wings had the same highly swept discontinuously tapered plan form with NACA 65A-series airfoil sections 4 percent thick at the root tapering linearly to 3 percent thick at the tip. The bodies were based on the area distribution of a Sears-Haack body of revolution for minimum drag with a given length and volume. These wings and bodies were used to determine the effects of wing twist, wing twist and camber, wing leading-edge droop, a change from circular to elliptical body cross-sectional shape, and body indentation by the area-rule and streamline methods. The supersonic test Mach numbers were 1.41 and 2.01. The transonic test Mach number range was from 0.6 to 1.2.

For the transition-fixed condition and at a Reynolds number of 2.7×10^6 based on the mean aerodynamic chord, the maximum value of lift-drag ratio at a Mach number of 1.41 was 9.6 for a combination with a twisted wing and an indented body of elliptical cross section.

The tests indicated that the transonic rise in minimum drag was low and did not change appreciably up to the highest test Mach number of 2.01. The lower values of lift-drag ratio obtained at a Mach number of 2.01 can be attributed to the increase of drag due to lift with Mach number.

INTRODUCTION

The reduction of the unavoidable losses in maximum lift-drag ratio at supersonic speeds to as small a value as possible is currently a matter of considerable aerodynamic interest. Various means of reducing the losses in maximum lift-drag ratio at low supersonic speeds are

recognized. A good plan form, thin wing sections, proper wing warp, and proper body indentation are among these. In the present investigation some of these means have been combined in several configurations in an effort to arrive at a configuration with high efficiency (as measured by maximum lift-drag ratio) at a Mach number of 1.41. Four differently indented bodies were tested with two differently warped wings. For comparison purposes, data for a plane wing and two nonindented bodies are also shown.

SYMBOLS

a_1, a_2	semimajor and semiminor axes, respectively, of ellipse
c	reference chord
$\bar{c}$	mean aerodynamic chord
C_D	drag coefficient, $\frac{\text{Drag}}{qS}$
C_L	lift coefficient, $\frac{\text{Lift}}{qS}$
C_m	pitching-moment coefficient about axis passing through one-quarter chord of reference chord (fig. 1) and perpendicular to plane of symmetry, $\frac{\text{Pitching moment}}{qS\bar{c}}$
$C_{D,min}$	minimum value of drag coefficient
$(C_L)_{C_{D,min}}$	value of lift coefficient when drag coefficient is a minimum
L/D	ratio of lift to drag
$(L/D)_{max}$	maximum value of lift-drag ratio
M	Mach number
q	dynamic pressure
r	radius of body cross section at any station
S	wing plan-form area (including that portion blanketed by the fuselage)

x	distance along body axis, measured from nose apex
X	distance used in defining coordinates of leading-edge inserts (fig. 2), measured from wing leading edge along a line parallel to body center line
Z	distance above reference plane used in defining leading-edge inserts (table I)
α	angle of attack
ϵ	drag-due-to-lift parameter
Λ	sweep angle of wing

Subscripts:

i	test values to be substituted in equation (A3)
o	leading term of Taylor series (eq. (A2))
le	leading edge
te	trailing edge
u	upper
l	lower

MODELS

Each of six different body configurations was tested in combination with five different wing variations, thus making a total of 30 wing-body combinations which were investigated. A general layout of the wing plan form along with certain of the body variations can be seen in figure 1. Figure 3 shows a photograph of a typical configuration.

Wings

The wing plan form employed for all configurations was the discontinuously tapered type with an aspect ratio of 2.91. Previous tests of a wing of identical plan form (ref. 1) indicated that such a shape gives higher values of maximum lift-drag ratio than a conventional swept wing of the same thickness; therefore, the discontinuously tapered type of wing was selected for the present tests.

All wings tested had the same spanwise variation in thickness ratio; namely, 4 percent at the root (body center line) and decreasing linearly to 3 percent at the tip. At the time of selection these thickness values were believed to be near the practical structural limits for the chosen plan form. Since the leading edge is subsonic at the design Mach number of 1.41, a round-nosed airfoil section was selected - specifically, an NACA 65A thickness distribution. The wings were all mounted in a midwing location on the bodies.

Linearized theory for supersonic speeds indicates that a lifting surface should generally be warped for highest L/D. For tapered swept-back wings with subsonic leading edges, a certain amount of washout as well as a certain amount of positive camber in the streamwise direction is known to be beneficial. Thus, the five wing variations tested were all related with regard to the manner in which the wing was warped. The design operating point was a lift coefficient of 0.2 and, although no calculations were made for the test plan form itself, the results of references 2 and 3 were used as a qualitative guide in choosing a camber and twist for the selected plan form.

One of the wings tested had neither camber nor twist and hereinafter is referred to as the plane wing. A second wing had no camber but was twisted linearly along the span from zero incidence at the root (body center line) to 4° of washout at the tip. A third wing had the same twist distribution as above and, in addition, was cambered with an NACA $a = 0$ mean camber line (ref. 4) in the streamwise direction. The amount of camber varied linearly along the span from 0 percent chord at the root to 4 percent chord at the wingtip. The investigation of two variations of the twisted and cambered wing was made possible by constructing the wing so that the forward portion of the wing near the body could be replaced by inserts of different camber: one referred to as medium droop and the other as large droop. Details of these inserts are presented in figure 2 and in table I. A general idea of the extent of the insert can be obtained from figure 3 which shows a photograph of one of the drooped configurations.

Bodies

Six different bodies were tested in combination with the previously described wings in order to evaluate the relative merits of various contours and cross-sectional shapes. The Sears-Haack body of minimum drag for a given length and volume was chosen as the basic body, and basic bodies of circular and elliptical cross section were constructed with the same Sears-Haack area distribution. The fineness ratio for the basic circular body was 15 from point to point, but the body was truncated to a fineness ratio of 12.5 to accommodate the sting support.

Additional bodies were designed by indentation of the two basic bodies. The basic body of circular cross section was indented for Mach numbers of 1.0 and 1.4 by area-rule methods (refs. 5 and 6) to preserve effectively, for the wing-body combination, the area distribution of the basic Sears-Haack body alone. The basic body of elliptical cross section was indented for a Mach number of 1.4 by the area-rule method of reference 6 and also by the so-called streamline method of reference 7 which contours the wing-body juncture in imitation of the streamlines over a two-dimensional wing swept behind the Mach lines.

L
2
6
0

Because of certain fixed model geometry (chiefly the diameter of the internal strain-gage balance) it was not possible to maintain the original elliptical cross section (1.5:1 ratio of axes) at every station on the indented bodies, particularly in the region where the largest indentation occurred. In this region, in order to maintain the desired area distribution, it was necessary to change the shape of the ellipse gradually to a circle. The same problem was present to a lesser extent in the case of the basic elliptical body which had to be made circular at the base because of limitations imposed by the sting diameter.

The coordinates of the six bodies investigated are presented in table II with sketches of typical cross sections of the circular and elliptical bodies.

Model Designation

For purposes of brevity, the various configurations will sometimes be referred to by a number designation. The following table presents the number designation and summarizes the different configurations investigated.

Number	Bodies		Wings	
	Contour	Cross section	Description	Inboard droop
1	Sears-Haack	Circular	Plane	
2	M = 1.0, area rule	Circular	Twisted	
3	M = 1.4, area rule	Circular	Cambered and twisted	None
4	Sears-Haack	Elliptical	Cambered and twisted	Medium
5	M = 1.4, area rule	Elliptical	Cambered and twisted	Large
6	M = 1.4, streamline	Elliptical		

TESTS AND ACCURACY

The supersonic tests were conducted at $M = 1.41$ and $M = 2.01$ in the Langley 4- by 4-foot supersonic pressure tunnel which is described in reference 8. The model was sting-mounted and normal force, chord force, and pitching moment were measured by means of an internal strain-gage balance. Base pressure was measured and the chord force was subsequently adjusted to correspond to the condition of free-stream pressure at the base.

The normal test condition at both Mach numbers was a stagnation pressure of 10 lb/sq in. abs and a stagnation temperature of 110° F ($q \approx 623$ lb/sq ft abs at $M = 1.41$ and $q \approx 510$ lb/sq ft abs at $M = 2.01$) with the model in the smooth condition. These conditions correspond to a Reynolds number (based on the mean aerodynamic chord) of 2.7×10^6 at $M = 1.41$ and 2.2×10^6 at $M = 2.01$. The angle-of-attack range for these test conditions was from -4° to 12°.

In addition, certain configurations were tested over a range of stagnation pressure up to 30 lb/sq in. abs with both fixed and natural transition. These special runs were made to detect changes in the total loads caused by flexure of the wings, as well as to obtain information on the extent of laminar flow and its variation with Reynolds number. Transition was fixed by means of 1/8-inch-wide roughness strips (composed of No. 60 carborundum) located at the 10-percent chord on the wing and 1/2 inch back from the nose apex on the body.

A limited amount of testing on several selected configurations was done in the Langley 8-foot transonic tunnel (ref. 9) and the results are reported herein. The Mach number range of these tests was from 0.6 to 1.2 and the Reynolds number (based on the mean aerodynamic chord) ranged from 2.9×10^6 to 3.5×10^6. These transonic tests were for the purpose of obtaining a measure of the drag rise experienced near $M = 1$ and were a logical extension of the subsonic results already reported in reference 10.

The uncertainties which are believed to hold for the data presented herein are tabulated below.

α, deg	±0.1
C_D	±0.0005
C_L	±0.005
C_m	±0.001

RESULTS AND DISCUSSION

Supersonic and Transonic Results

Supersonic.- The basic supersonic data obtained from the tests are presented in figures 4 and 5 for the test Mach numbers of 1.41 and 2.01. Variations of C_D, C_m, α, and L/D with C_L are shown for all the various wing-body combinations tested. These data are all taken at the normal test conditions and with natural transition. In figures 6 to 9, the effects of changes in dynamic pressure and of fixing transition are shown in the same manner as in figures 4 and 5. The results obtained from tests of the basic circular body alone are presented in figure 10.

In general, the results indicate that relatively high values of L/D were obtained at the design Mach number of 1.41 with natural transition. The maximum value obtained was about 10.8 for the twisted wing in combination with the elliptical body indented by the area rule for $M = 1.4$ (fig. 4(j)). A repeat run of this model (also with natural transition) yielded a maximum value of L/D of 10.5 (fig. 7(b)), and with transition fixed the value was reduced to about 9.6.

At a Mach number of 2.01, the maximum values of L/D are lower than at $M = 1.41$ and the differences between configurations are smaller. For the configuration with body 5 and wing 2, which yielded an $(L/D)_{max}$ of 10.8 at $M = 1.41$, the corresponding value with natural transition at $M = 2.01$ was about 8.0. (See fig. 5(j).) A repeat run resulted in an $(L/D)_{max}$ of 8.2 and fixing transition reduced the $(L/D)_{max}$ to about 7.6. (See fig. 9(b).) The plane wing in combination with body 5 resulted in about the same value of $(L/D)_{max}$ (fig. 5(j)).

As discussed previously, the twisted wing (wing 2) generally gave the highest values of L/D at both test Mach numbers of 1.41 and 2.01. However, at the higher lift coefficients (particularly at $M = 1.41$), the cambered and twisted wings are more efficient than either the plane or the twisted wing. Such a result indicates that the wing camber was excessive at the design lift coefficient. The data for the cambered and twisted wings with droop (figs. 4 and 5) indicate that the inboard leading-edge droop was detrimental. As in the case of the cambered and twisted wing (wing 3), the indication is that the shape changes embodied in wings 4 and 5 were too large. The comparatively poor showing of the cambered and twisted wings indicates that, unless improvement in lift-drag ratio is desired only at the higher lift coefficients, the designer must avoid an excess of camber.

Transonic.- Tests were made of bodies 2 and 5 in combination with the plane and the twisted wings through the Mach number range from 0.6 to 1.2. The variation of C_D, C_m, and α with C_L for these configurations with natural transition is shown in figures 11 to 13.

In figure 14, the variation of $C_{D,min}$ with Mach number is presented for the configurations tested. The transonic rise in minimum drag is shown by figure 14 to be relatively small, about 0.0020. In addition to the transonic data (M = 0.6 to 1.2) appearing in figure 14, there is also plotted a data point for the body 5 - wing 2 configuration (with fixed transition) at a Mach number of 1.41. Comparable supersonic data are not presented for the configurations with natural transition since it was believed that differences in the extent of laminar flow on the models in the two wind tunnels (mainly due to differences in tunnel turbulence level) would render any valid comparison impossible and possibly lead to erroneous conclusions.

L 2 6 0

In addition to obtaining a measure of the drag rise, the other main reason for the transonic tests was to investigate the pitching-moment characteristics in this speed range. Results of this phase of the investigation indicated the absence of any abrupt destabilizing tendency up to a lift coefficient of about 0.6 (figs. 11 to 13). Additional data to even higher lift coefficients (C_L = 1.0) are presented in figure 15 for the body 2 - wing 2 configuration at M = 0.6 and 0.8. These data indicate the same absence of a destabilizing tendency, with the possible exception of the point of highest lift at M = 0.6.

Analysis of Supersonic Results

Method of analysis.- The method of least squares was selected for data analysis because for a given set of data and an assumed function, the results are unique. Linear theory indicates that the variation of drag with lift is a parabolic function. Only in theory, of course, is the variation exactly parabolic; actual variations are parabolic only for the lower lift coefficients. The basis of curve fitting by least squares is explained in reference 11. The details of application to the present data are given in the appendix. The parabolas used to fit the present data are of the form

$$C_D = C_{D,min} + \epsilon\left[C_L - (C_L)_{C_{D,min}}\right]^2$$

The minimum drag coefficient $C_{D,min}$, the drag-rise factor ϵ, and the lift coefficient at minimum drag $(C_L)_{C_{D,min}}$ are the parameters

extracted from the data by the method of least squares. The values of these parameters are tabulated for each model and test condition in tables III and IV.

If the measured maximum L/D values were compared with those computed with the parameter values of tables III and IV, a deviation of less than 2 percent would be found for any case. For most cases a deviation less than 1 percent is found. Hence, although the parameter values in tables III and IV may be relatively inaccurate individually, the accuracy of the computed L/D function is very good near maximum L/D.

Drag-due-to-lift parameter.- An approximate independence of ϵ and $C_{D,min}$ may be expected in these tests, due to the approximate independence of lifting and thickness effects. The variation of ϵ with $C_{D,min}$ is shown for three test wings in figures 16 and 17. The values are taken from tables III and IV. As expected, figures 16 and 17 show that ϵ does not vary systematically with $C_{D,min}$. There is an appreciable scatter in the data. The average of the ϵ values has been indicated to give a representative value of ϵ for each wing.

A comparison of these average values shows the superiority of the twisted wing at $M = 1.41$ (fig. 16), since the minimum drag level is about the same as for the plane wing and ϵ is lower. Although the cambered and twisted wing has a lower ϵ than does the plane wing, the minimum drag level is much higher. At $M = 2.01$ (fig. 17) the cambered and twisted wing has a lower average ϵ than either the plane or the twisted wings. This lower ϵ is more than offset by the increase in $C_{D,min}$ level introduced by the camber.

Tip twist.- The variation of ϵ with dynamic pressure q is shown in figure 18 for the twisted wing at $M = 1.41$. This variation of ϵ can be a clue to the optimum amount of twist. Also shown in figure 18 are the corresponding values of $C_{D,min}$. The dynamic pressure corresponding to normal test conditions is marked with a vertical line. It appears from the figure that at the normal test dynamic pressure the wing is operating near the minimum in the ϵ variation. Unpublished measurements of wingtip deflection have been taken with a model of this twisted wing alone at $M = 1.61$. These measurements indicate that at the normal dynamic pressure and near $(L/D)_{max}$ the wing has about 1° of additional washout at the tip due to aeroelastic deflection. Thus, the indication is that a rigid wing of the same plan form, thickness distribution, and twist distribution as the test model should have slightly more washout for best performance at $M = 1.41$.

The large variations in $C_{D,min}$ shown in figure 18 must be strongly associated with changes in the boundary-layer flow. Since the changes in

ϵ due to changes in the boundary-layer flow are unknown, the indication of the proper amount of tip twist given above is subject to question.

Minimum drag.- Comparative minimum drag coefficients for the test bodies in combination with the plane wing are shown in figures 19 and 20. The relative merit of the bodies can be most easily judged in this manner. It is recognized that this simple approach is not strictly correct, since changes of wing-body interference with lift are neglected.

In figure 19, for the design condition of $M = 1.41$, there is little to choose between the indented bodies considered as a group, or between the Sears-Haack bodies considered as a pair. That there is a substantial gain due to indentation is evident. When a body is indented, however, a certain amount of volume is lost and the comparisons are perhaps unfair to the Sears-Haack bodies. In order to eliminate this injustice the relative drag of indented configurations of the same volume as the non-indented configurations is also shown in figure 19. On this equal-volume basis there is still a noticeable gain due to indentation. (A parameter often used in discussing different wing-body combinations is the ratio $\frac{\text{Volume}^{2/3}}{\text{Wing area}}$ where the volume includes both the body and wing. As a matter of general interest, this ratio was computed for the present configurations and found to be about 0.17 for the configurations with indented bodies and about 0.19 for the configurations with the basic bodies.)

For $M = 2.01$, similar comparisons are made in figure 20. The improvement due to indentation is less than at $M = 1.41$, and on an equal-volume basis there is no improvement for the circular bodies.

The foregoing comparisons have all been for natural transition. In figure 20 minimum drag coefficients are also shown for three of the bodies for fixed transition. There is a shift in the relative merits of the three bodies when the transition is fixed. For the nonindented bodies, the elliptical section is better than the circular section. The advantage of the indented over the nonindented elliptical body is somewhat reduced.

A calculation of the turbulent skin friction by the results of Van Driest (ref. 12) gives the values 0.0086 and 0.0083 shown on the right side of figures 19 and 20, respectively. The body and wing have been considered separately in this calculation. Values for laminar flow were taken from the results of Blasius. The Reynolds numbers used in the calculations for the body and wing were based on the body length and mean aerodynamic chord, respectively. For turbulent skin friction, figure 20 indicates that some 0.0024 in the drag coefficient of body 5 on the plane wing is due to wave drag. If the wave drag coefficient is assumed to be 0.0024 at $M = 1.41$, the actual skin friction is as shown

in figure 19 for body 5 on the plane wing. It is apparent that considerable laminar flow existed on the test models at $M = 1.41$ when transition was not fixed. For this reason, the relative minimum wave drag of the bodies may be somewhat different from that indicated by figure 19. The values of drag coefficient with fixed transition are shown for body 1 in figure 10. If the calculated skin-friction coefficient of 0.0037 is subtracted from the total of 0.0056, an increment of 0.0019 remains for the wave drag. This is some 0.0005 less than the estimated wave drag of the wing-body combination previously mentioned. The minimum drag rise in the transonic speed range of the wing-body combination is about the same as the estimated wave drag of the body alone at $M = 1.41$ and 2.01.

L
2
6
0

L/D at Full Scale

If the combination of body 5 and wing 2 is considered, with turbulent flow (fig. 7), the maximum value of lift-drag ratio at the normal test pressure is 9.6. This result is somewhat poorer than the 10.5 value attained with natural transition. If the estimate of 0.0086 for turbulent skin-friction coefficient is correct, figure 7(b) indicates the wave drag coefficient to be 0.0024. If the approximate formula

$$\left(\frac{L}{D}\right)_{max} = \frac{0.5}{\sqrt{C_{D,min}\,\epsilon}} \qquad (C_L)_{C_{D,min}} \approx 0$$

is assumed, and if ϵ is assumed not to vary with increasing Reynolds number, then

$$\frac{(L/D)_{max,1}}{(L/D)_{max,2}} = \sqrt{\frac{(C_{D,min})_2}{(C_{D,min})_1}}$$

With the test model assumed to be 1/20 scale, a computation of $(L/D)_{max,2}$ for full scale yields

$$\left(\frac{L}{D}\right)_{max,2} = \sqrt{\frac{0.0110}{0.0024 + 0.0051}}(9.6) = 11.6$$

This result shows the importance of scale effects on lift-drag ratio, and, of course, applies to a full-scale wing-body configuration, not a complete airplane.

CONCLUDING REMARKS

The most efficient test configuration at the design condition of a Mach number of 1.41 was a twisted wing in combination with a body of elliptical cross section indented for this design Mach number. This combination gave a maximum lift-drag ratio $(L/D)_{max}$ of about 10.5 with natural transition. With transition fixed, the $(L/D)_{max}$ of this combination was 9.6. The twisted wing had a lower drag due to lift than did the plane wing and also had a small penalty in minimum drag. Wings designed with both camber and twist were less successful because excessive camber was used. Improvement over the plane wing was noted at the higher lifts for the cambered wings. Symmetric body indentation reduced the minimum drag even for equal-volume configurations, but there was little to choose between methods of indentation. Large amounts of laminar flow are shown to have existed for the data with natural transition at a Mach number of 1.41.

The small amount of data with a completely turbulent boundary layer taken at a Mach number of 2.01 indicated that caution should be used in comparing minimum drag coefficients for the test configurations. At a Mach number of 2.01 the differences between configurations appeared smaller than at a Mach number of 1.41. As was to be expected, the $(L/D)_{max}$ was lower and drag due to lift was higher. The $(L/D)_{max}$ attained with natural transition was 8.0 for the same configuration that gave the highest value at a Mach number of 1.41. With a turbulent boundary layer the $(L/D)_{max}$ of this configuration was 7.6.

The drag rise indicated by the transonic tests was about 0.0020. This value is slightly less than the wave drag of 0.0024 which was estimated from the supersonic results for two of the indented configurations.

Langley Research Center,
National Aeronautics and Space Administration,
Langley Field, Va., May 18, 1960.

APPENDIX

DETAILS OF DATA ANALYSIS

General

As applied to drag polars, the method of least squares passes a parabola through the data in such a manner as to minimize the sum of the squares of the differences between the data drag coefficients and the calculated parabola drag coefficients. If the variation of drag with lift is truly parabolic with random errors superposed, the theory of probability indicates that the least-squares parabola is the one most likely to be correct (ref. 9).

The assumed parabolic variation of drag coefficient is

$$C_D = C_{D,min} + \epsilon\left[C_L - (C_L)_{C_{D,min}}\right]^2 \tag{A1}$$

with $C_{D,min}$, ϵ, and $(C_L)_{C_{D,min}}$ as parameters. Expansion of formula (A1) in a Taylor series about approximate parameter values equal to ϵ_o, $C_{D,o}$, and $C_{L,o}$ will provide a linear relation for C_D if only the first-order terms are retained. If these parameters are defined

$$\left.\begin{aligned} C_{D,min} &= C_{D,o} + \Delta C_{D,min} \\ \epsilon &= \epsilon_o + \Delta\epsilon \\ (C_L)_{C_{D,min}} &= C_{L,o} + \Delta(C_L)_{C_{D,min}} \end{aligned}\right\} \tag{A2}$$

and the first terms of a Taylor series for C_D about ϵ_o, $C_{D,o}$, and $C_{L,o}$ are used, the three linear equations for $\Delta(C_L)_{C_{D,min}}$, $\Delta\epsilon$, $\Delta C_{D,min}$ result when the derivatives of the sum of the squares of the differences are set equal to zero:

$$\left[\sum_{i=1}^{n}\left(C_{L,i} - C_{L,o}\right)^{j}\right]\Delta C_{D,min} + \left[\sum_{i=1}^{n}\left(C_{L,i} - C_{L,o}\right)^{j+2}\right]\Delta\epsilon$$

$$+\left[\sum_{i=1}^{n} -2\epsilon_o\left(C_{L,i} - C_{L,o}\right)^{j+1}\right]\Delta\left(C_L\right)_{C_{D,min}} = \sum_{i=1}^{n}\left(C_{D,i} - \bar{C}_{D,i}\right)\left(C_{L,i} - C_{L,o}\right)^{j}$$

$$j = 0,\ 1,\ 2 \qquad \text{(A3)}$$

In formula (A3) $C_{D,i}$ and $C_{L,i}$ are the test values. $\bar{C}_{D,i}$ is the value of C_D from formula (A1) when $C_L = C_{L,i}$ and ϵ, $C_{D,min}$, $\left(C_L\right)_{C_{D,min}}$ are equal to ϵ_o, $C_{D,o}$, $C_{L,o}$, respectively. The number of data points is denoted by n.

Specific

The values of ϵ_o and $C_{L,o}$ used for the various configurations of this paper are tabulated below. Also shown is the range of C_L used in fitting the parabolas. The smallest measured C_D was used for $C_{D,o}$ in all cases.

Wing	M = 1.41			M = 2.01		
	ϵ_o	$C_{L,o}$	C_L range	ϵ_o	$C_{L,o}$	C_L range
1	0.30	0	-0.2 to 0.2	0.45	0	-0.2 to 0.2
2	.30	0	-.02 to .2	.45	0	-.02 to .2
3	.30	.03	-.02 to .2	.45	0	-.02 to .2
4	.30	.03	-.02 to .2	.45	0	-.02 to .2
5	.30	.03	-.02 to .2	.45	0	-.02 to .2

REFERENCES

1. Sevier, John R., Jr.: Investigation of the Effects of Body Indentation and of Wing-Plan-Form Modification on the Longitudinal Characteristics of a 60° Swept-Wing-Body Combination at Mach Numbers of 1.41, 1.61, and 2.01. NACA RM L55E17, 1955.

2. Tucker, Warren A.: A Method for the Design of Sweptback Wings Warped To Produce Specified Flight Characteristics at Supersonic Speeds. NACA Rep. 1226, 1955. (Supersedes NACA RM L51F08.)

3. Grant, Frederick C.: The Proper Combination of Lift Loadings for Least Drag on a Supersonic Wing. NACA Rep. 1275, 1956. (Supersedes NACA TN 3533.)

4. Abbott, Ira H., von Doenhoff, Albert E., and Stivers, Louis S., Jr.: Summary of Airfoil Data. NACA Rep. 824, 1945. (Formerly NACA WR L-560.)

5. Whitcomb, Richard T.: A Study of the Zero-Lift Drag-Rise Characteristics of Wing-Body Combinations Near the Speed of Sound. NACA Rep. 1273, 1956. (Supersedes NACA RM L52H08.)

6. Whitcomb, Richard T., and Fischetti, Thomas L.: Development of a Supersonic Area Rule and an Application to the Design of a Wing-Body Combination Having High Lift-to-Drag Ratios. NACA RM L53H31a, 1953.

7. Hilton, W. F.: Tests of a Fairing To Reduce the Drag of a Supersonic Swept-Wing Root. Jour. Aero. Sci., vol. 22, no. 3, Mar. 1955, pp. 173-178, 188.

8. Cooper, Morton, Smith, Norman F., and Kainer, Julian H.: A Pressure-Distribution Investigation of a Supersonic Aircraft Fuselage and Calibration of the Mach Number 1.59 Nozzle of the Langley 4- by 4-Foot Supersonic Tunnel. NACA RM L9E27a, 1949.

9. Wright, Ray H., Ritchie, Virgil S., and Pearson, Albin O.: Characteristics of the Langley 8-Foot Transonic Tunnel With Slotted Test Section. NACA Rep. 1389, 1958. (Supersedes NACA RM L51H10 by Wright and Ritchie and NACA RM L51K14 by Ritchie and Pearson.)

10. Fournier, Paul G.: Wind-Tunnel Investigation of the High-Subsonic Static Longitudinal Stability Characteristics of Several Wing-Body Configurations Designed for High Lift-Drag Ratios at a Mach Number of 1.4. NACA TN 4340, 1958.

11. Scarborough, James B.: Numerical Mathematical Analysis. Second ed., The Johns Hopkins Press (Baltimore), 1950, pp. 451-469.

12. Van Driest, E. R.: Turbulent Boundary Layer in Compressible Fluids. Jour. Aero. Sci., vol. 18, no. 3, Mar. 1951, pp. 145-160, 216.

TABLE I.- ORDINATES OF LEADING-EDGE INSERTS

[Reference plane is parallel to and located 1 inch below the plane of the body center line and leading edge of the plane wing]

Station A			Station B			Station C			Station D			Station E		
X	Z_u	Z_l	X	Z_u	Z_l	X	Z_u	Z_l	X	Z_u	Z_l	X	Z_u	Z_l
Large droop														
0.000	0.499	0.499	0.000	0.601	0.601	0.000	0.761	0.761	0.000	0.920	0.920	0.000	1.000	1.000
.076	.587	.484	.070	.677	.588	.060	.823	.750	.050	.968	.908	.045	1.037	.987
.191	.653	.503	.175	.738	.600	.150	.870	.756	.125	1.000	.908	.113	1.065	.985
.382	.744	.540	.350	.816	.631	.300	.933	.780	.250	1.044	.920	.225	1.095	.986
.764	.893	.621	.700	.949	.704	.600	1.031	.827	.500	1.107	.945	.450	1.142	.997
1.146	1.018	.693	1.050	1.056	.764	.900	1.115	.871	.750	1.162	.965	.675	1.180	1.007
1.528	1.120	.751	1.400	1.146	.815	1.200	1.182	.905	1.000	1.204	.980	.900	1.212	1.014
2.292	1.263	.828	2.100	1.273	.878	1.800	1.283	.951	1.500	1.273	1.003	1.350	1.265	1.026
3.056	1.334	.842	2.800	1.339	.897	2.400	1.340	.968	2.000	1.319	1.018	1.800	1.306	1.036
3.820	1.363	.832	3.500	1.370	.890	3.000	1.370	.968	2.500	1.353	1.025	2.250	1.328	1.037
Medium droop														
0.000	0.805	0.805	0.000	0.845	0.845	0.000	0.907	0.907	0.000	0.969	0.969	0.000	1.000	1.000
.076	.873	.775	.070	.905	.819	.060	.960	.888	.050	1.014	.954	.045	1.037	.987
.191	.917	.773	.175	.947	.815	.150	.997	.887	.125	1.042	.953	.113	1.065	.985
.382	.973	.777	.350	1.000	.820	.300	1.041	.891	.250	1.080	.957	.225	1.095	.986
.764	1.058	.797	.700	1.083	.843	.600	1.112	.912	.500	1.133	.972	.450	1.142	.997
1.146	1.132	.814	1.050	1.147	.860	.900	1.169	.929	.750	1.177	.983	.675	1.180	1.007
1.528	1.189	.826	1.400	1.205	.877	1.200	1.218	.943	1.000	1.215	.993	.900	1.212	1.014
2.292	1.282	.847	2.100	1.287	.894	1.800	1.290	.960	1.500	1.278	1.008	1.250	1.265	1.026
3.056	1.334	.842	2.800	1.339	.897	2.400	1.340	.968	2.000	1.319	1.018	1.800	1.306	1.036
3.820	1.363	.832	3.500	1.370	.890	3.000	1.370	.968	2.500	1.353	1.025	2.250	1.328	1.037

TABLE II.- BODY COORDINATES

[All dimensions are in inches]

x	Circular cross section			Elliptical cross section					
	Body 1	Body 2	Body 3	Body 4		Body 5		Body 6	
	r	r	r	a_1	a_2	a_1	a_2	a_1	a_2
0	0	0	0	0	0	0	0	0	0
1	.243	.243	.243	.297	.198	.297	.198	.297	.198
2	.401	.401	.401	.492	.328	.492	.328	.492	.328
3	.535	.535	.535	.655	.437	.655	.437	.655	.437
4	.652	.652	.652	.799	.533	.799	.533	.799	.533
5	.758	.758	.758	.928	.619	.928	.619	.928	.619
6	.853	.853	.853	1.045	.696	1.045	.696	1.045	.696
7	.940	.940	.940	1.151	.767	1.151	.767	1.151	.767
8	1.019	1.019	1.019	1.248	.832	1.248	.832	1.248	.832
9	1.092	1.092	1.092	1.337	.891	1.337	.891	1.337	.891
10	1.158	1.158	1.158	1.418	.945	1.418	.945	1.418	.945
11	1.218	1.218	1.218	1.492	.995	1.492	.995	1.492	.995
12	1.273	1.273	1.273	1.559	1.040	1.559	1.040	1.559	1.040
13	1.323	1.323	1.323	1.620	1.080	1.620	1.080	1.620	1.080
14	1.367	1.366	1.356	1.674	1.116	1.666	1.116	1.675	1.116
15	1.407	1.392	1.370	1.723	1.149	1.666	1.149	1.699	1.149
16	1.441	1.392	1.372	1.765	1.177	1.645	1.175	1.690	1.175
17	1.472	1.379	1.361	1.802	1.202	1.609	1.190	1.656	1.190
18	1.497	1.361	1.337	1.834	1.223	1.551	1.195	1.610	1.195
19	1.518	1.334	1.308	1.860	1.240	1.482	1.195	1.558	1.195
20	1.535	1.301	1.275	1.880	1.254	1.399	1.195	1.497	1.195
21	1.548	1.266	1.241	1.896	1.264	1.325	1.195	1.437	1.195
22	1.556	1.231	1.210	1.905	1.270	1.257	1.195	1.381	1.195
23	1.560	1.202	1.193	1.910	1.273	1.198	1.195	1.327	1.195
24	1.559	1.186	1.202	1.910	1.273	1.211	1.195	1.281	1.195
25	1.555	1.184	1.222	1.904	1.269	1.260	1.195	1.243	1.195
26	1.546	1.198	1.258	1.893	1.262	1.332	1.195	1.215	1.195
27	1.532	1.227	1.313	1.877	1.251	1.446	1.195	1.198	1.195
28	1.515	1.267	1.340	1.855	1.237	1.514	1.195	1.197	1.195
29	1.493	1.321	1.356	1.828	1.219	1.542	1.195	1.210	1.195
30	1.466	1.362	1.361	1.795	1.197	1.554	1.195	1.232	1.195
31	1.435	1.355	1.353	1.752	1.175	1.534	1.195	1.249	1.195
32	1.399	1.328	1.335	1.696	1.154	1.489	1.195	1.255	1.195
33	1.359	1.294	1.309	1.630	1.133	1.433	1.195	1.240	1.195
34	1.313	1.253	1.272	1.552	1.111	1.369	1.182	1.210	1.182
35	1.263	1.211	1.226	1.463	1.090	1.303	1.155	1.170	1.155
36	1.207	1.166	1.173	1.363	1.068	1.231	1.117	1.125	1.117
37	1.145	1.119	1.113	1.253	1.047	1.155	1.072	1.077	1.072
38	1.078	1.068	1.047	1.133	1.025	1.067	1.025	1.027	1.025
39	1.004	1.004	.975	1.004	1.004	.975	.975	.975	.975

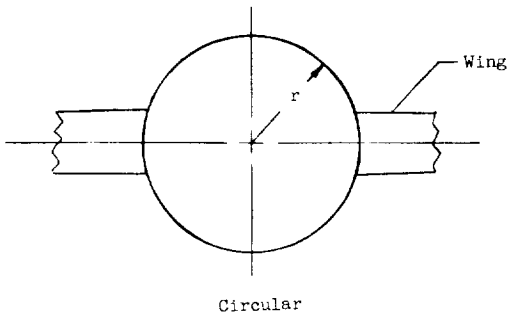

Circular

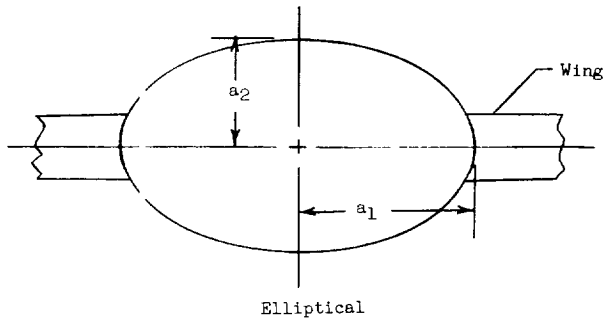

Elliptical

TABLE III.- PARAMETERS DEFINING THE DRAG POLAR

AT THE NORMAL TEST CONDITIONS

[Natural transition]

(a) M = 1.41; q ≈ 623 lb/sq ft abs

Configurations		ϵ	$C_{D,min}$	$(C_L)_{C_{D,min}}$	$(L/D)_{max}$
Body	Wing				
1	1	0.346	0.0090	-0.001	8.91
2	1	.329	.0074	.001	10.20
3	1	.329	.0075	-.001	10.03
4	1	.339	.0089	.002	9.18
5	1	.323	.0077	-.001	9.94
6	1	.344	.0076	.002	9.96
1	2	.285	.0096	-.005	9.26
2	2	.247	.0077	-.014	10.61
3	2	.271	.0076	-.006	10.62
4	2	.299	.0093	.001	9.54
5	2	.266	.0074	-.008	10.82
6	2	.282	.0081	-.002	10.31
1	3	.331	.0130	.043	9.49
2	3	.300	.0113	.034	10.22
3	3	.310	.0109	.039	10.57
4	3	.310	.0125	.036	9.60
5	3	.295	.0113	.035	10.37
6	3	.301	.0114	.034	10.16
1	4	.290	.0137	.034	9.29
2	4	.283	.0122	.035	10.05
3	4	.282	.0118	.034	10.23
4	4	.291	.0131	.036	9.59
5	4	.280	.0118	.034	10.25
6	4	.279	.0127	.035	9.90
1	5	.284	.0151	.038	8.86
2	5	.274	.0140	.037	9.52
3	5	.284	.0136	.041	9.67
4	5	.291	.0142	.040	9.31
5	5	.308	.0135	.047	9.71
6	5	.302	.0139	.046	9.52

TABLE III.- PARAMETERS DEFINING THE DRAG POLAR

AT THE NORMAL TEST CONDITIONS - Concluded

(b) M = 2.01; q ≈ 510 lb/sq ft abs

Configurations		ϵ	$C_{D,min}$	$(C_L)_{C_{D,min}}$	$(L/D)_{max}$
Body	Wing				
1	1	0.478	0.0096	0.002	7.47
2	1	.471	.0091	.001	7.70
3	1	.470	.0089	.000	7.75
4	1	.457	.0100	.001	7.45
5	1	.454	.0088	.001	7.98
6	1	.467	.0086	.001	7.91
1	2	.444	.0103	.003	7.52
2	2	.432	.0089	-.007	7.71
3	2	.438	.0096	.002	7.83
4	2	.429	.0098	.002	7.79
5	2	.444	.0093	.004	8.01
6	2	.422	.0097	.001	7.88
1	3	.427	.0140	.018	7.14
2	3	.388	.0132	.009	7.34
3	3	.398	.0132	.011	7.42
4	3	.428	.0135	.020	7.36
5	3	.421	.0128	.017	7.51
6	3	.419	.0126	.014	7.47
1	4	.392	.0141	.010	7.08
2	4	.391	.0138	.009	7.13
3	4	.451	.0134	.019	7.17
4	4	.397	.0137	.015	7.33
5	4	.397	.0135	.013	7.34
6	4	.505	.0129	.029	7.42
1	5	.406	.0159	.015	6.73
2	5	.413	.0153	.013	6.73
3	5	.407	.0154	.014	6.77
4	5	.439	.0149	.022	6.99
5	5	.398	.0147	.014	7.03
6	5	.398	.0145	.011	6.99

TABLE IV.- PARAMETERS DEFINING THE DRAG POLAR

AT SPECIAL TEST CONDITIONS

L
2
6
0

Configuration		q, lb/sq ft abs	ϵ	$C_{D,min}$	$(C_L)_{C_{D,min}}$	$(L/D)_{max}$
Body	Wing					
M = 1.41; natural transition						
1	1	623	0.346	0.0090	-0.001	8.91
		1,248	.266	.0092	-.021	9.06
4	1	623	.399	.0089	.002	9.18
		1,251	.282	.0095	-.011	9.14
5	1	252	.338	.0081	-.006	9.20
		623	.323	.0077	-.001	9.94
		1,244	.296	.0085	.001	10.06
		1,843	.292	.0084	-.001	10.02
5	2	187	.327	.0092	.018	10.17
		312	.291	.0077	.002	10.69
		623	.266	.0074	-.008	10.82
		1,246	.255	.0077	-.014	10.42
		1,869	.300	.0086	.009	10.38
M = 2.01; fixed transition						
1	1	510	0.431	0.0120	-0.002	6.87
4	1	510	.441	.0112	-.001	7.04
5	1	510	.431	.0106	.001	7.43

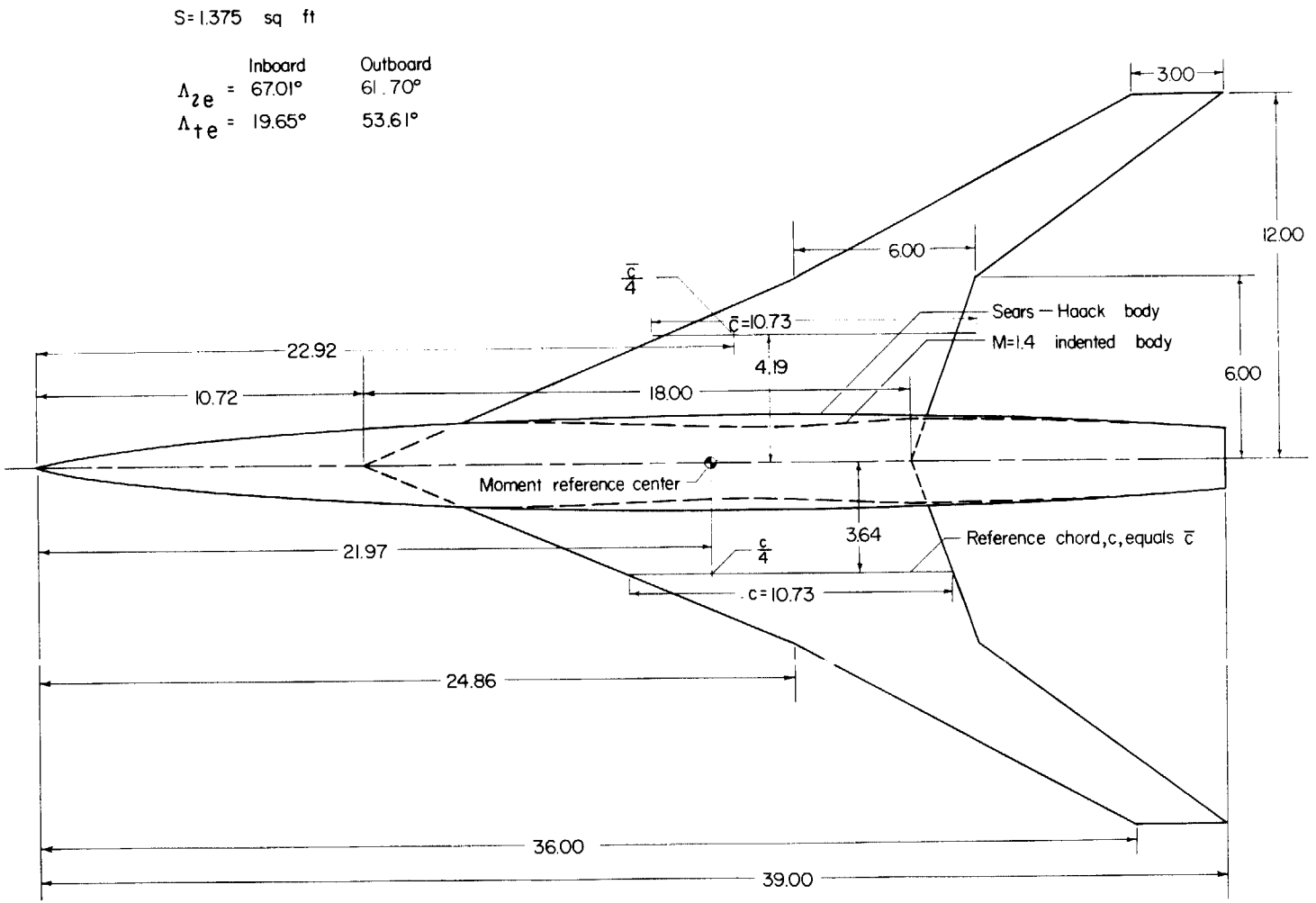

(a) Circular bodies.

Figure 1.- Sketch of configurations. All dimensions are in inches unless otherwise noted.

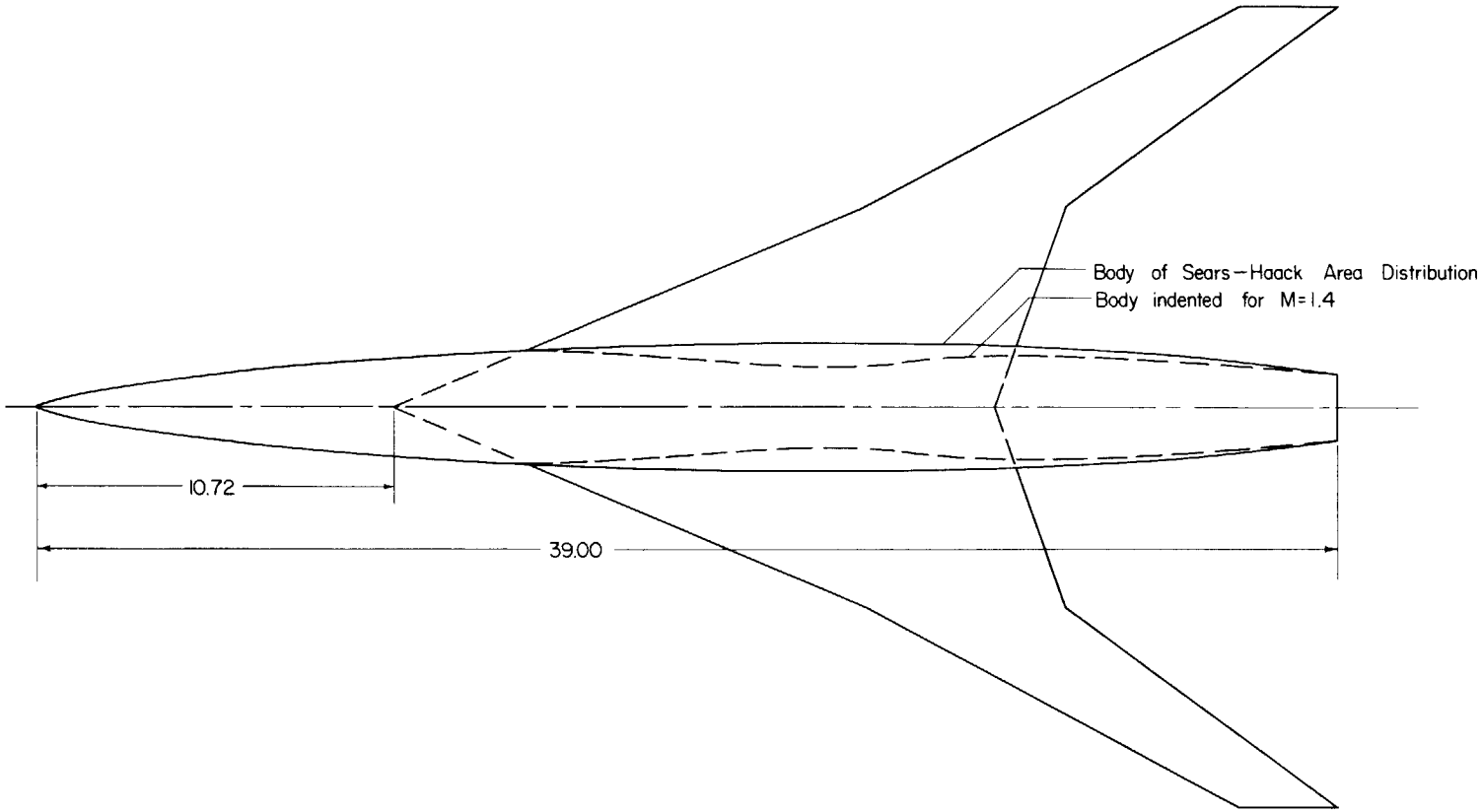

(b) Elliptical bodies.

Figure 1.- Concluded.

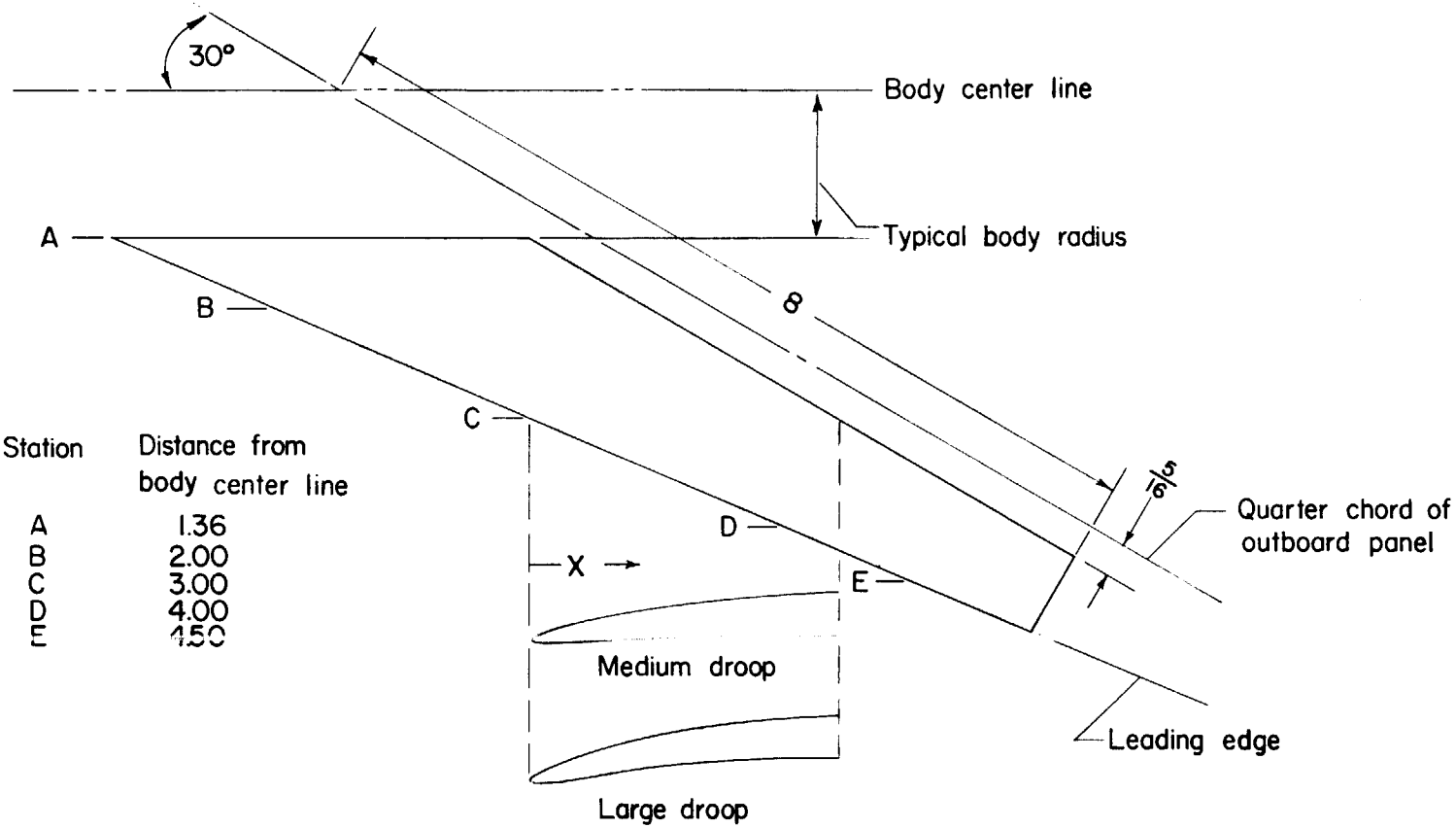

Figure 2.- Sketch of leading-edge inserts. Linear dimensions are in inches.

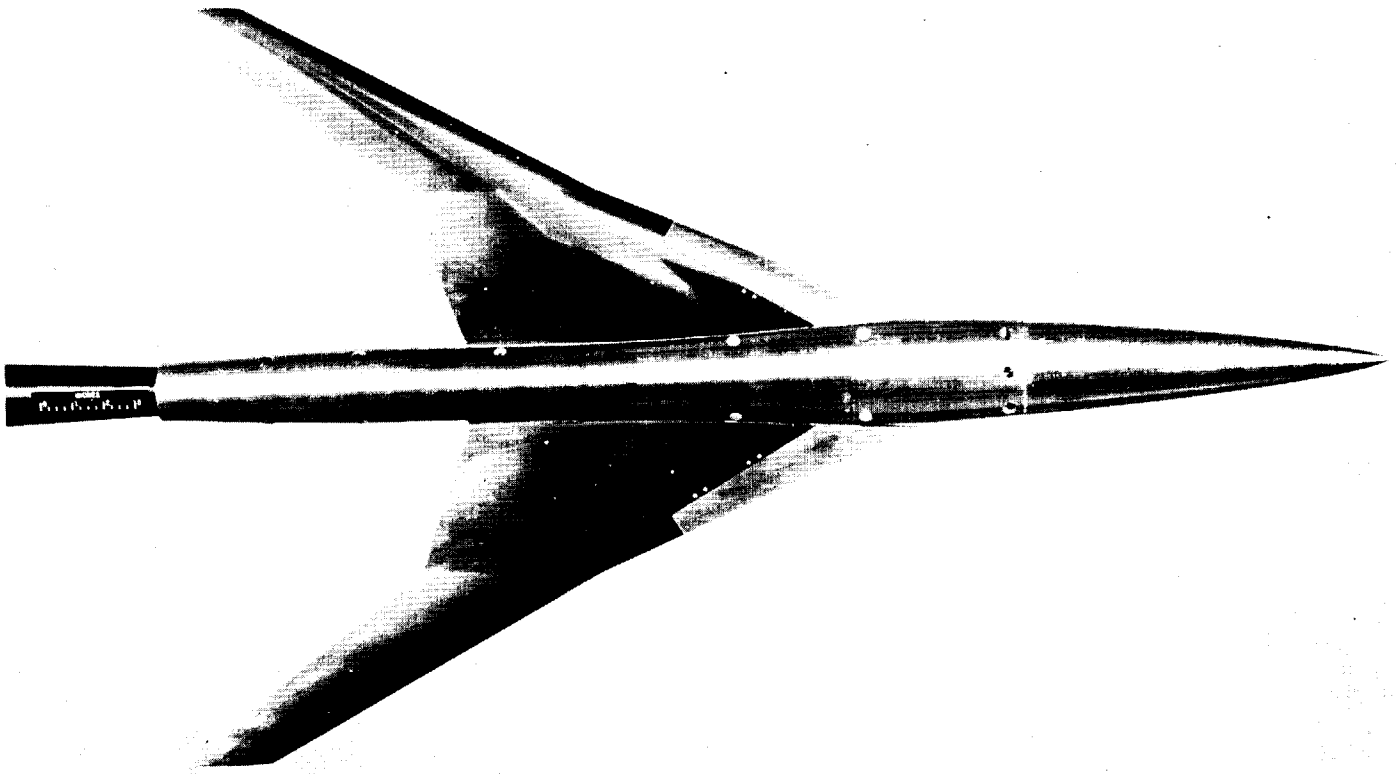

L-95570

Figure 3.- Photograph of typical test model, showing inboard leading-edge inserts.

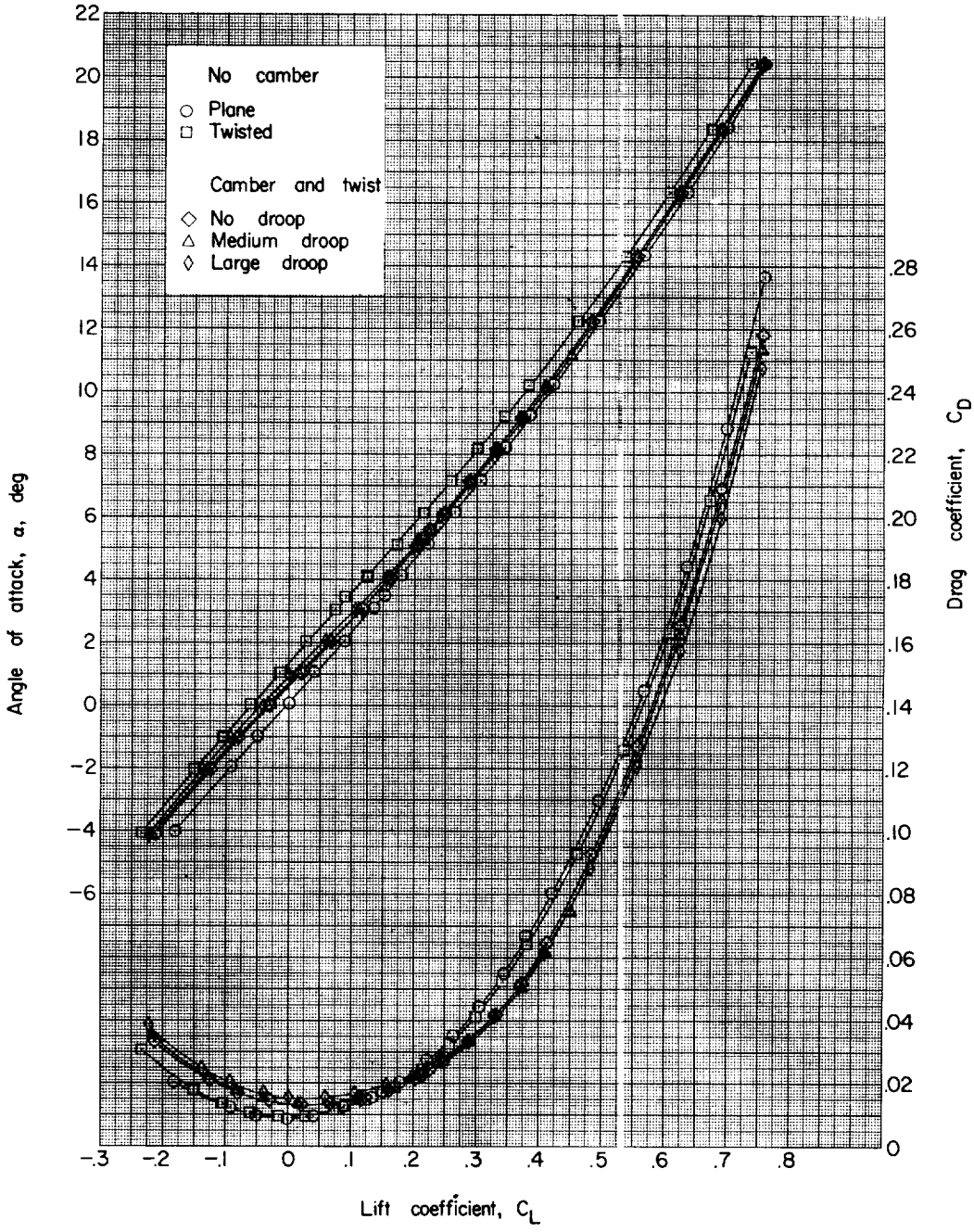

(a) Angle of attack and drag coefficient. Body 1.

Figure 4.- Variation of aerodynamic parameters with lift coefficient. M = 1.41; q ≈ 620 lb/sq ft abs; natural transition.

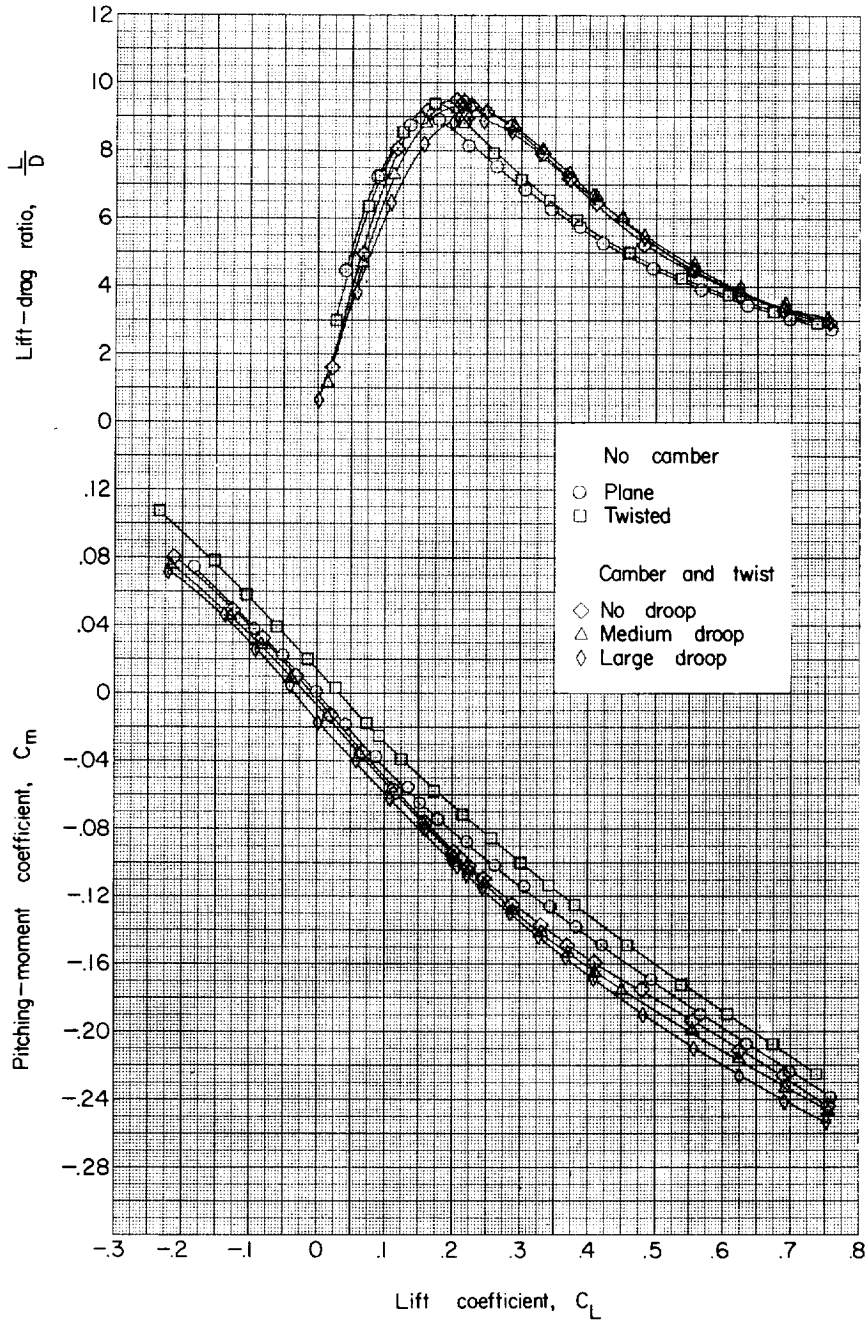

(b) Pitching-moment coefficient and lift-drag ratio. Body 1.

Figure 4.- Continued.

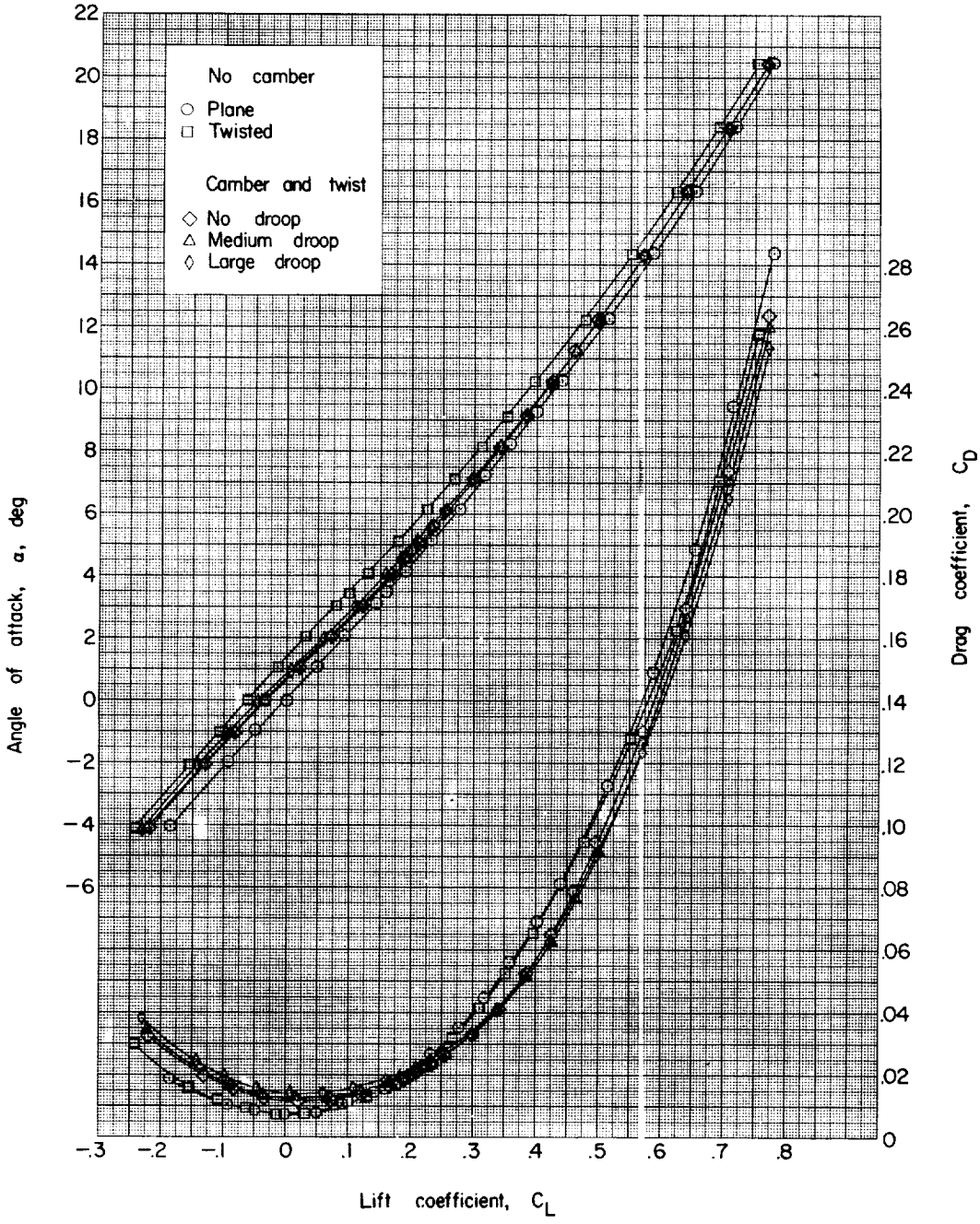

(c) Angle of attack and drag coefficient. Body 2.

Figure 4.- Continued.

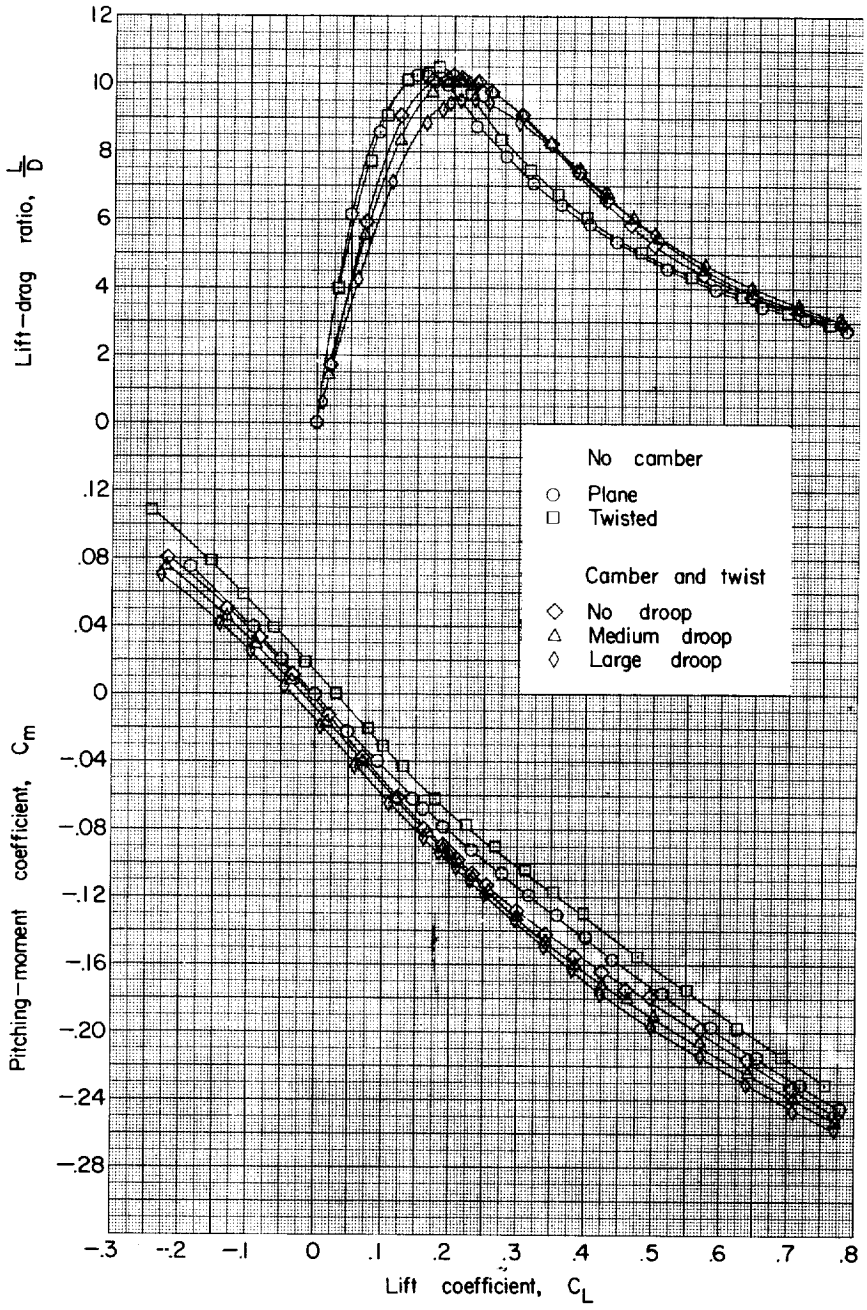

(d) Pitching-moment coefficient and lift-drag ratio. Body 2.

Figure 4.- Continued.

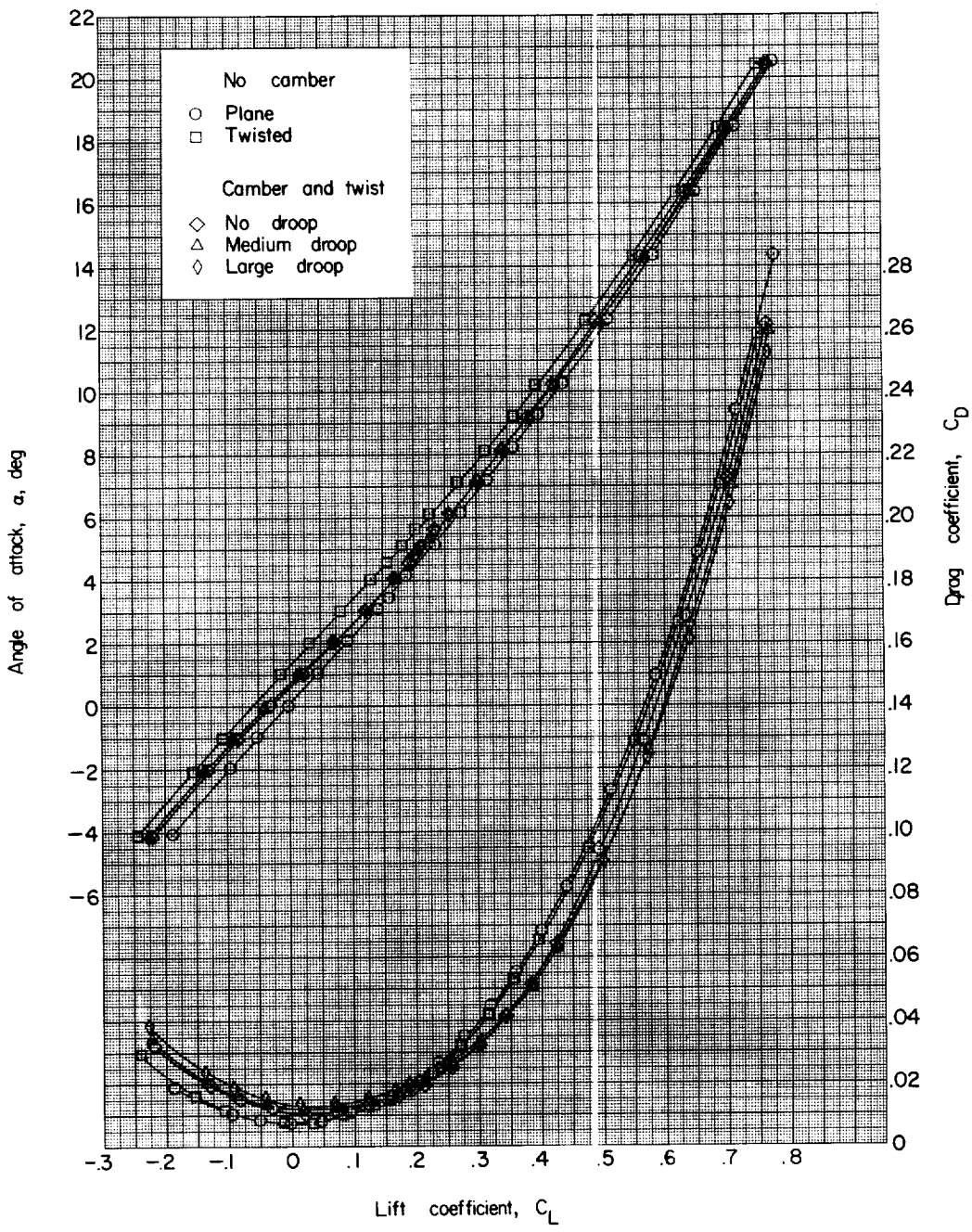

(e) Angle of attack and drag coefficient. Body 3.

Figure 4.- Continued.

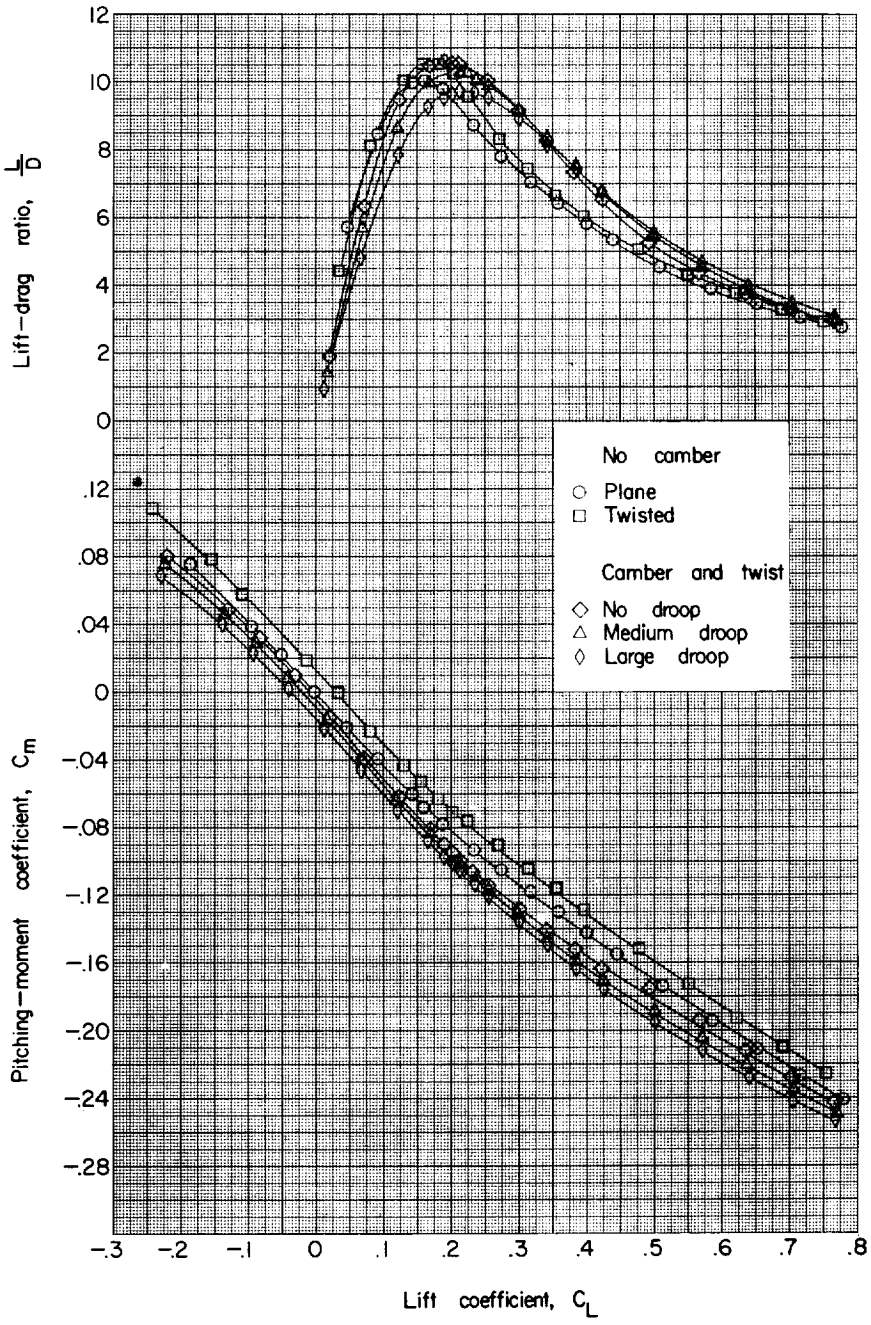

(f) Pitching-moment coefficient and lift-drag ratio. Body 3.

Figure 4.- Continued.

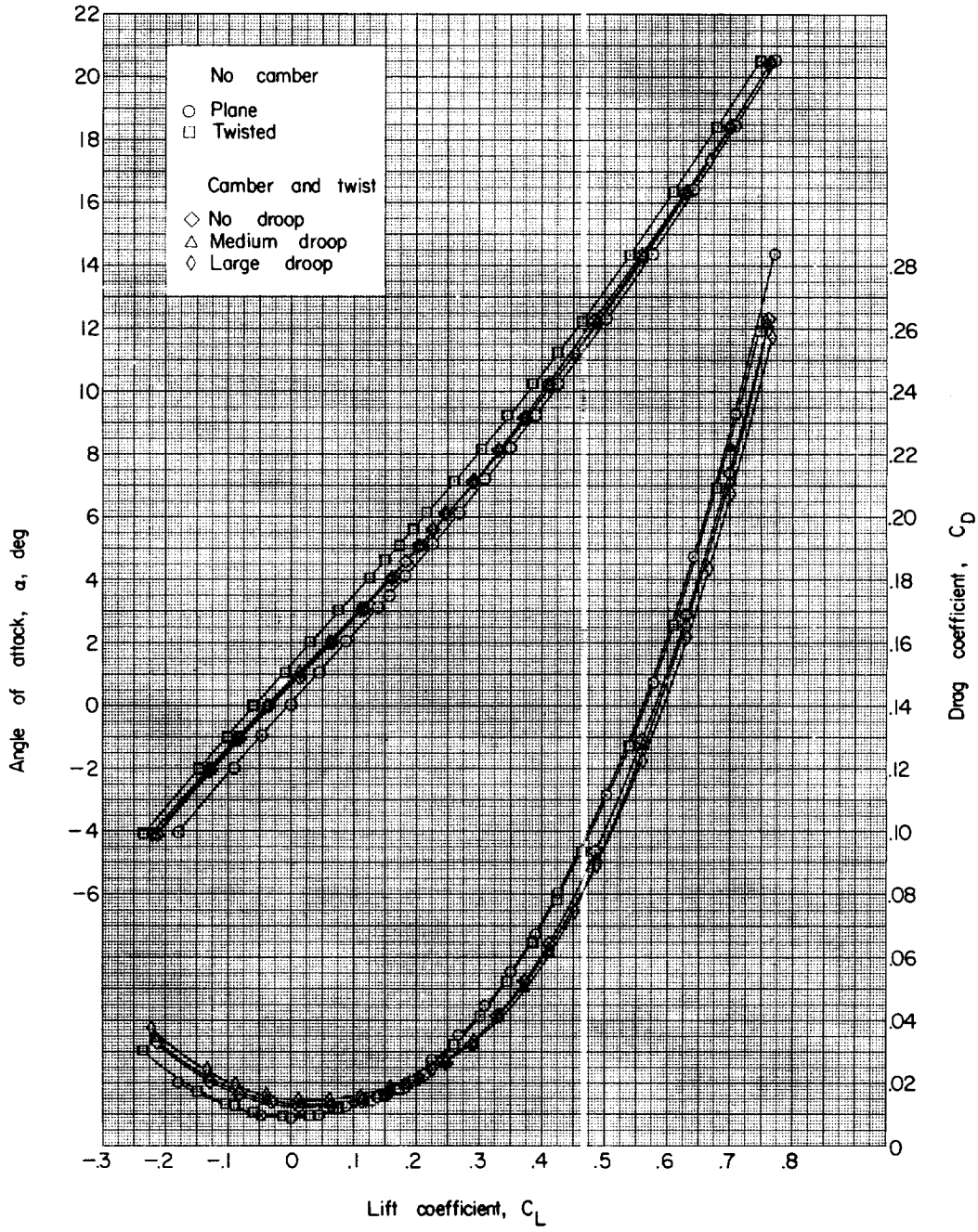

(g) Angle of attack and drag coefficient. Body 4.

Figure 4.- Continued.

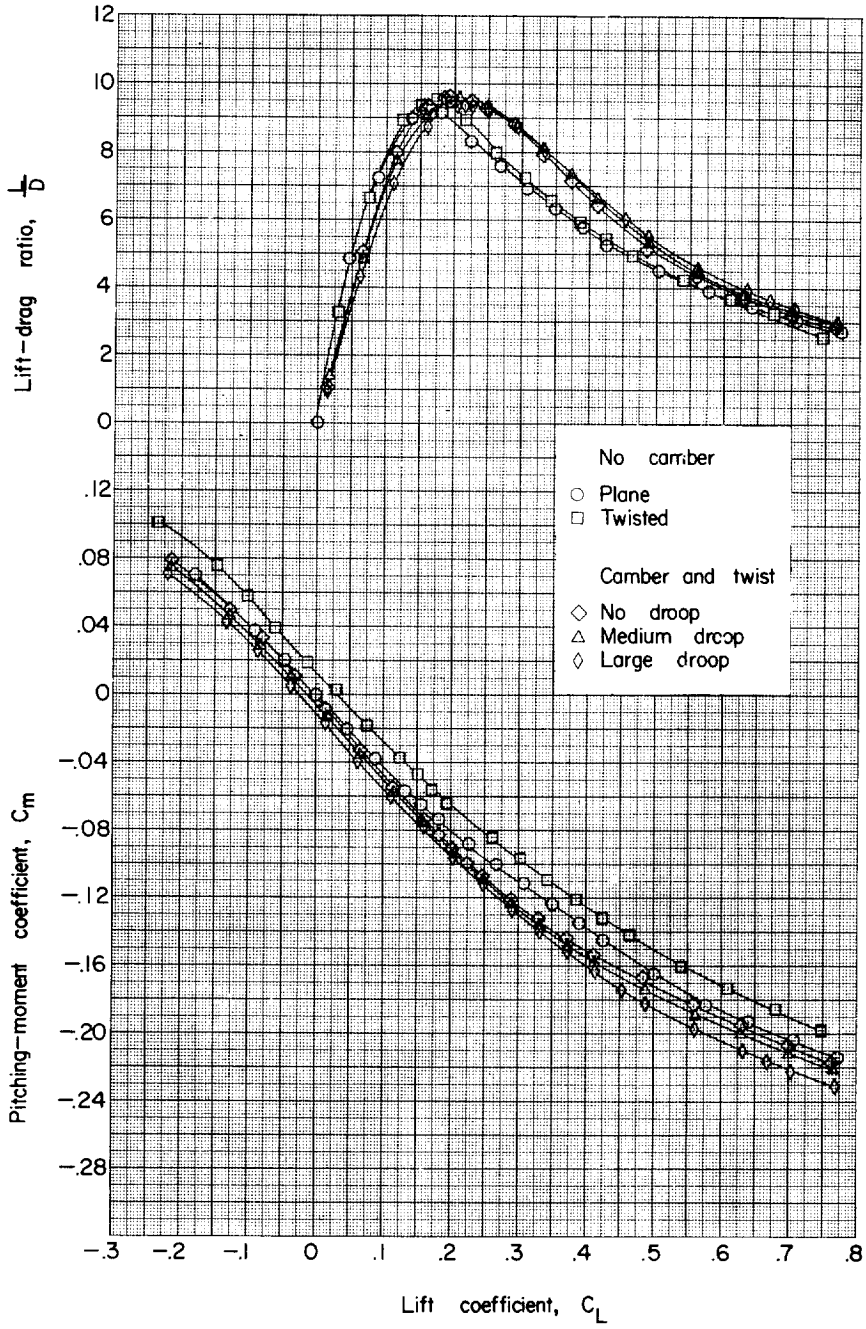

(h) Pitching-moment coefficient and lift-drag ratio. Body 4.

Figure 4.- Continued.

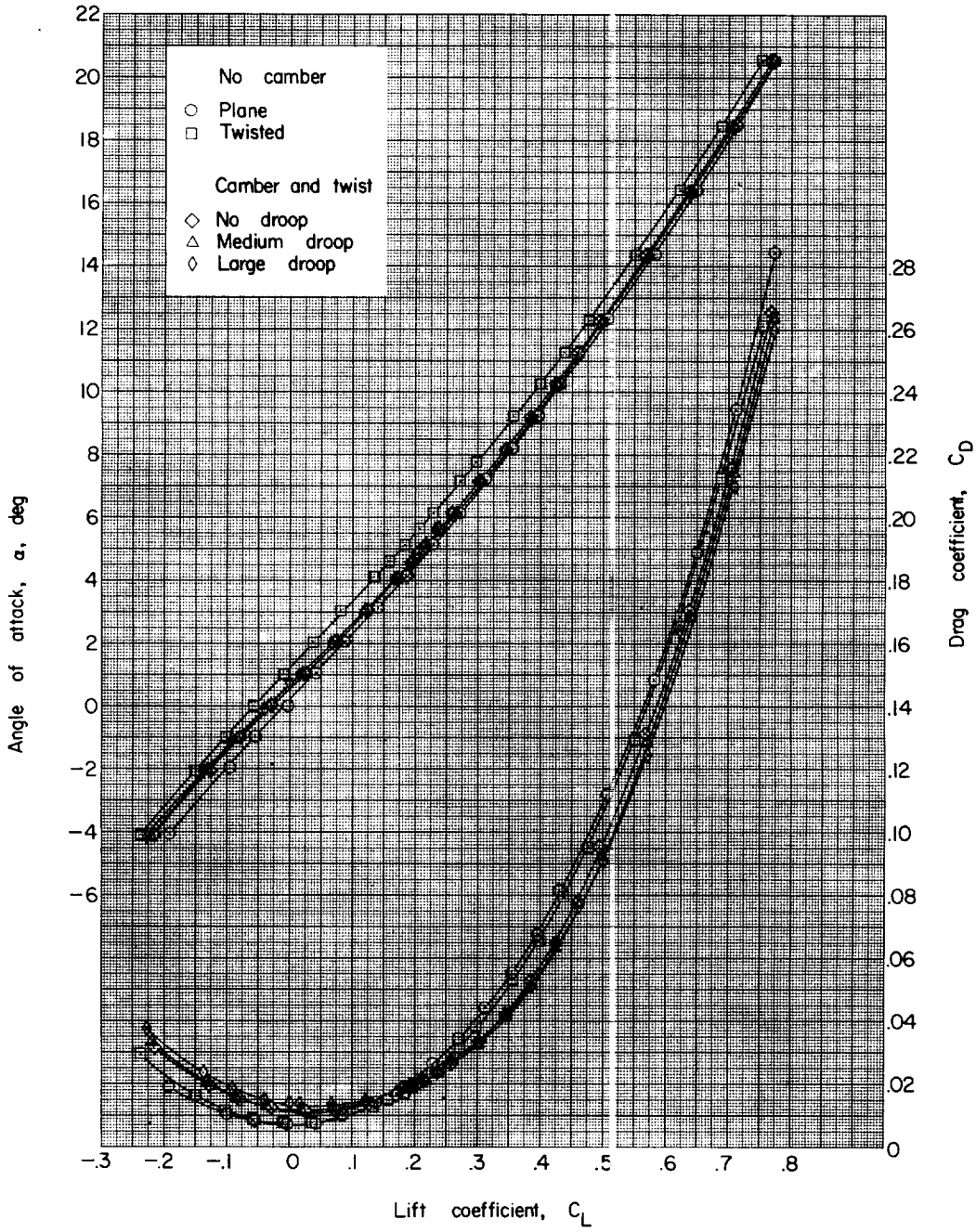

(i) Angle of attack and drag coefficient. Body 5.

Figure 4.- Continued.

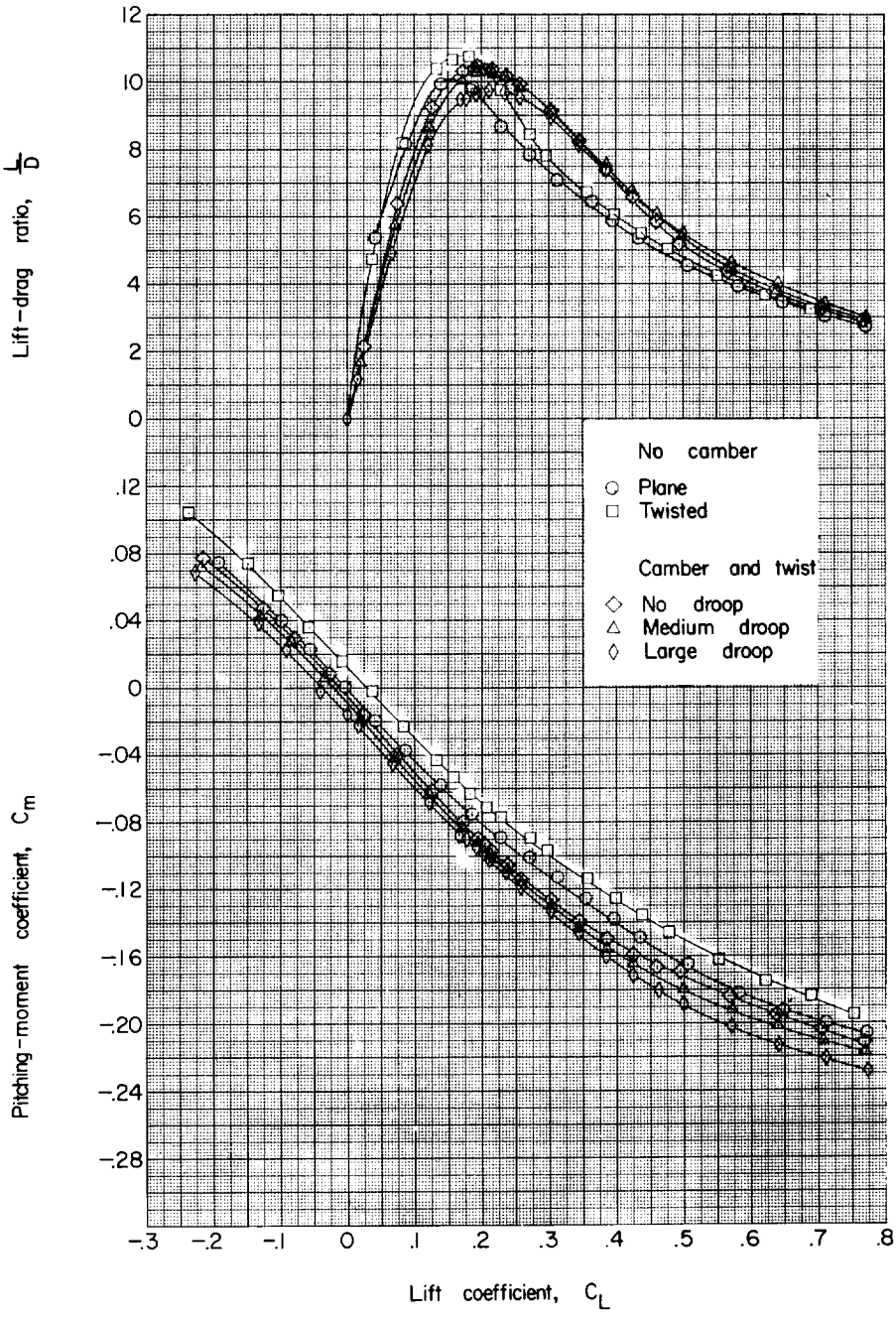

(j) Pitching-moment coefficient and lift-drag ratio. Body 5.

Figure 4.- Continued.

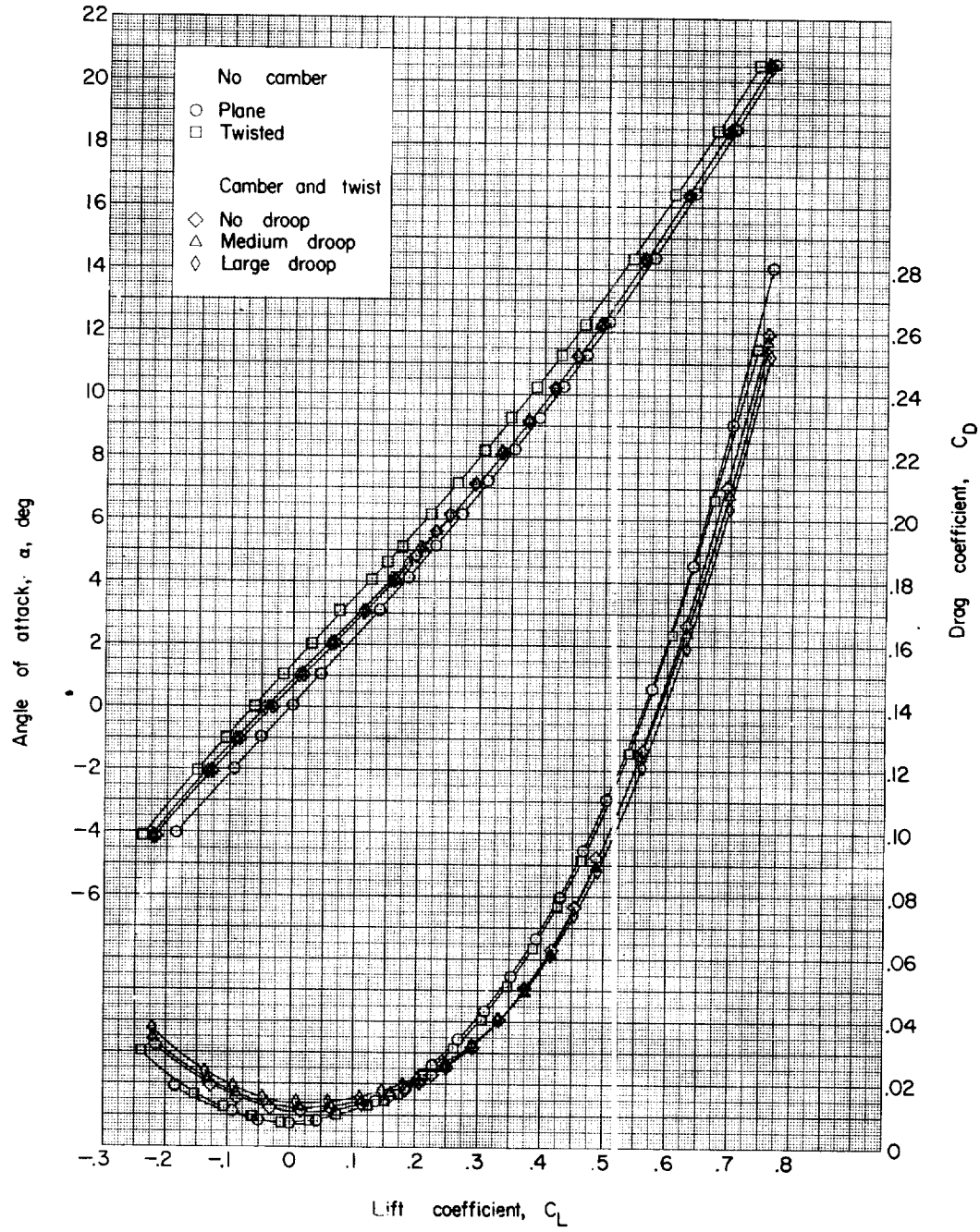

(k) Angle of attack and drag coefficient. Body 6.

Figure 4.- Continued.

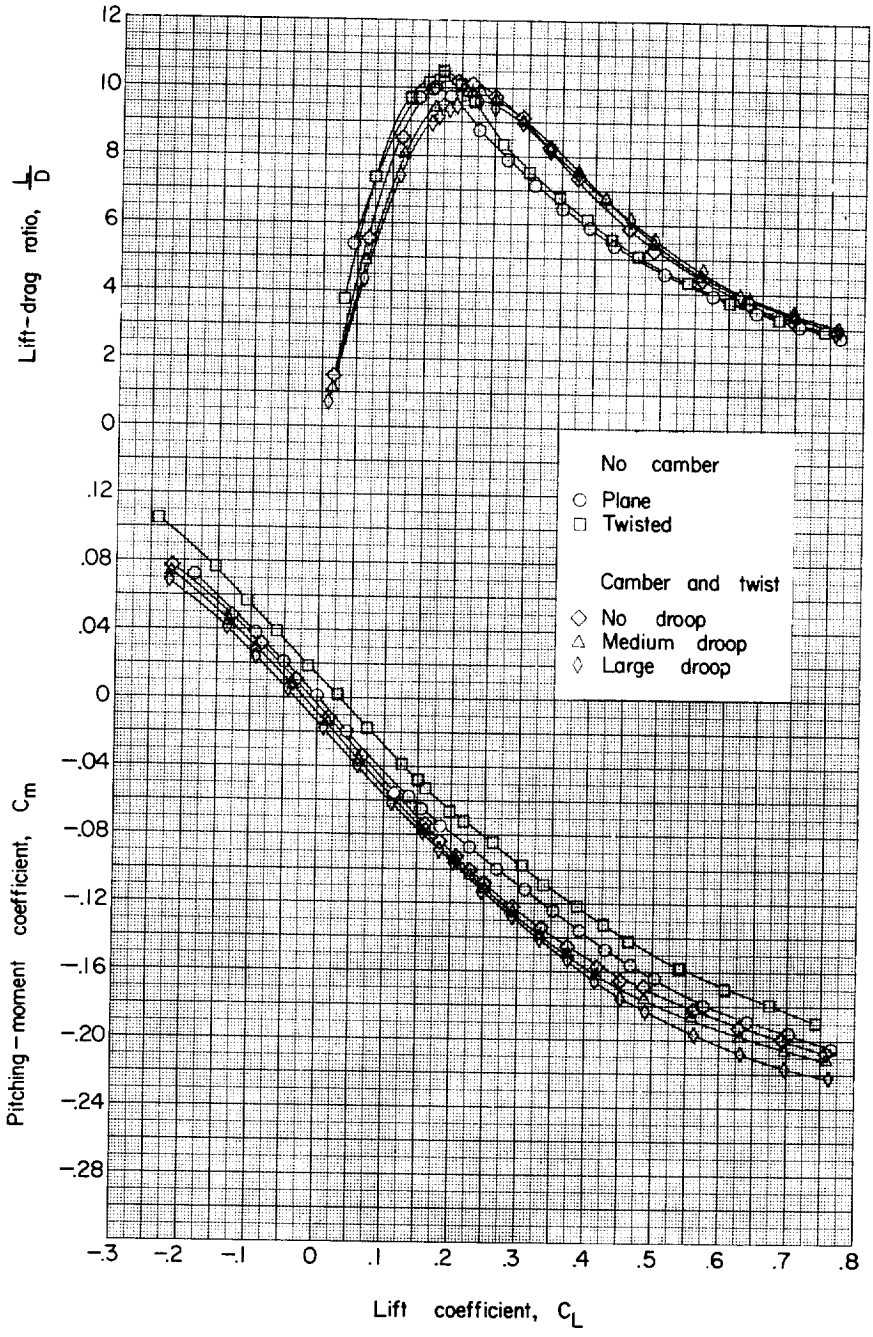

(l) Pitching-moment coefficient and lift-drag ratio. Body 6.

Figure 4.- Concluded.

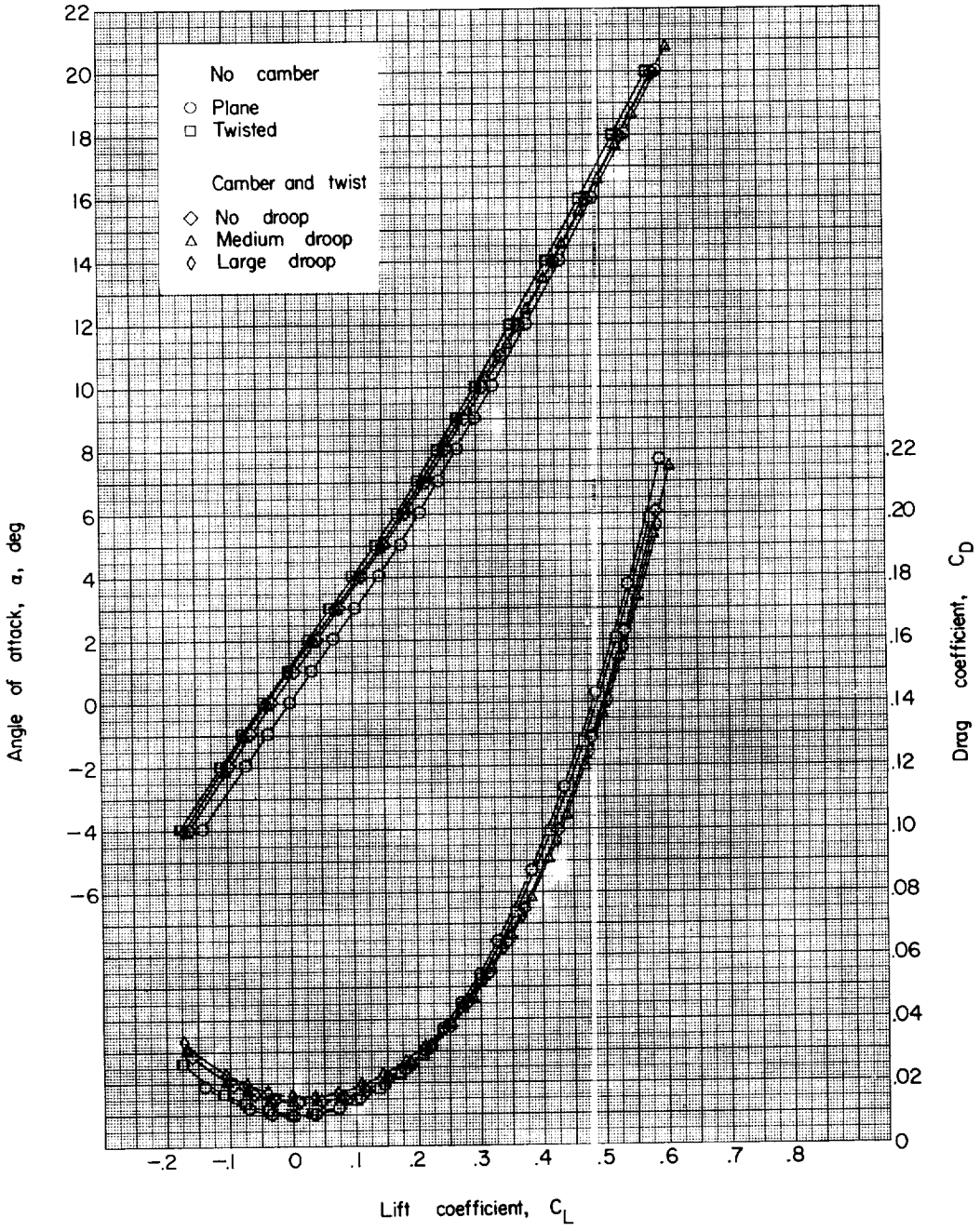

(a) Angle of attack and drag coefficient. Body 1.

Figure 5.- Variation of aerodynamic parameters with lift coefficient. M = 2.01; q ≈ 510 lb/sq ft abs; natural transition.

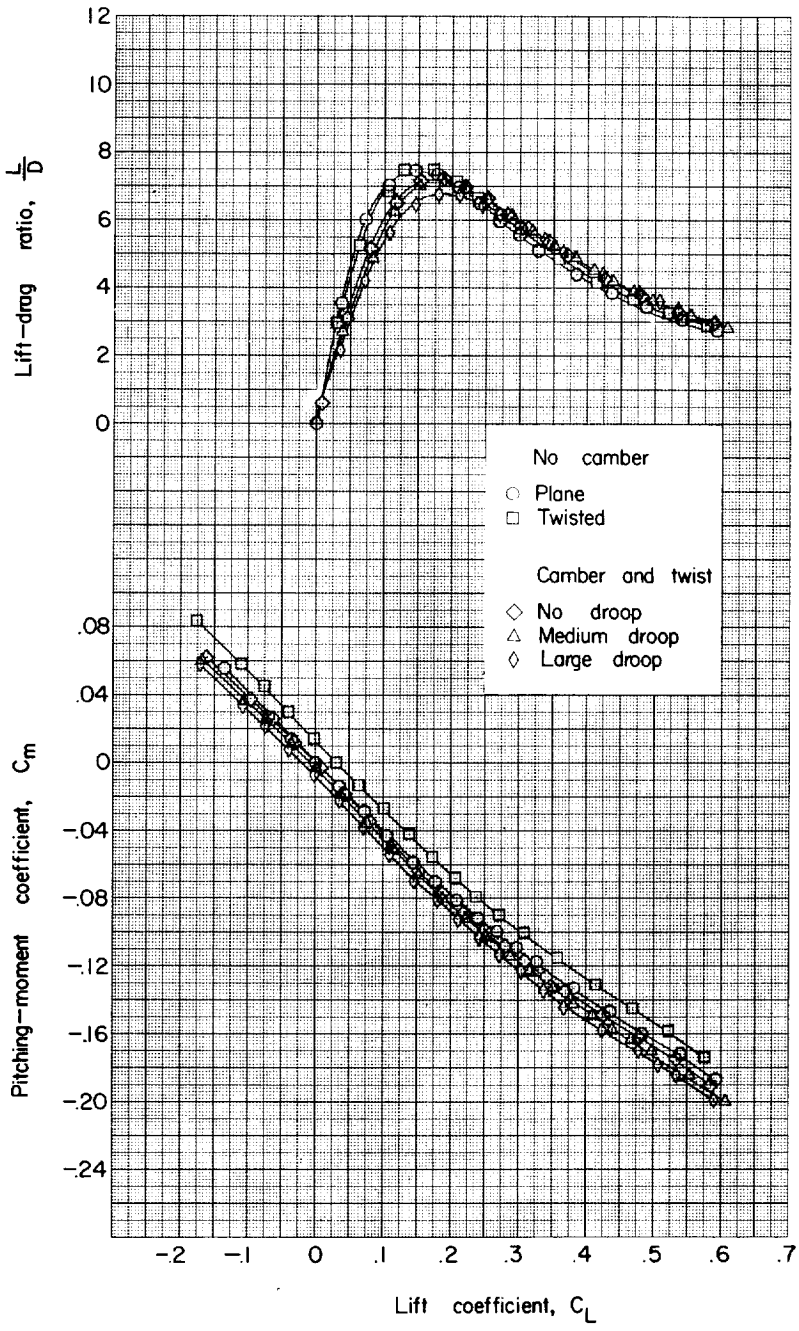

(b) Pitching-moment coefficient and lift-drag ratio. Body 1.

Figure 5.- Continued.

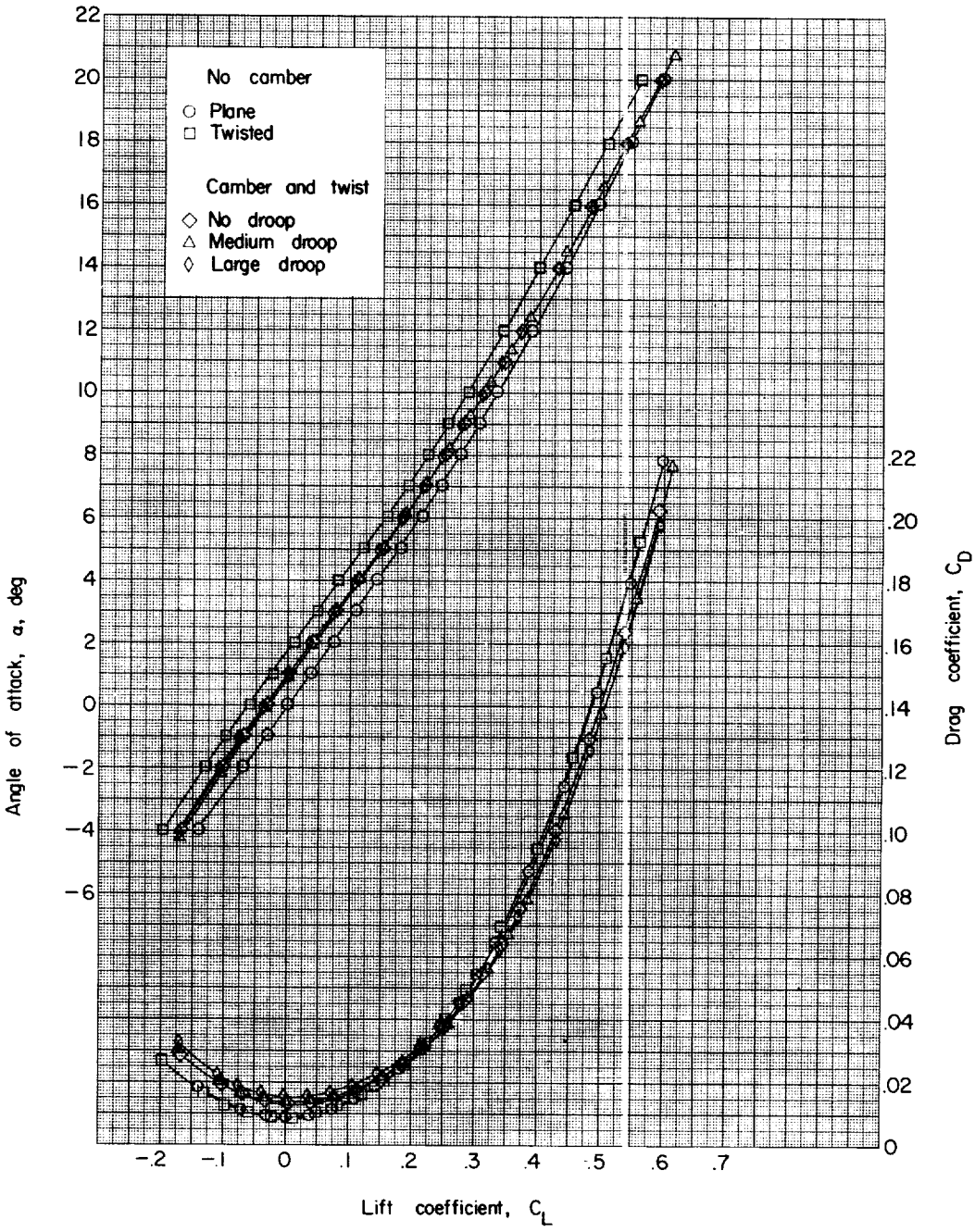

(c) Angle of attack and drag coefficient. Body 2.

Figure 5.- Continued.

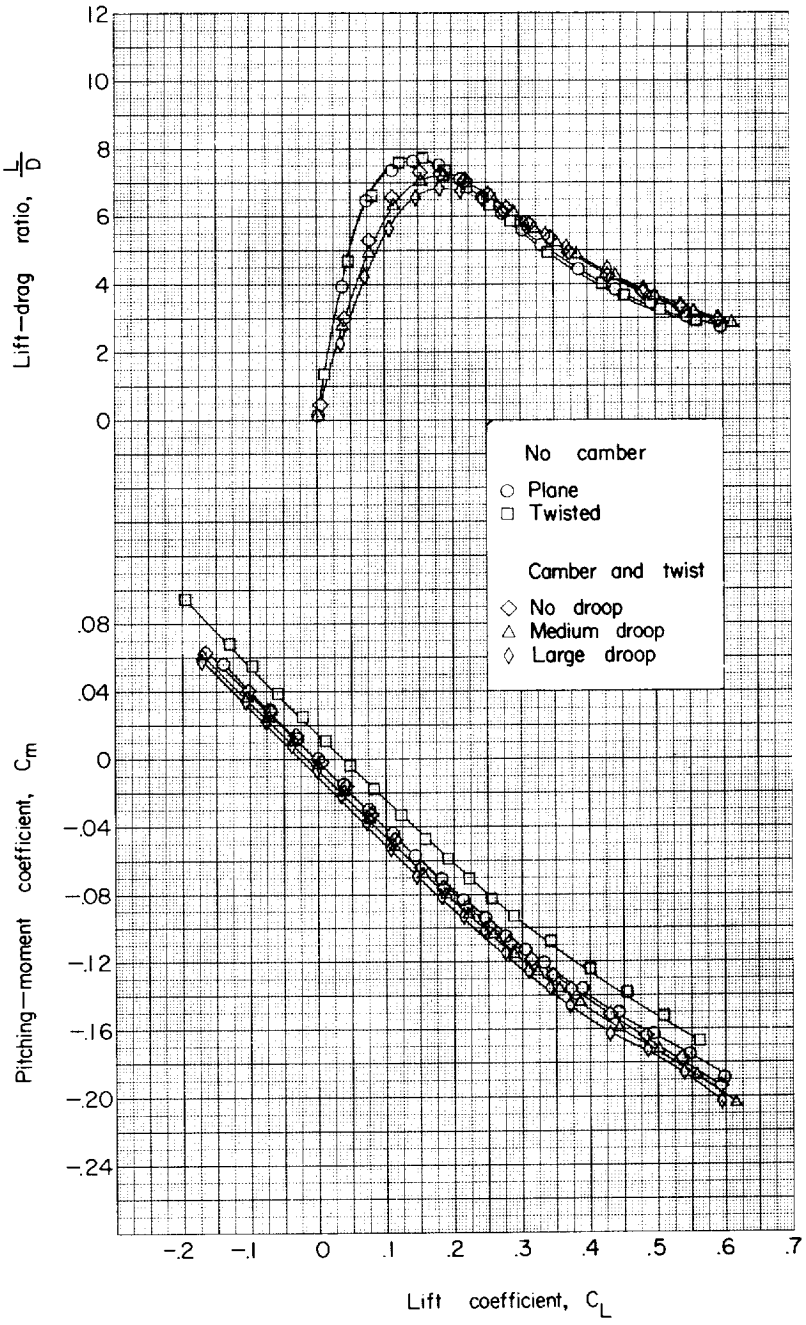

(d) Pitching-moment coefficient and lift-drag ratio. Body 2.

Figure 5.- Continued.

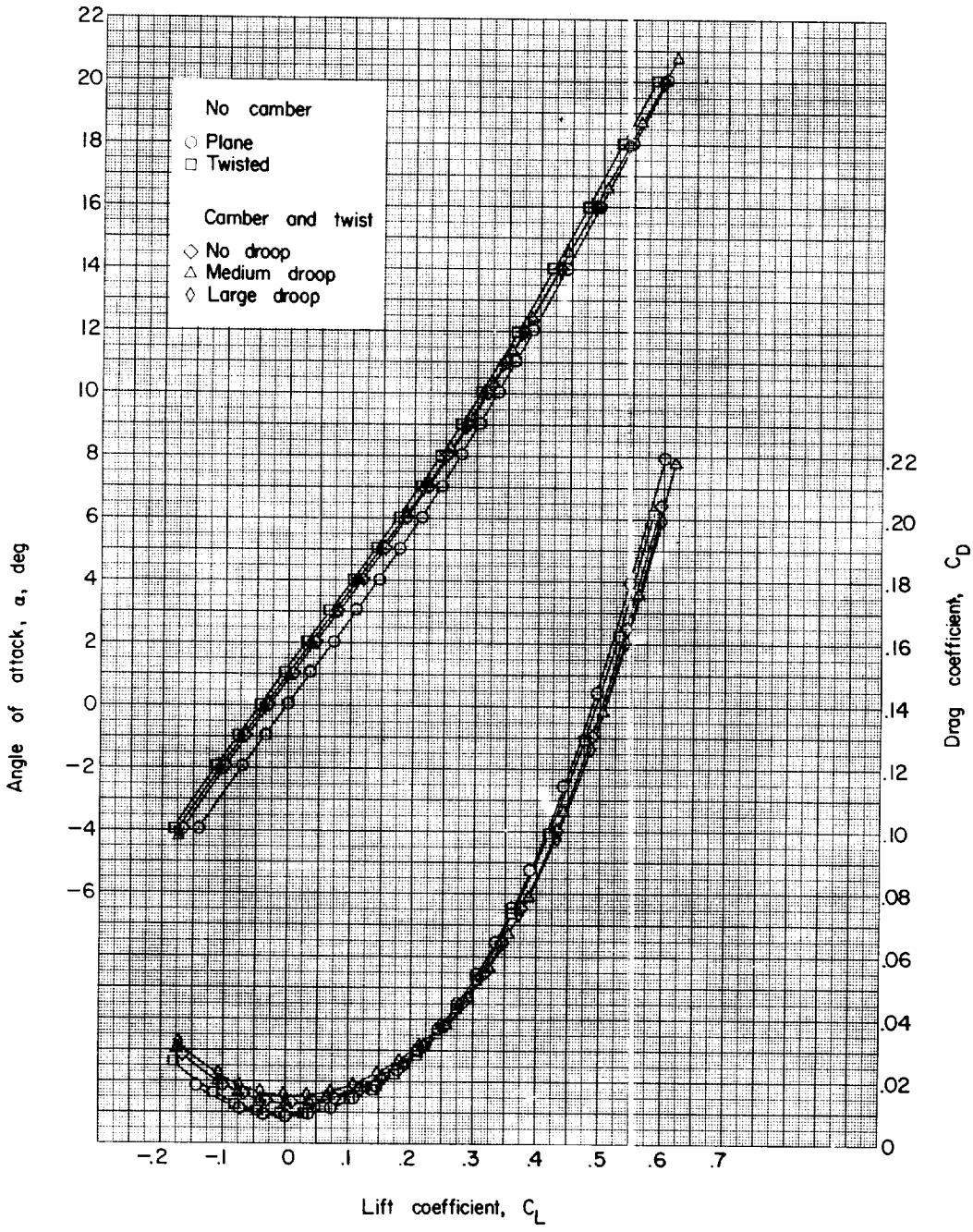

(e) Angle of attack and drag coefficient. Body 3.

Figure 5.- Continued.

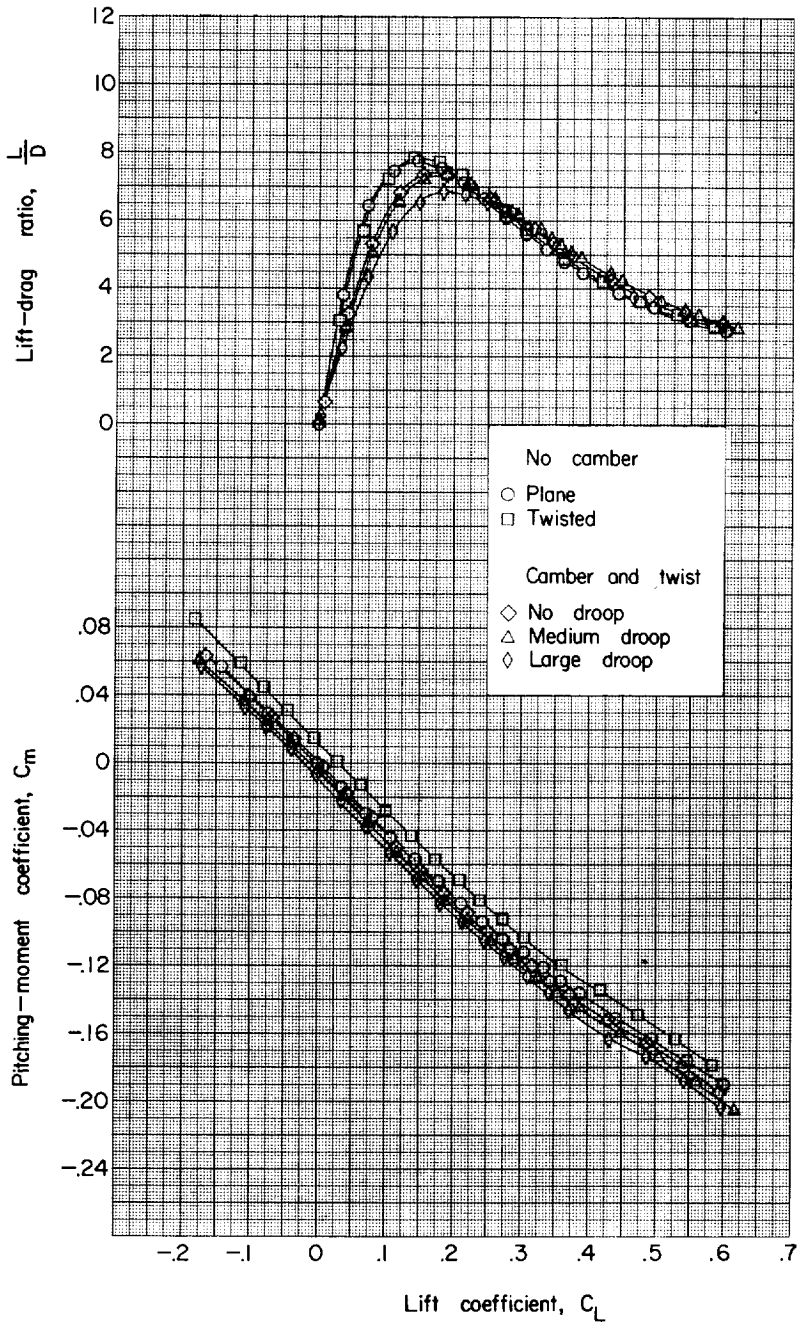

(f) Pitching-moment coefficient and lift-drag ratio. Body 3.

Figure 5.- Continued.

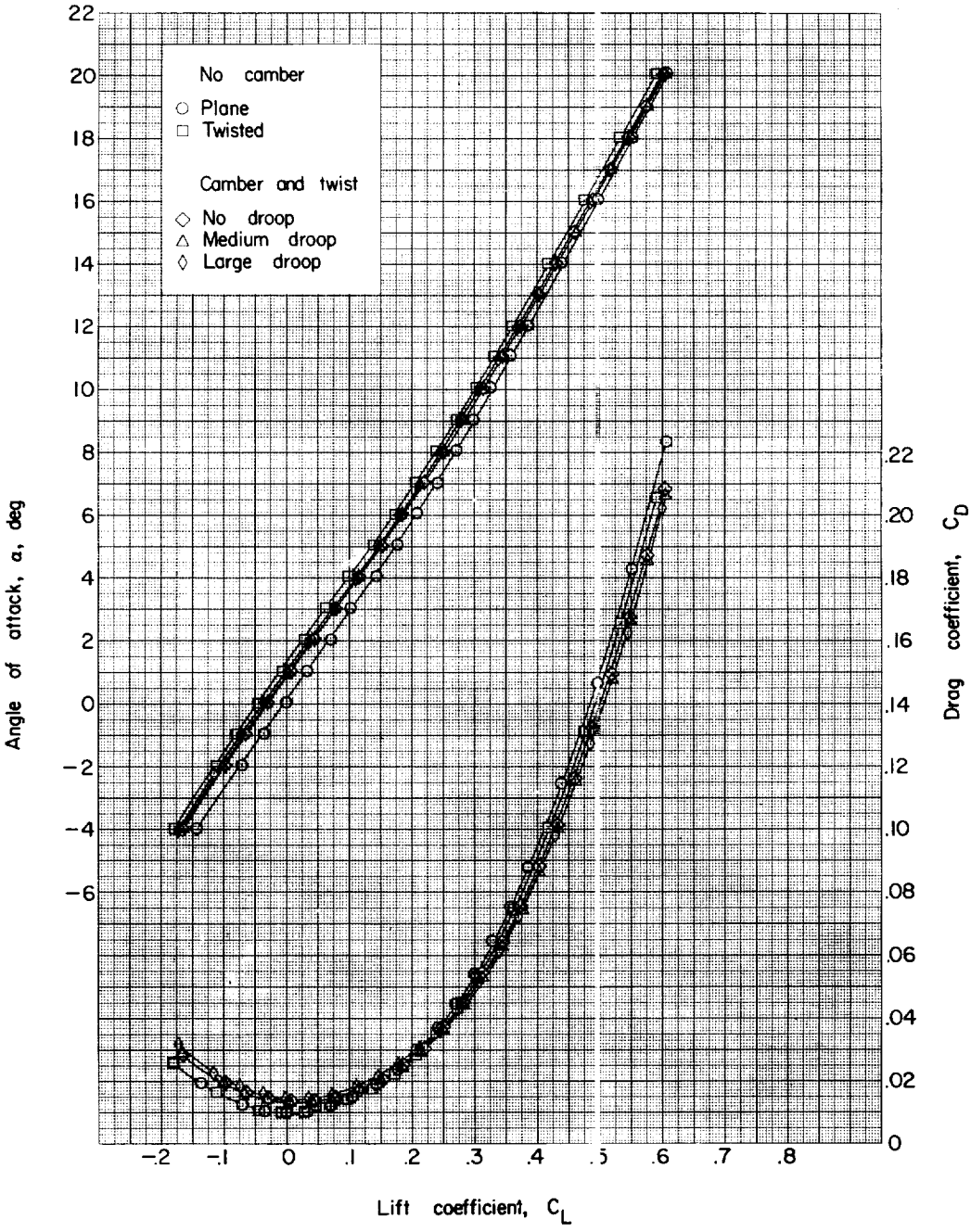

(g) Angle of attack and drag coefficient. Body 4.

Figure 5.- Continued.

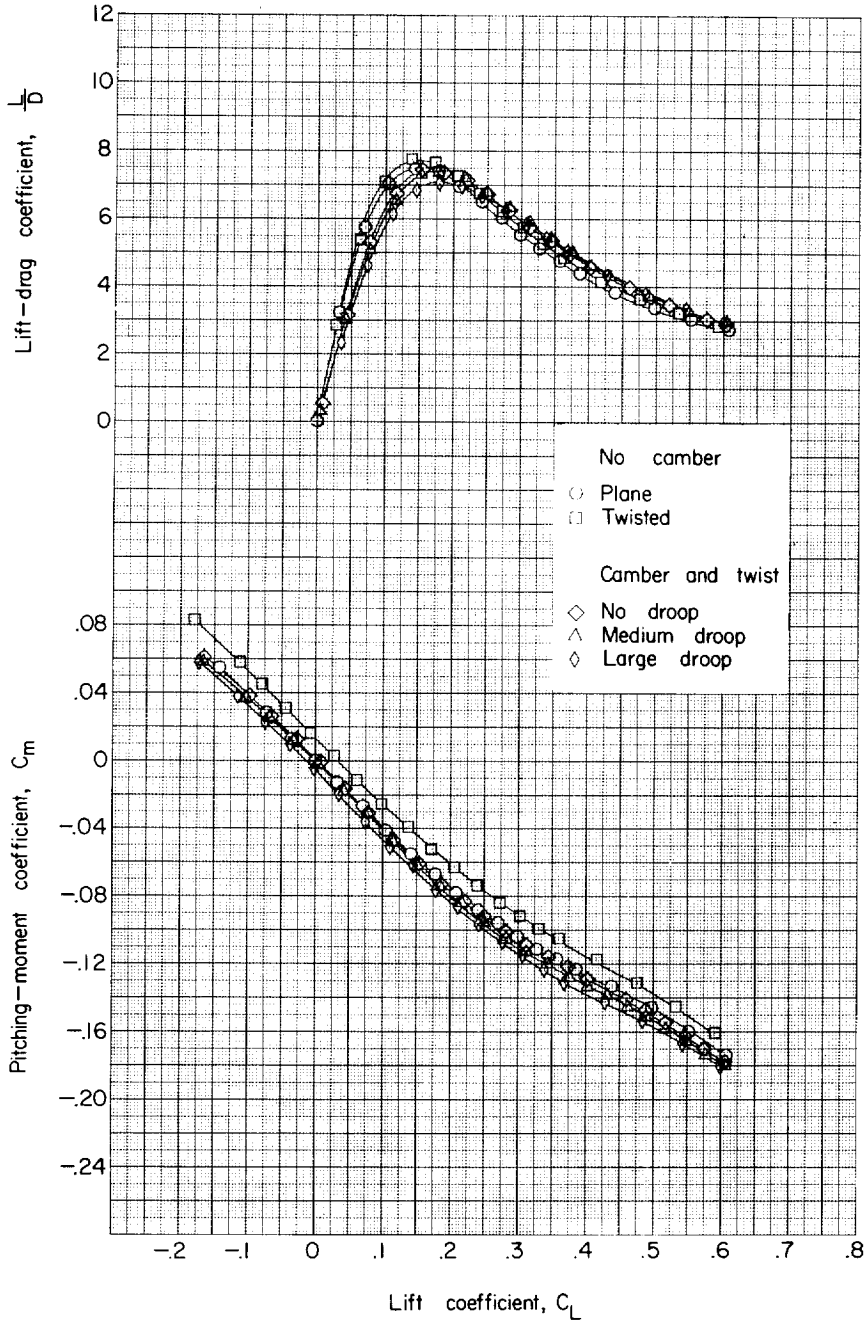

(h) Pitching-moment coefficient and lift-drag ratio. Body 4.

Figure 5.- Continued.

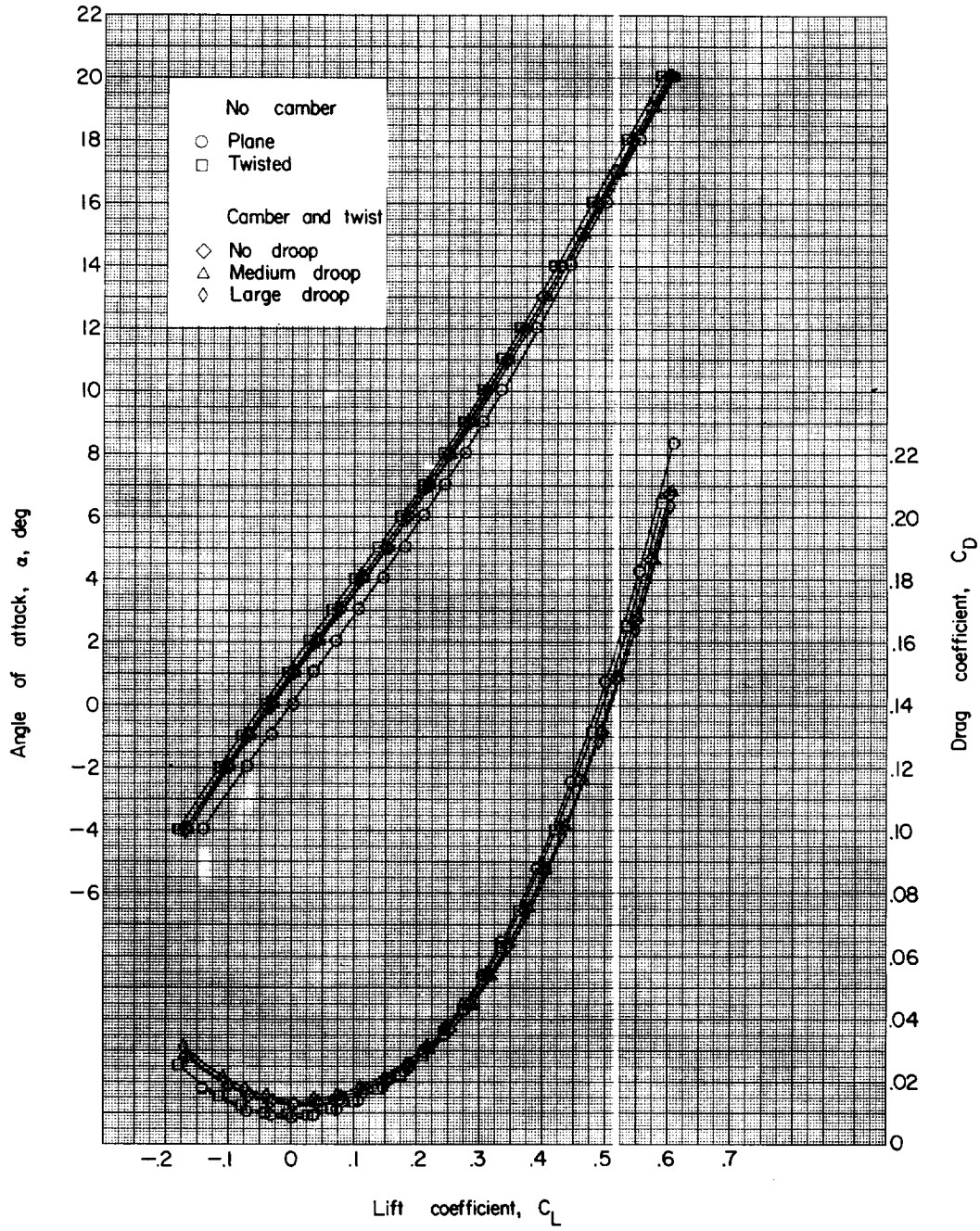

(i) Angle of attack and drag coefficient. Body 5.

Figure 5.- Continued.

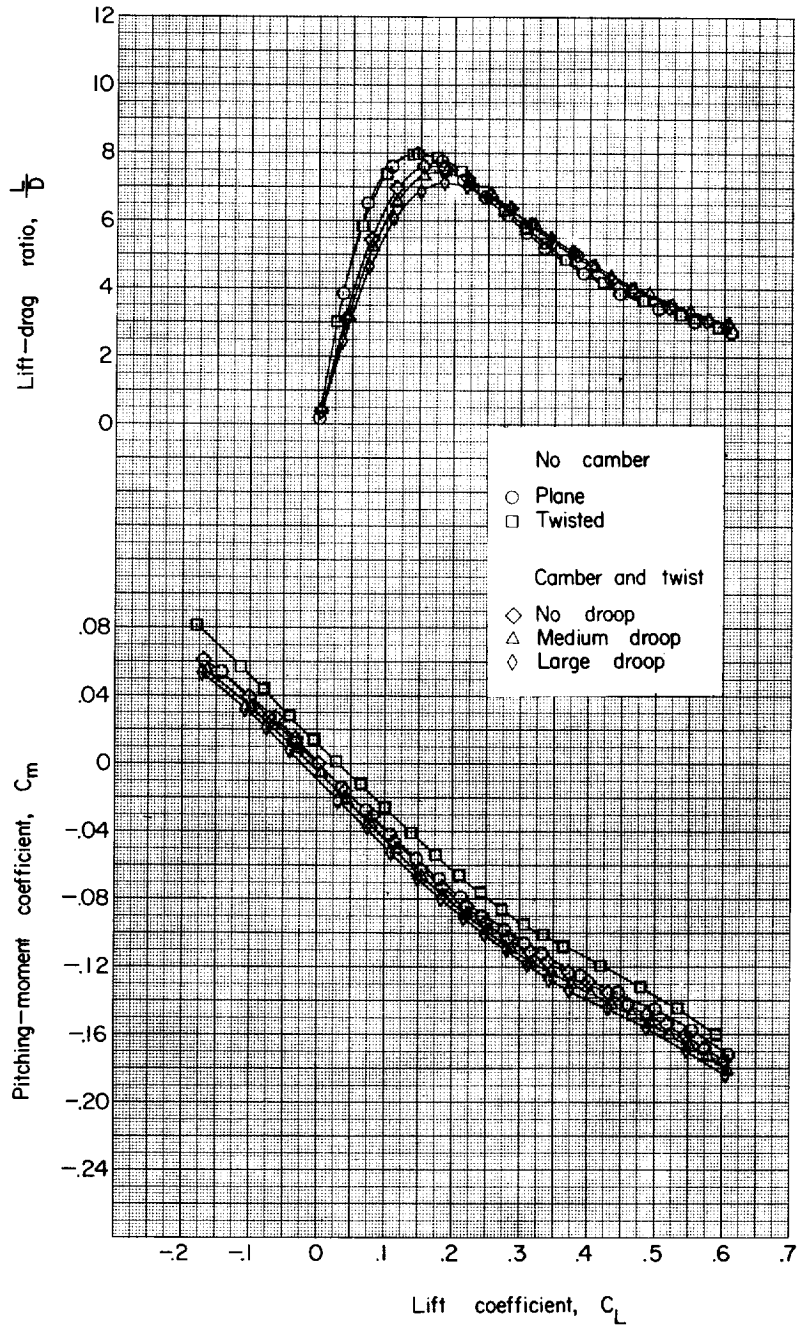

(j) Pitching-moment coefficient and lift-drag ratio. Body 5.

Figure 5.- Continued.

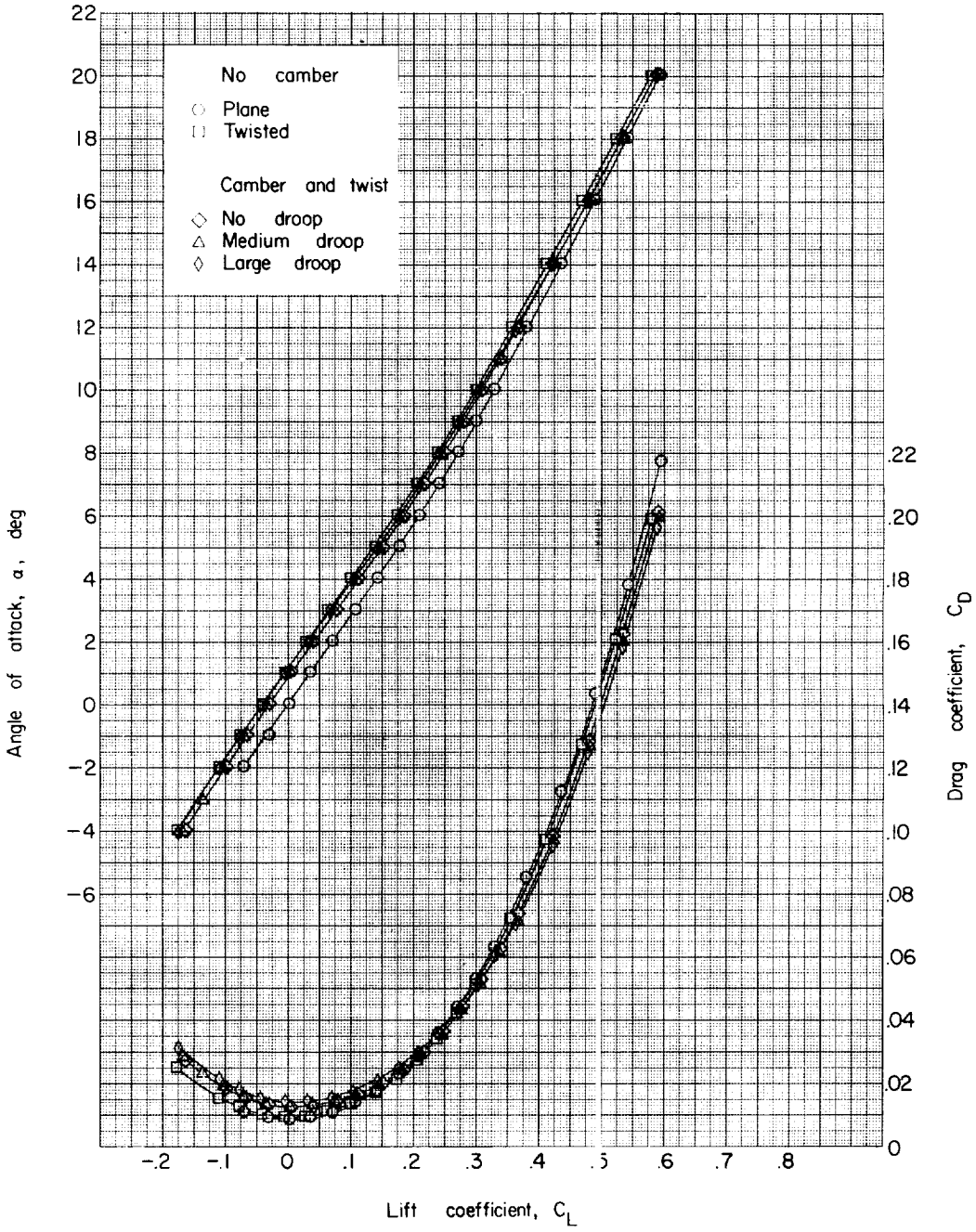

(k) Angle of attack and drag coefficient. Body 6.

Figure 5.- Continued.

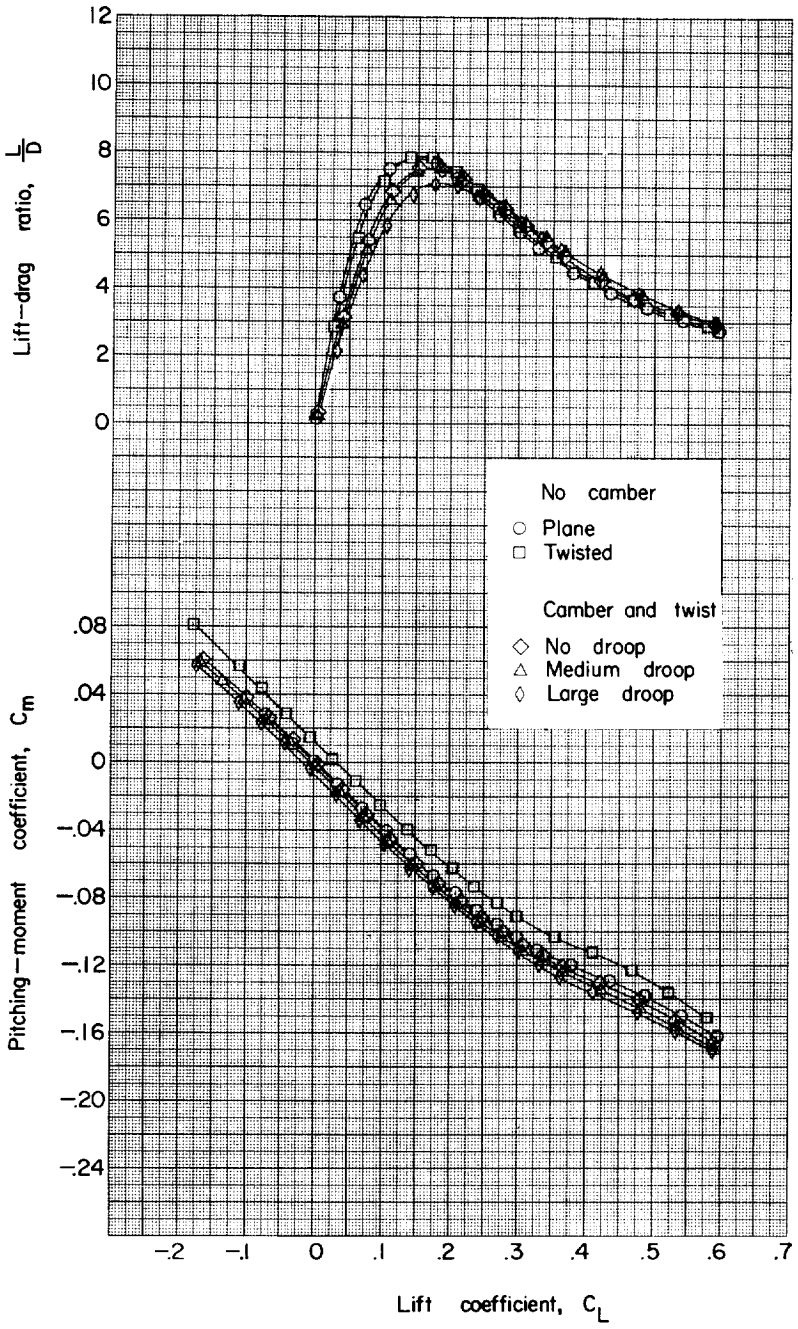

(l) Pitching-moment coefficient and lift-drag ratio. Body 6.

Figure 5.- Concluded.

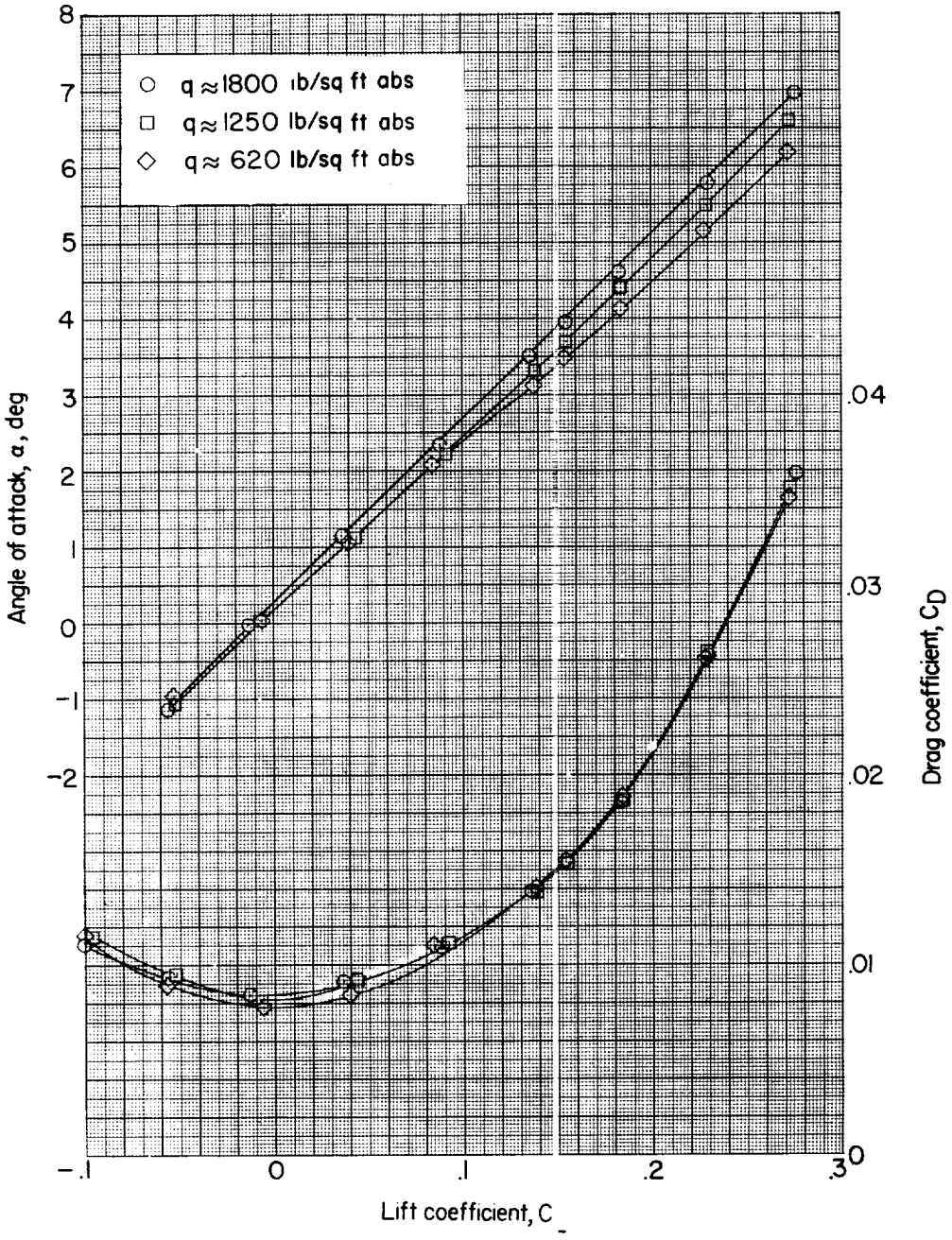

(a) Angle of attack and drag coefficient.

Figure 6.- Variation of aerodynamic parameters with lift coefficient for various dynamic pressures. Body 5 - wing 1 configuration; M = 1.41; natural transition.

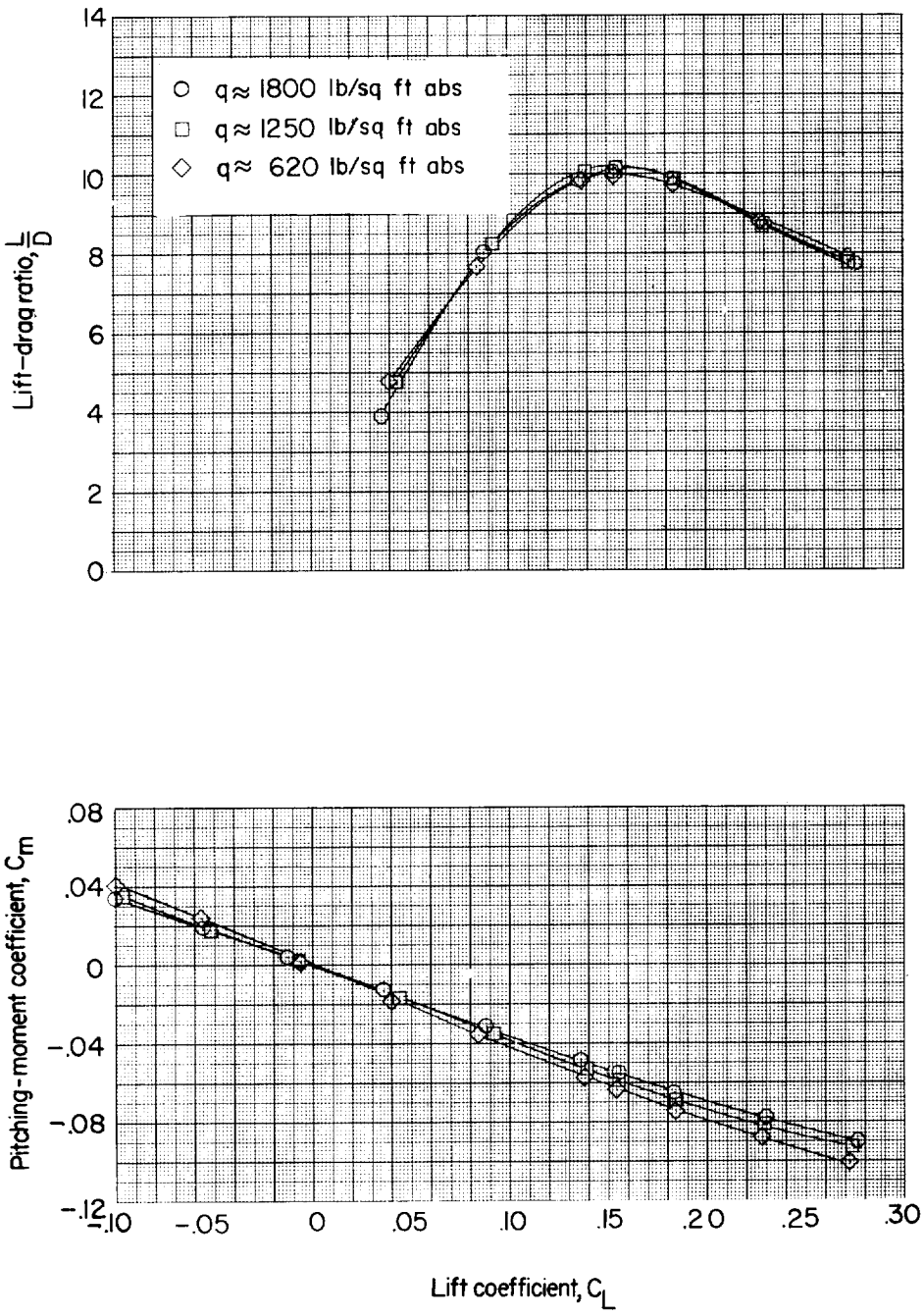

(b) Pitching-moment coefficient and lift-drag ratio.

Figure 6.- Concluded.

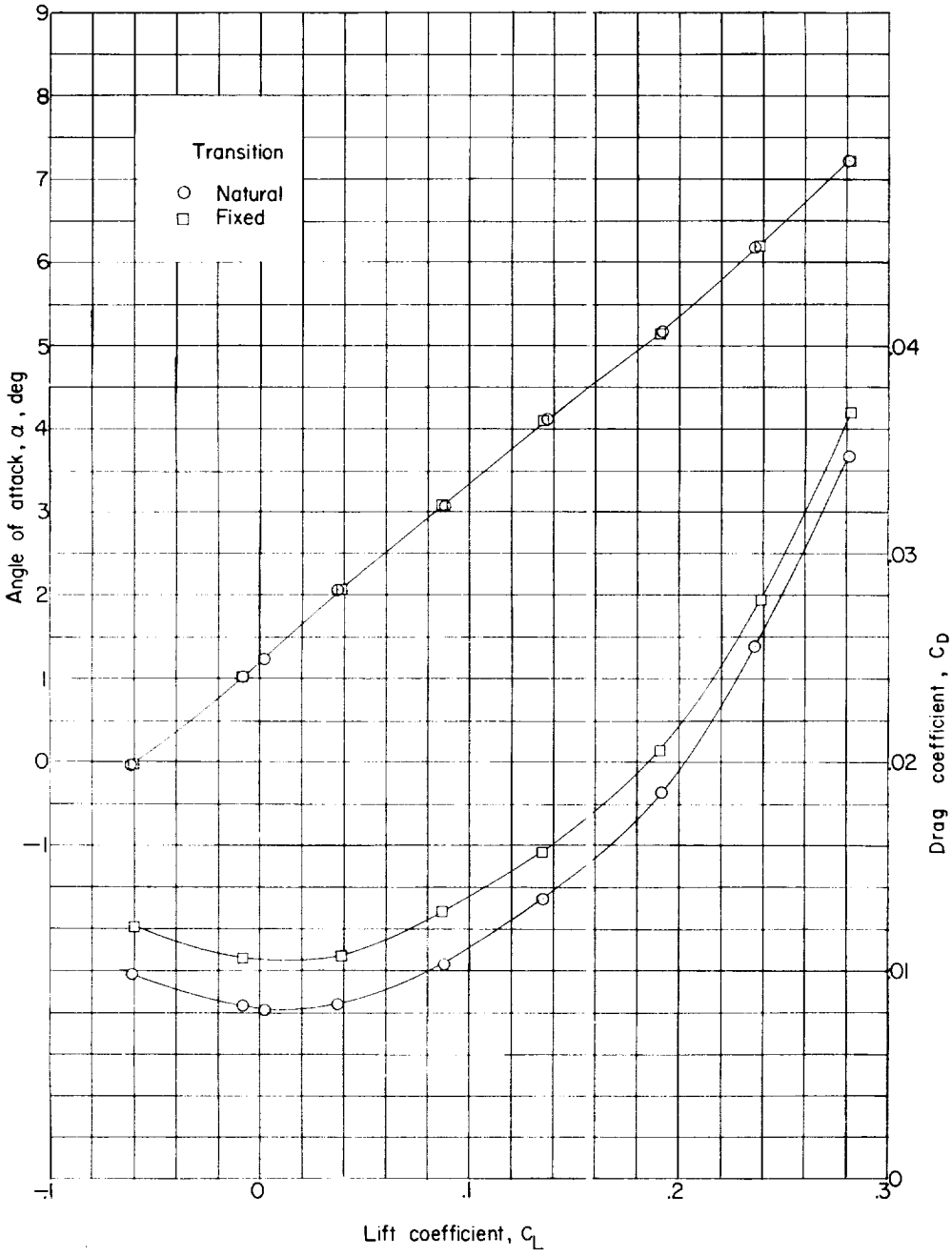

(a) $q \approx 315$ lb/sq ft abs.

Figure 7.- Effect of fixing transition on the body 5 - wing 2 configuration at $M = 1.41$ and at various values of dynamic pressure.

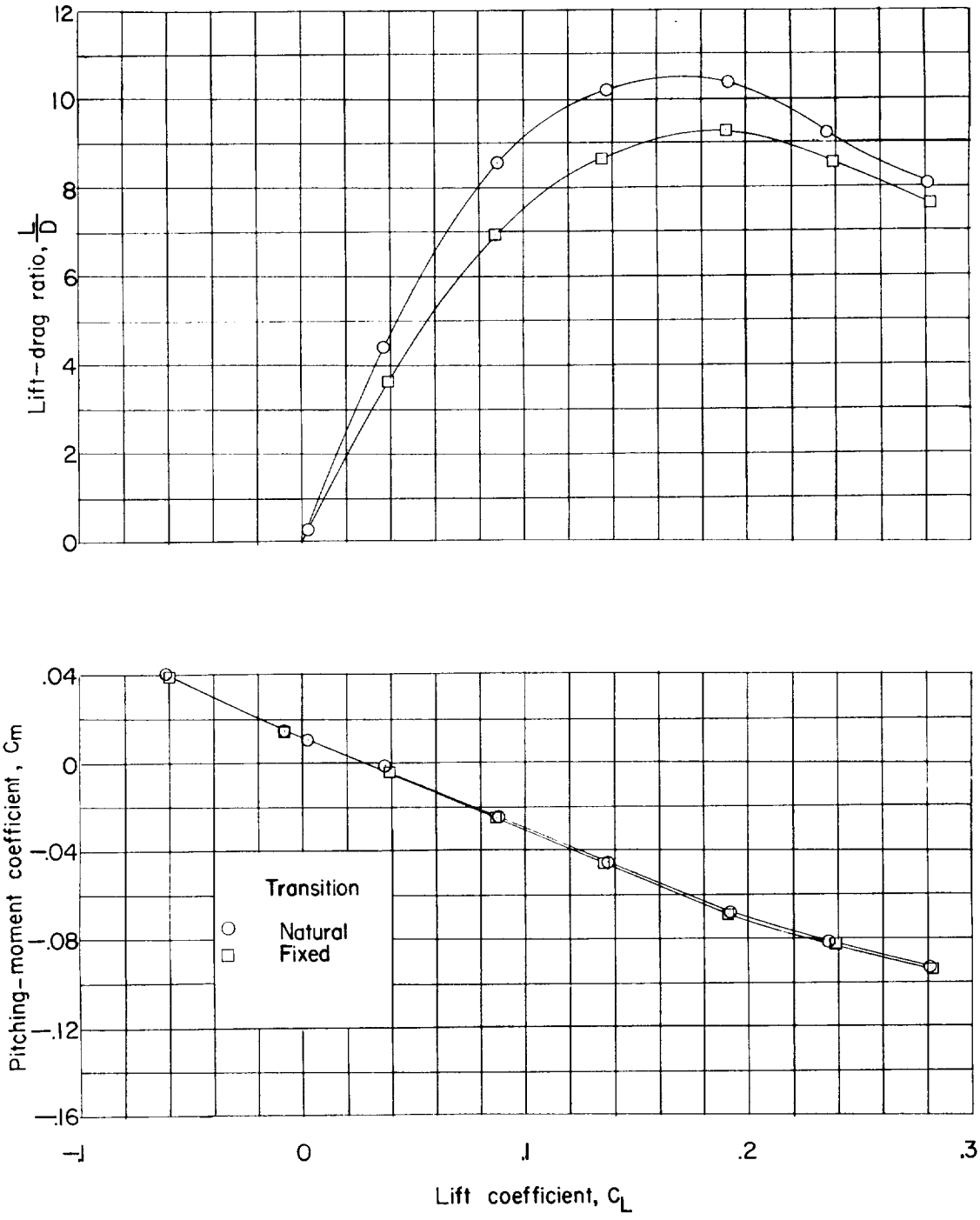

(a) $q \approx 315$ lb/sq ft abs. Concluded.

Figure 7.- Continued.

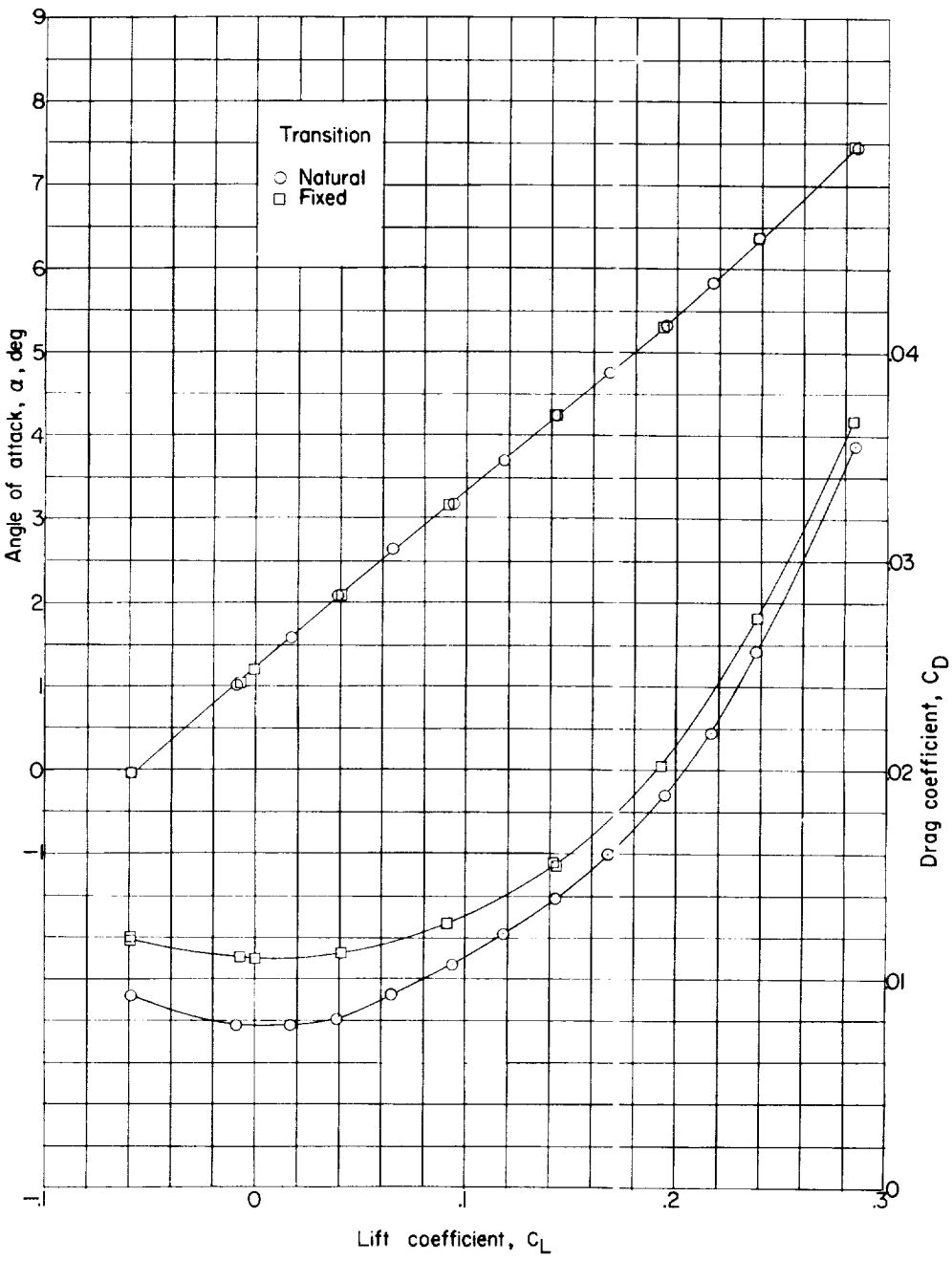

(b) $q \approx 623$ lb/sq ft abs.

Figure 7.- Continued.

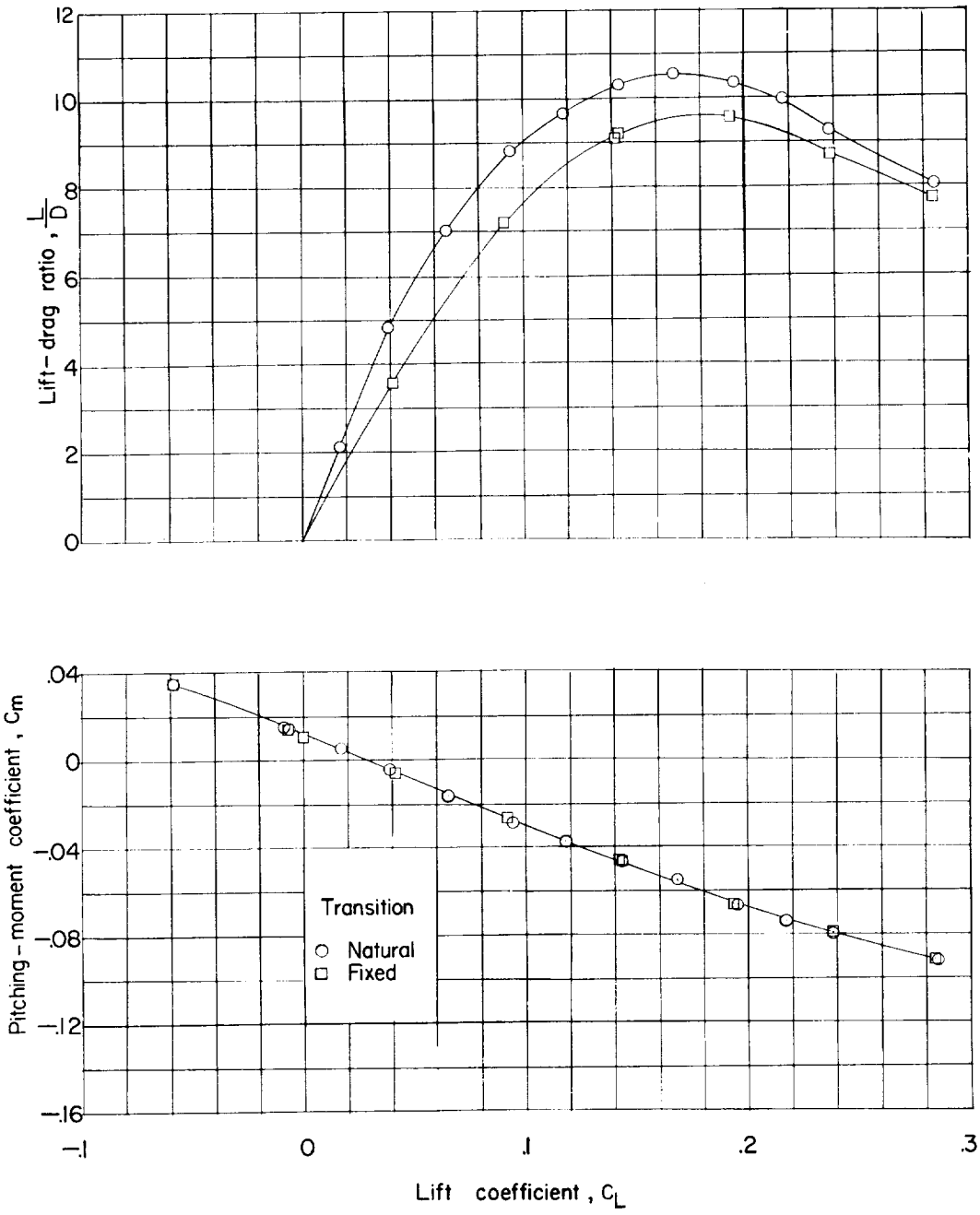

(b) $q \approx 623$ lb/sq ft abs. Concluded.

Figure 7.- Continued.

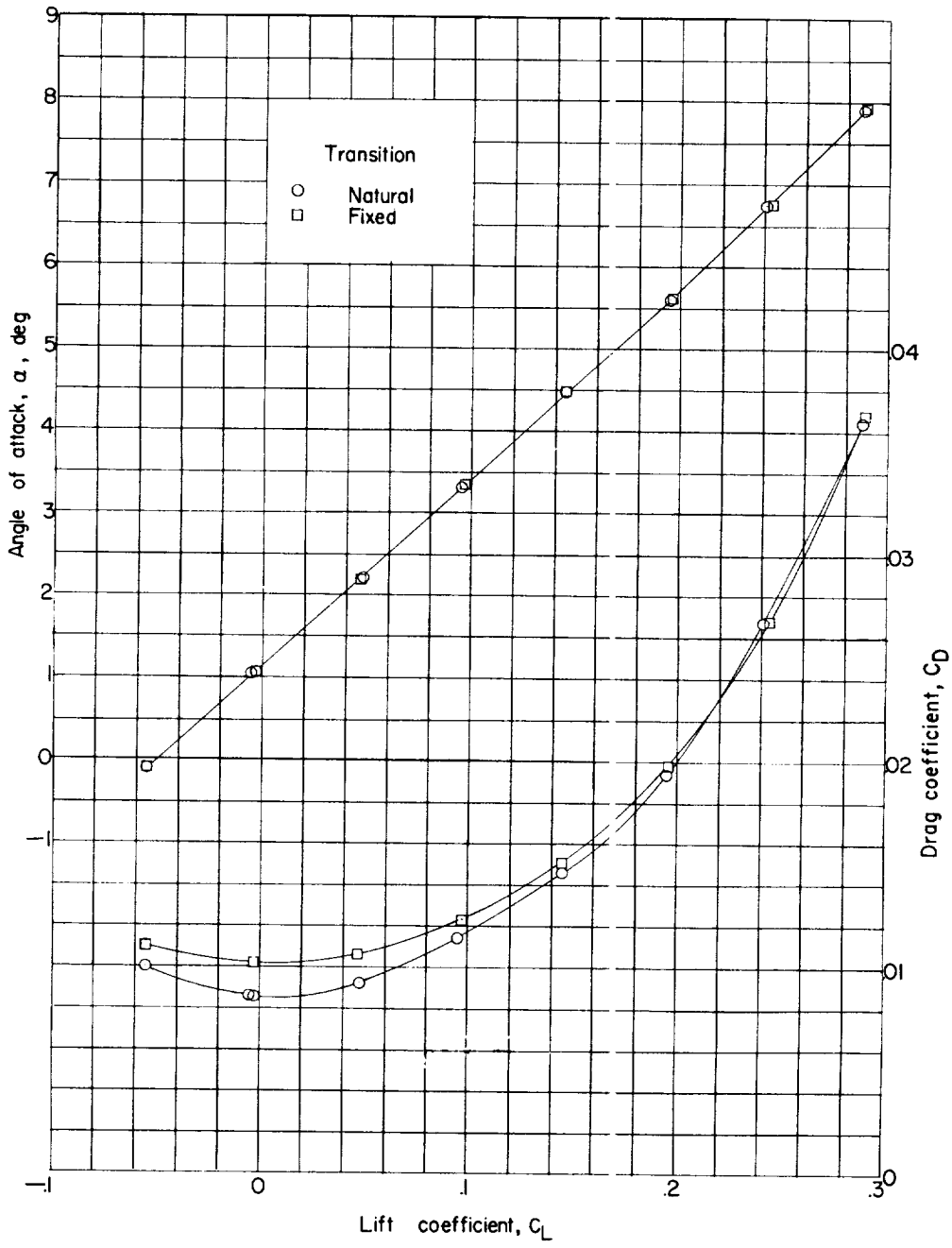

(c) $q \approx 1{,}245$ lb/sq ft abs.

Figure 7.- Continued.

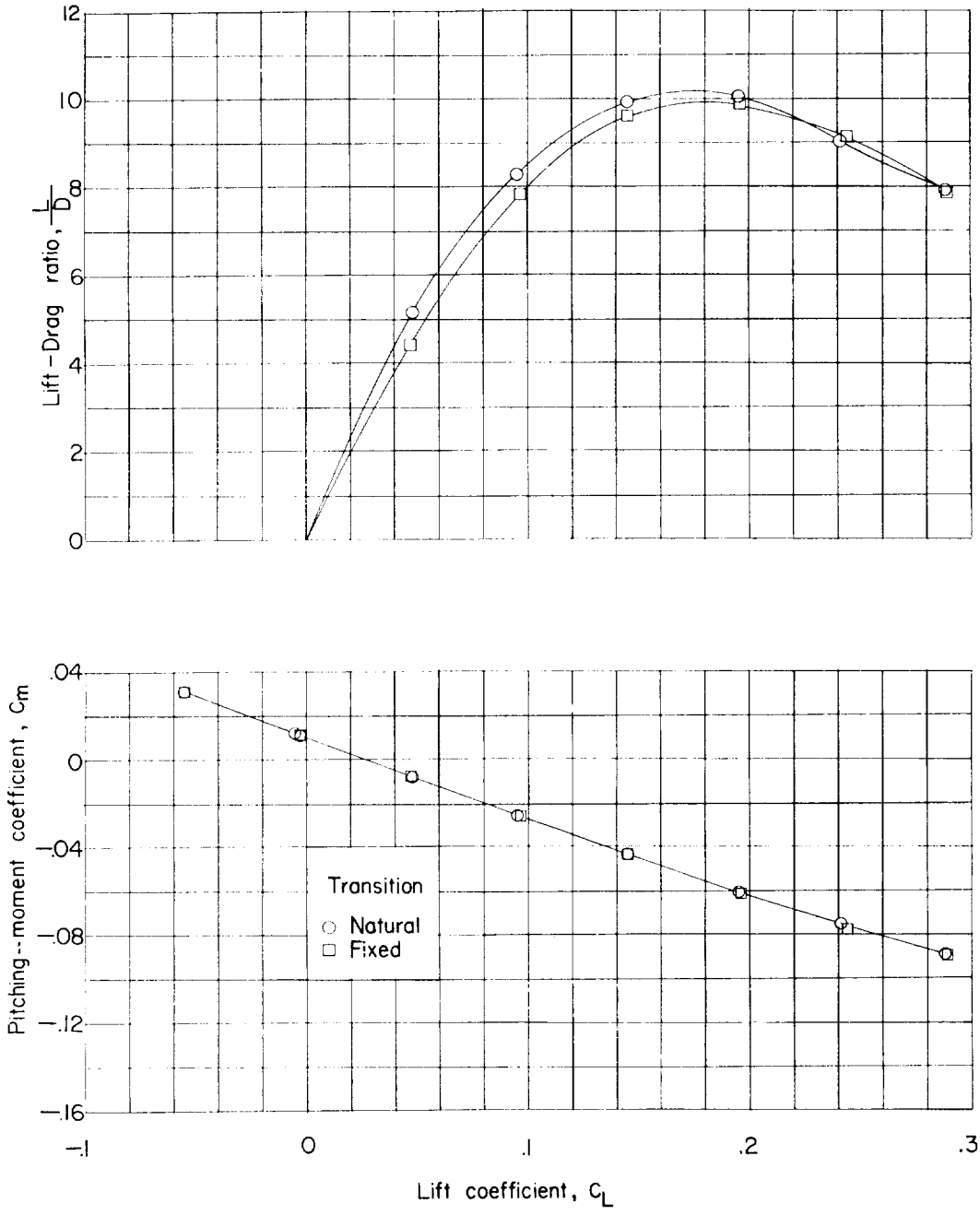

(c) $q \approx 1{,}245$ lb/sq ft abs. Concluded.

Figure 7.- Continued.

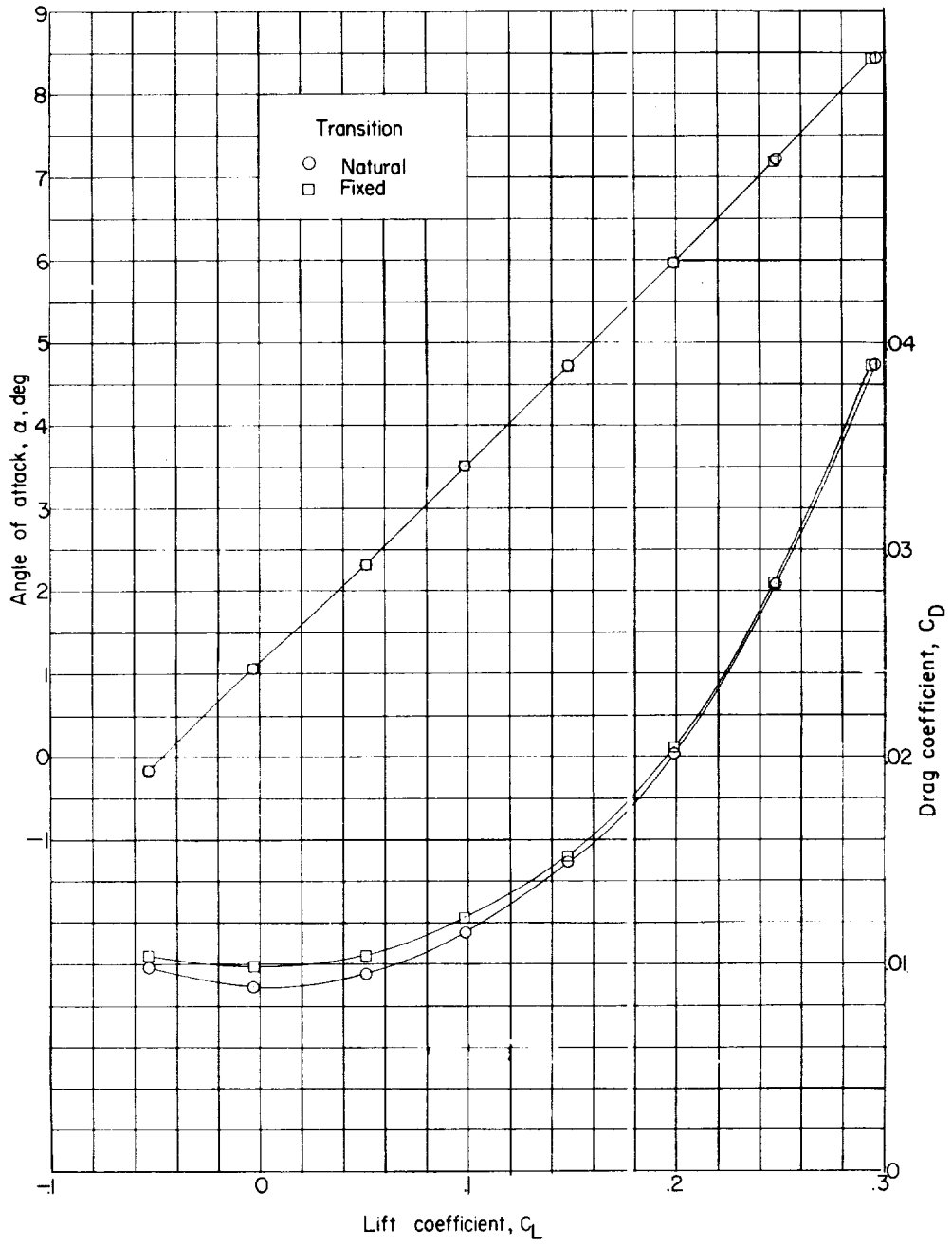

(d) $q \approx 1{,}860$ lb/sq ft abs.

Figure 7.- Continued.

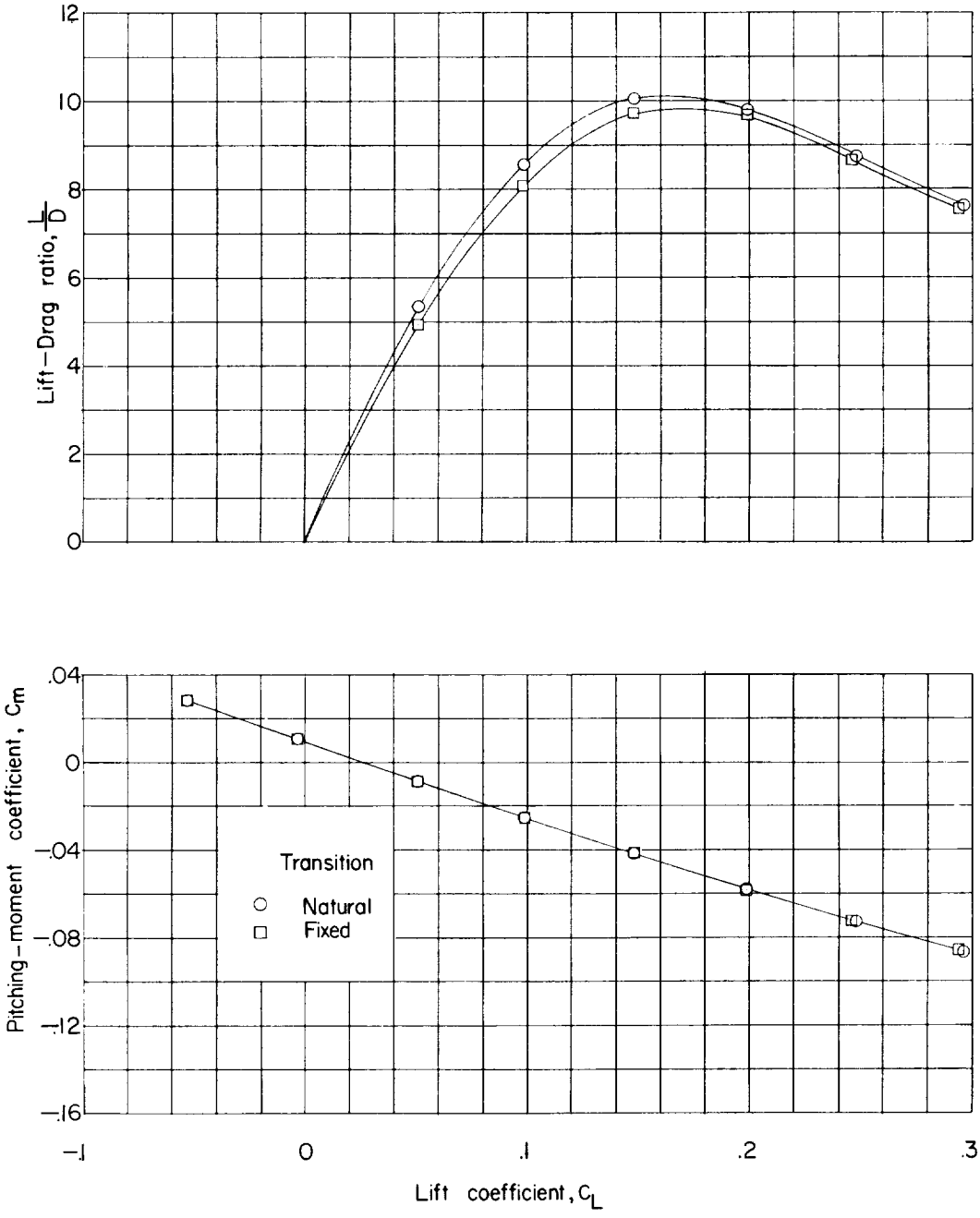

(d) $q \approx 1{,}860$ lb/sq ft abs. Concluded.

Figure 7.- Concluded.

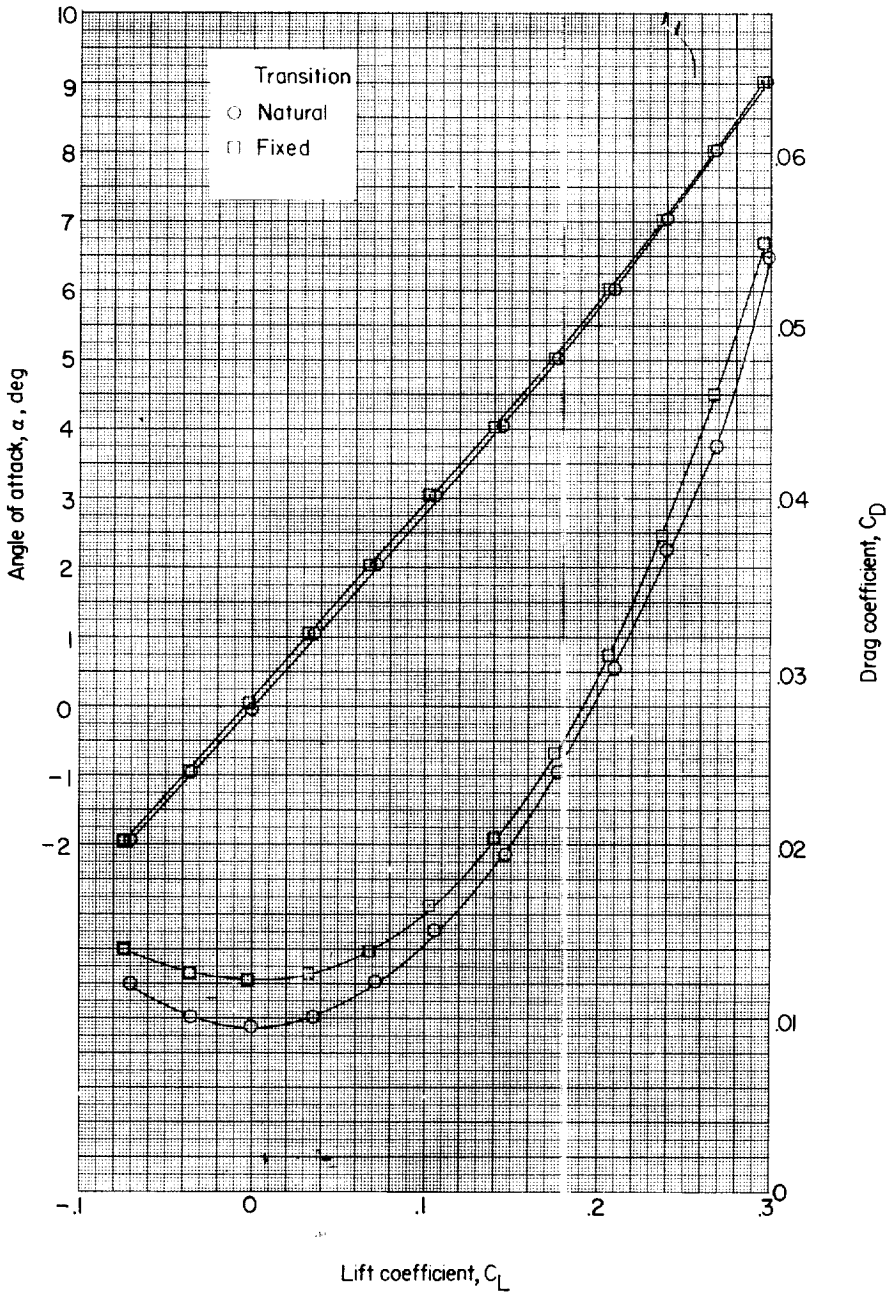

(a) Angle of attack and drag coefficient. Body 1.

Figure 8.- Variation of aerodynamic parameters with lift coefficient for fixed transition. Plane wing; M = 2.01; q ≈ 510 lb/sq ft abs.

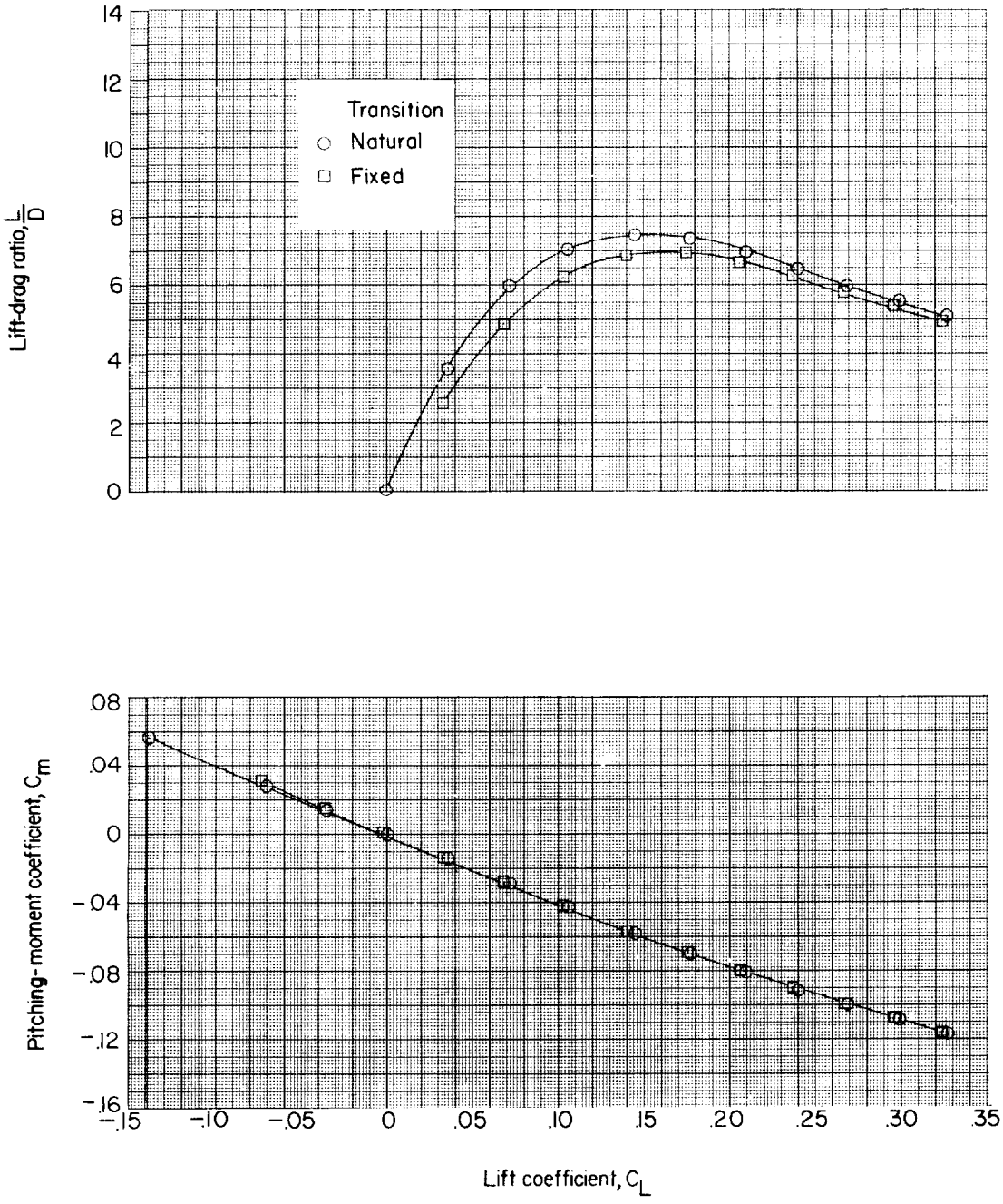

(b) Pitching-moment coefficient and lift-drag ratio. Body 1.

Figure 8.- Continued.

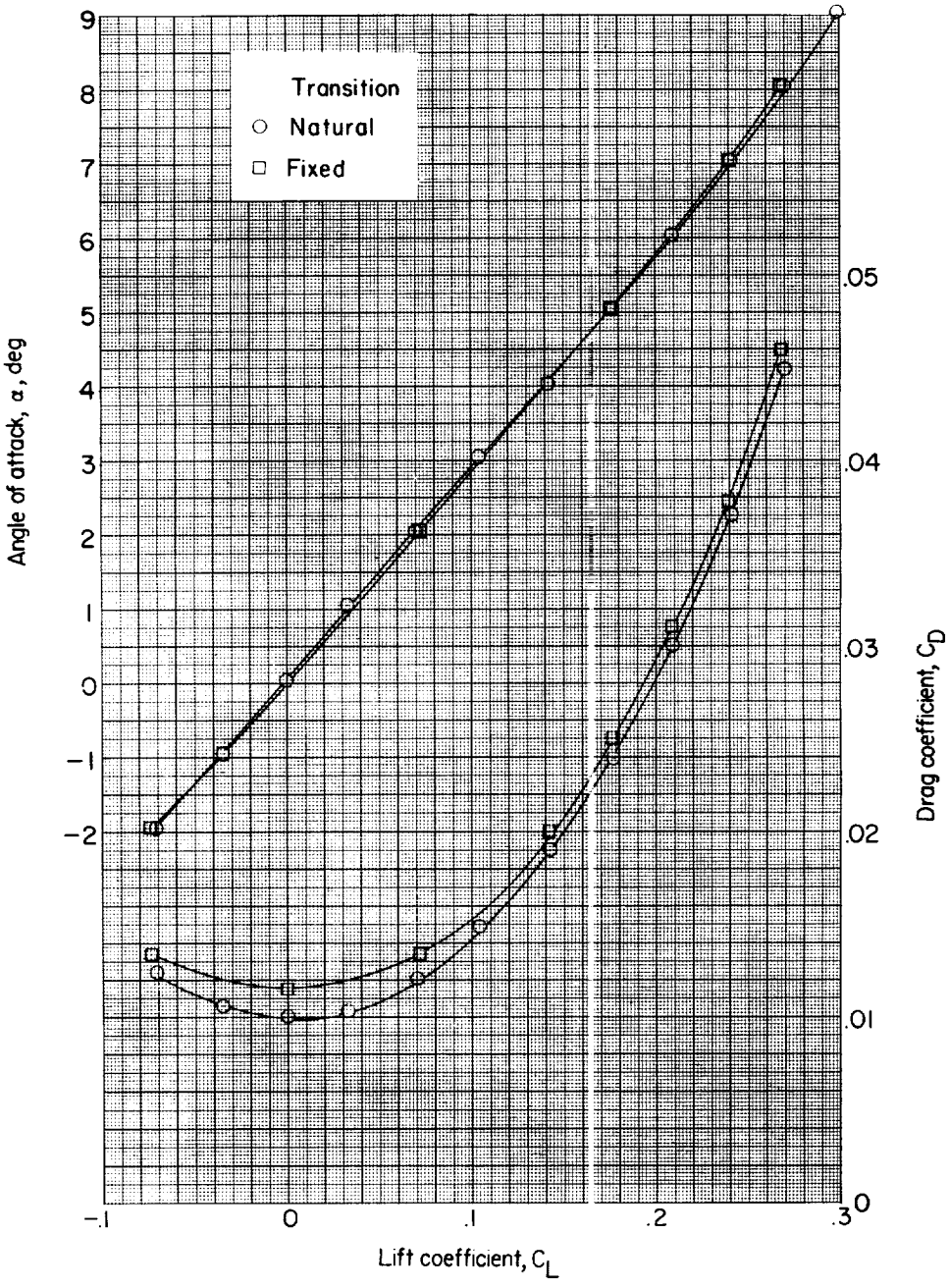

(c) Angle of attack and drag coefficient. Body 4.

Figure 8.- Continued.

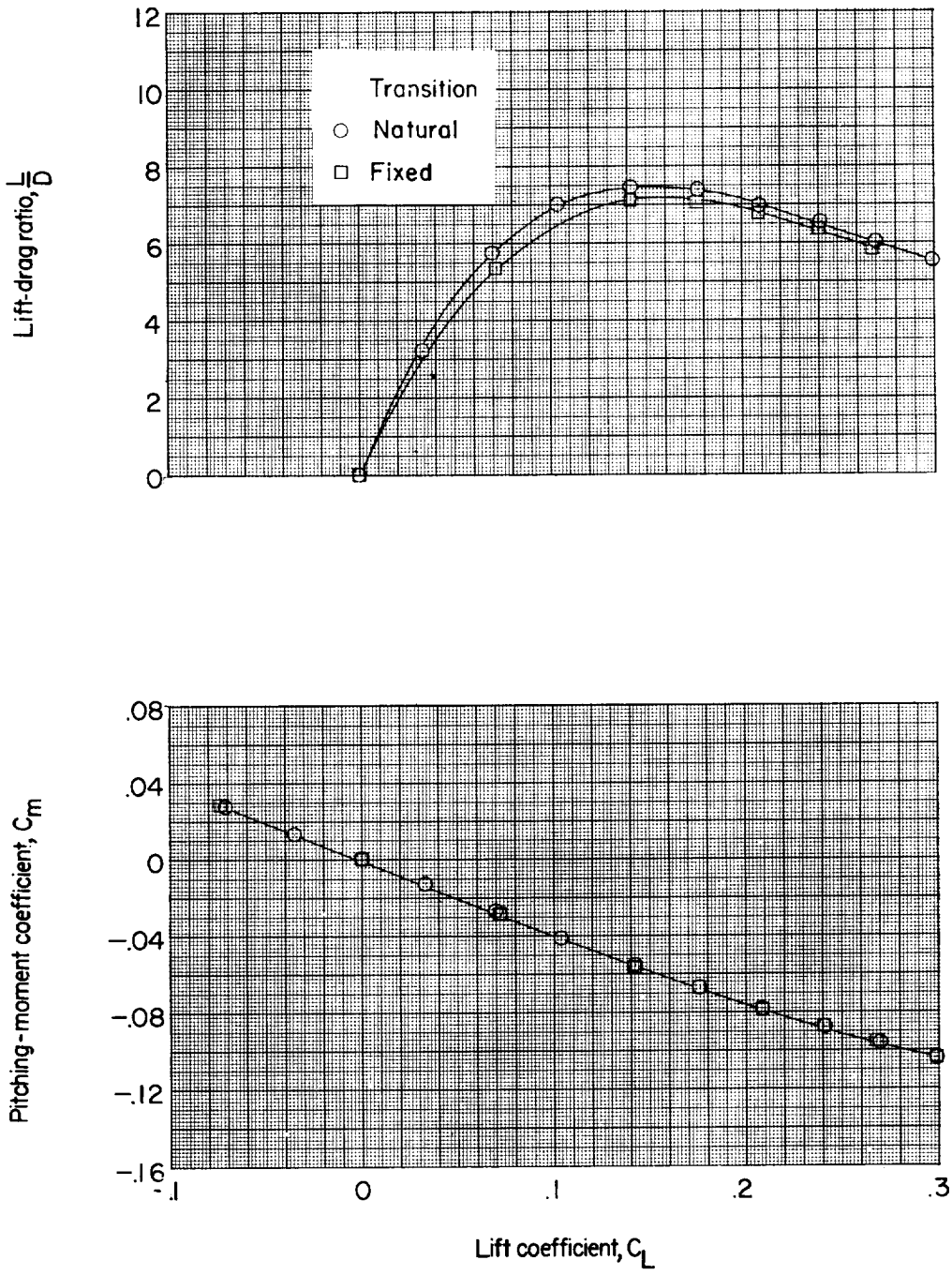

(d) Pitching-moment coefficient and lift-drag ratio. Body 4.

Figure 8.- Continued.

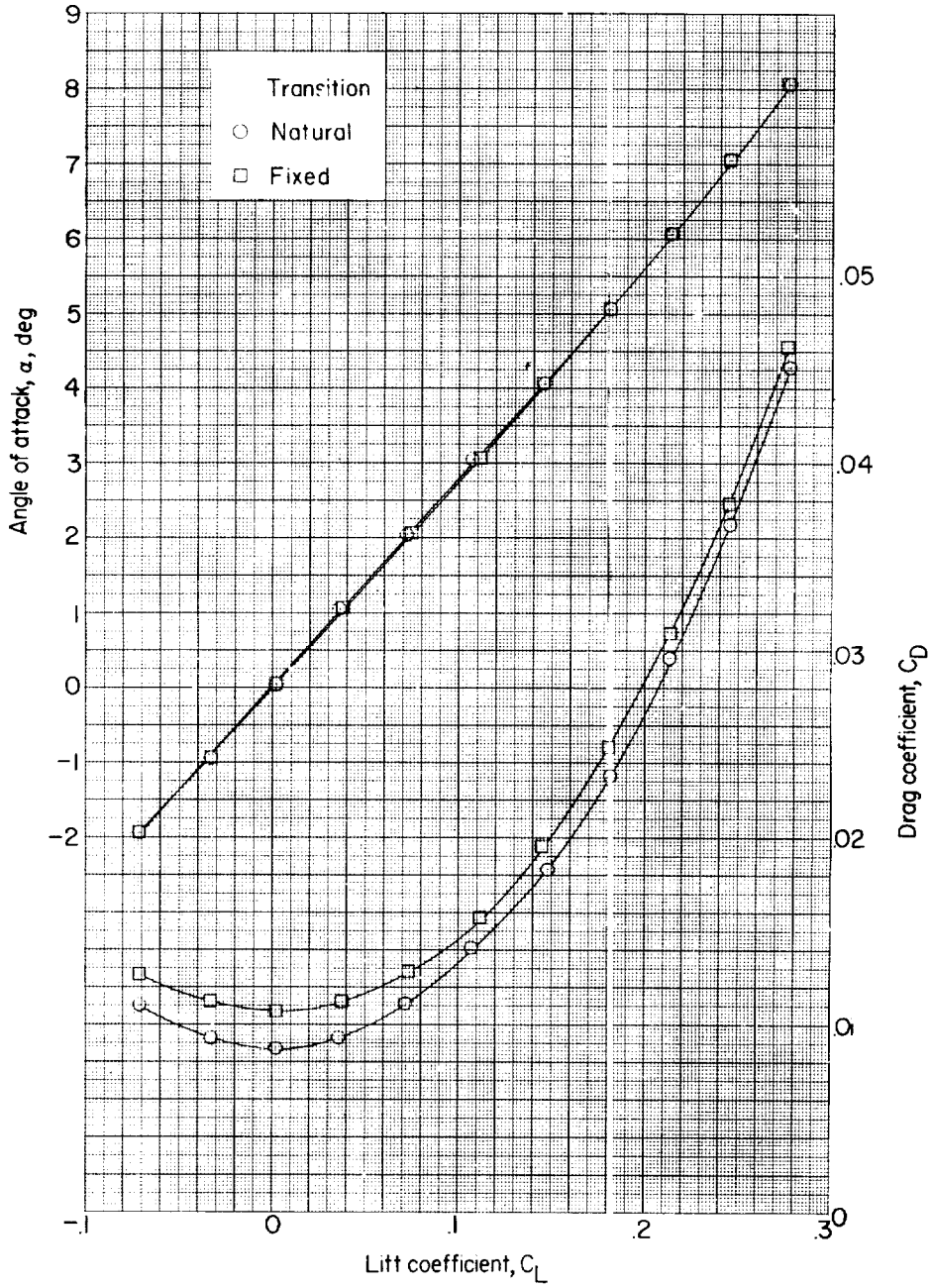

(e) Angle of attack and drag coefficient. Body 5.

Figure 8.- Continued.

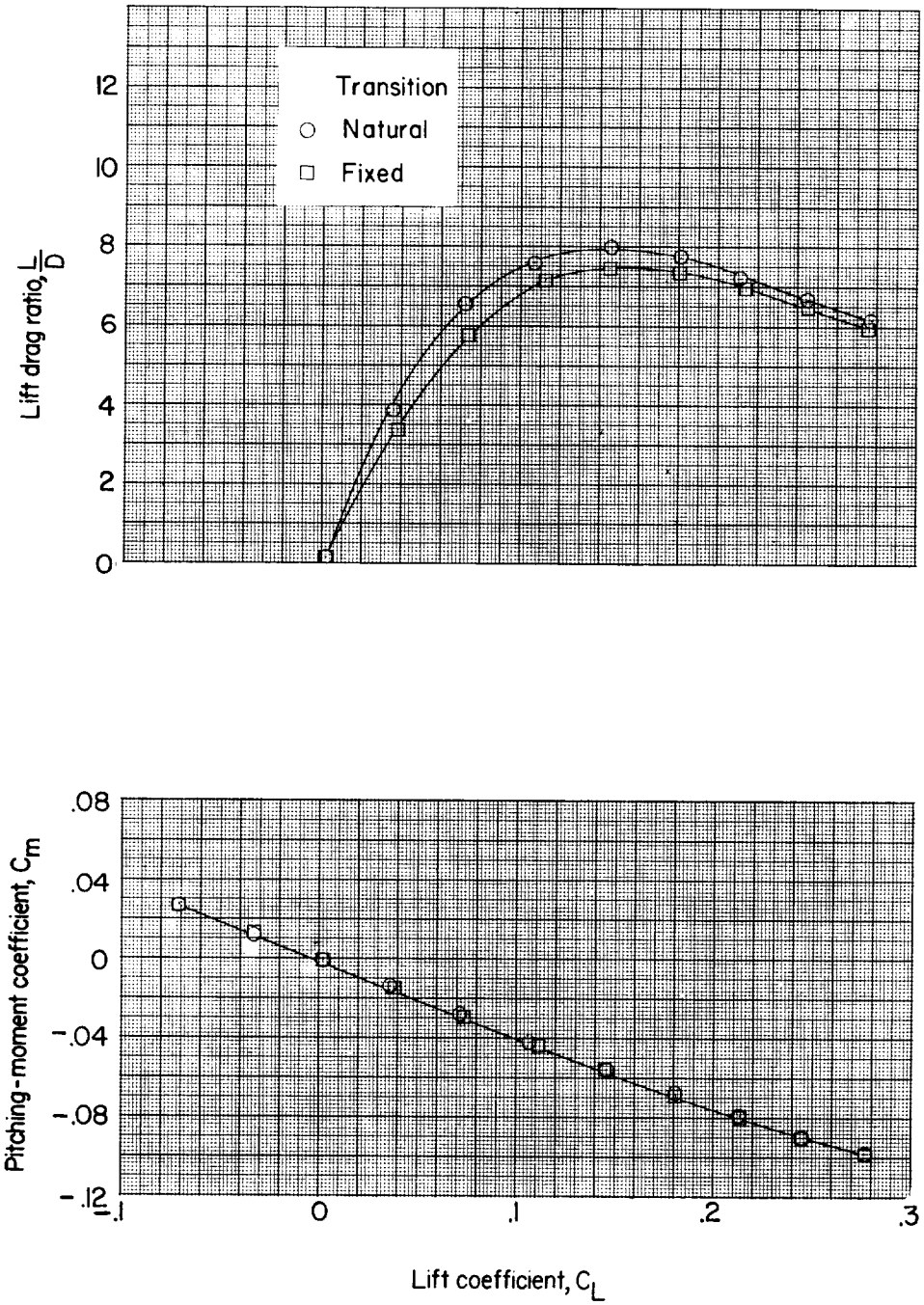

(f) Pitching-moment coefficient and lift-drag ratio. Body 5.

Figure 8.- Concluded.

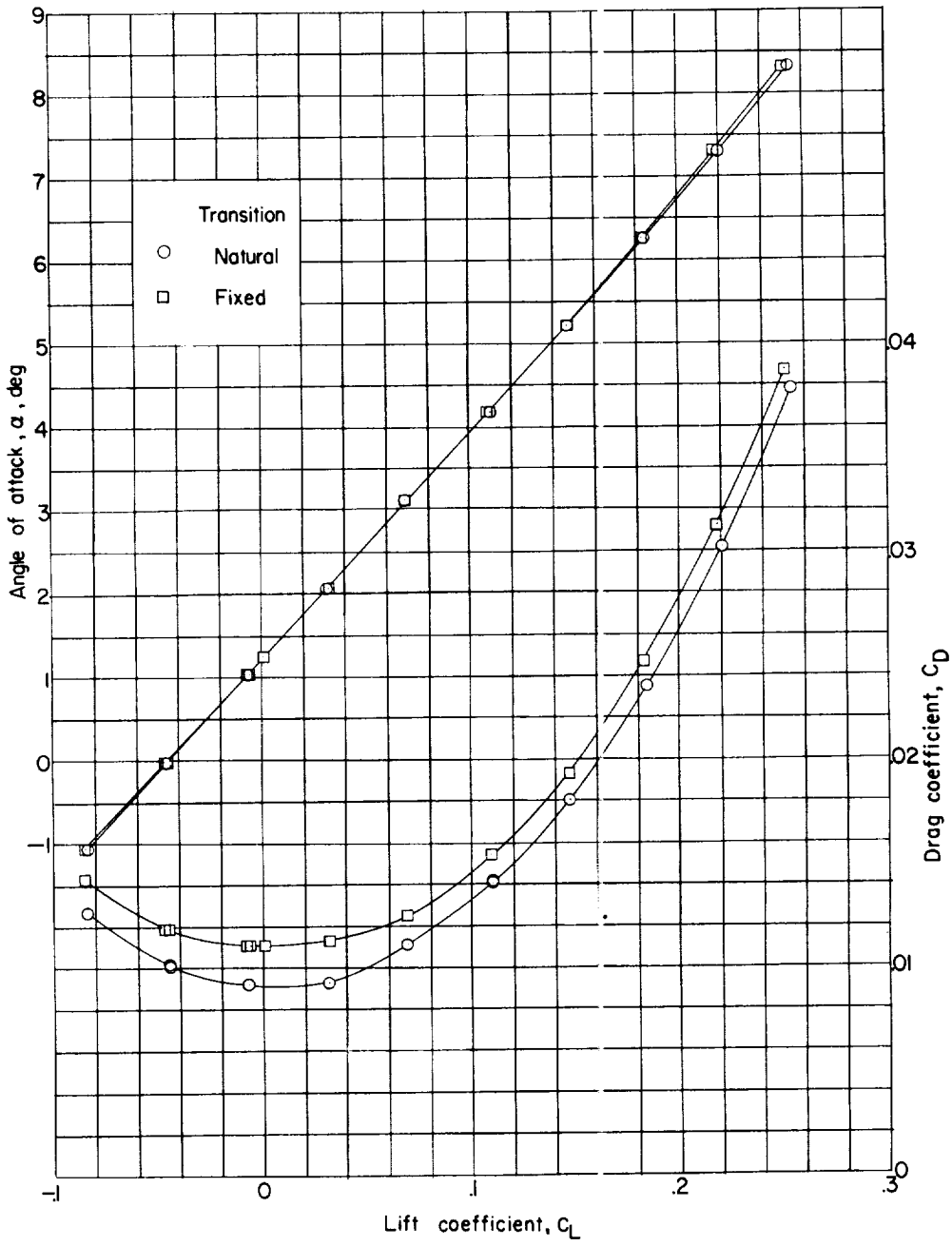

(a) Angle of attack and drag coefficient plotted against lift coefficient.

Figure 9.- Effect of fixing transition on body 5 - wing 2 configuration. M = 2.01; q ≈ 510 lb/sq ft abs.

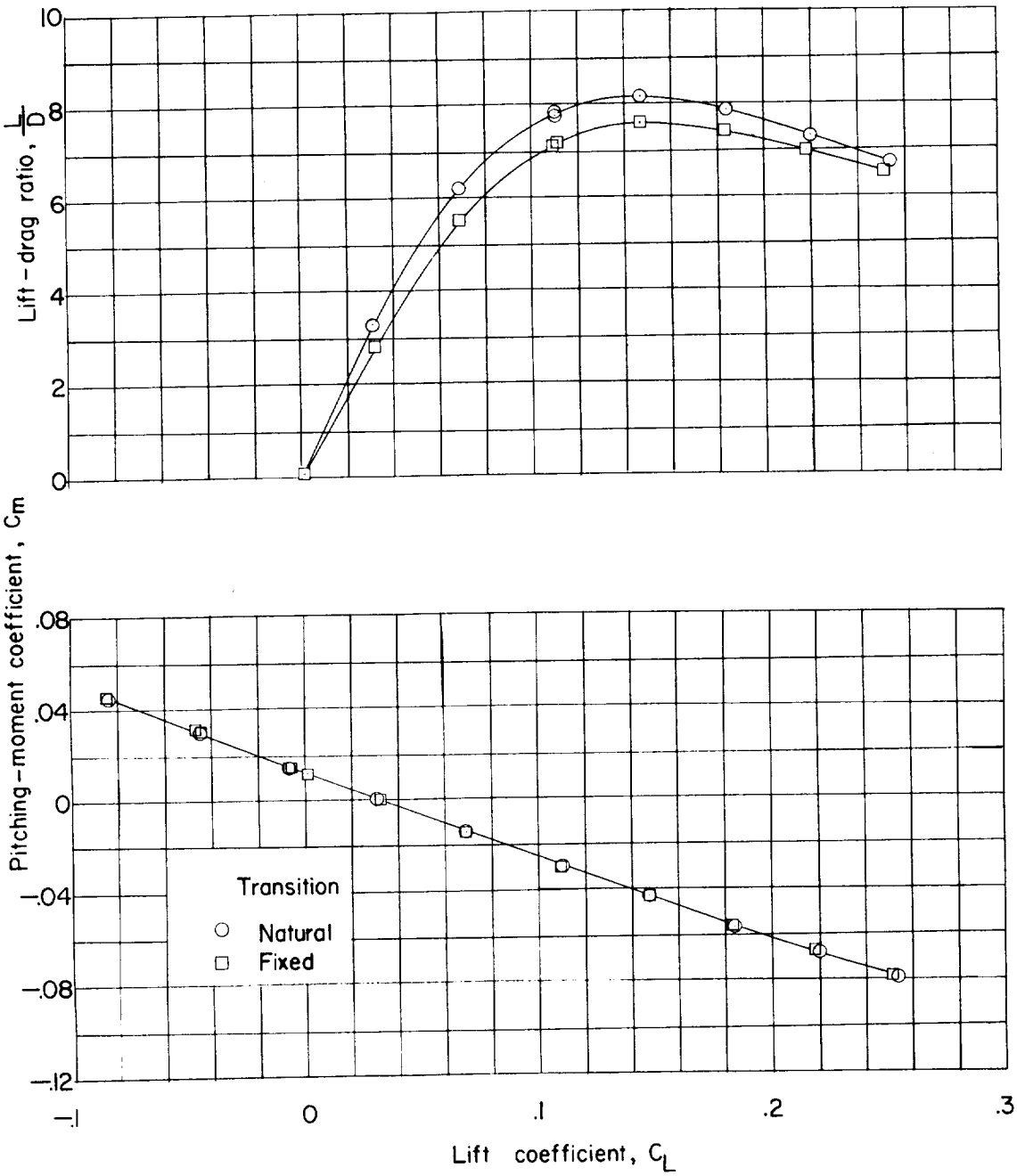

(b) Pitching-moment coefficient and lift-drag ratio plotted against lift coefficient.

Figure 9.- Concluded.

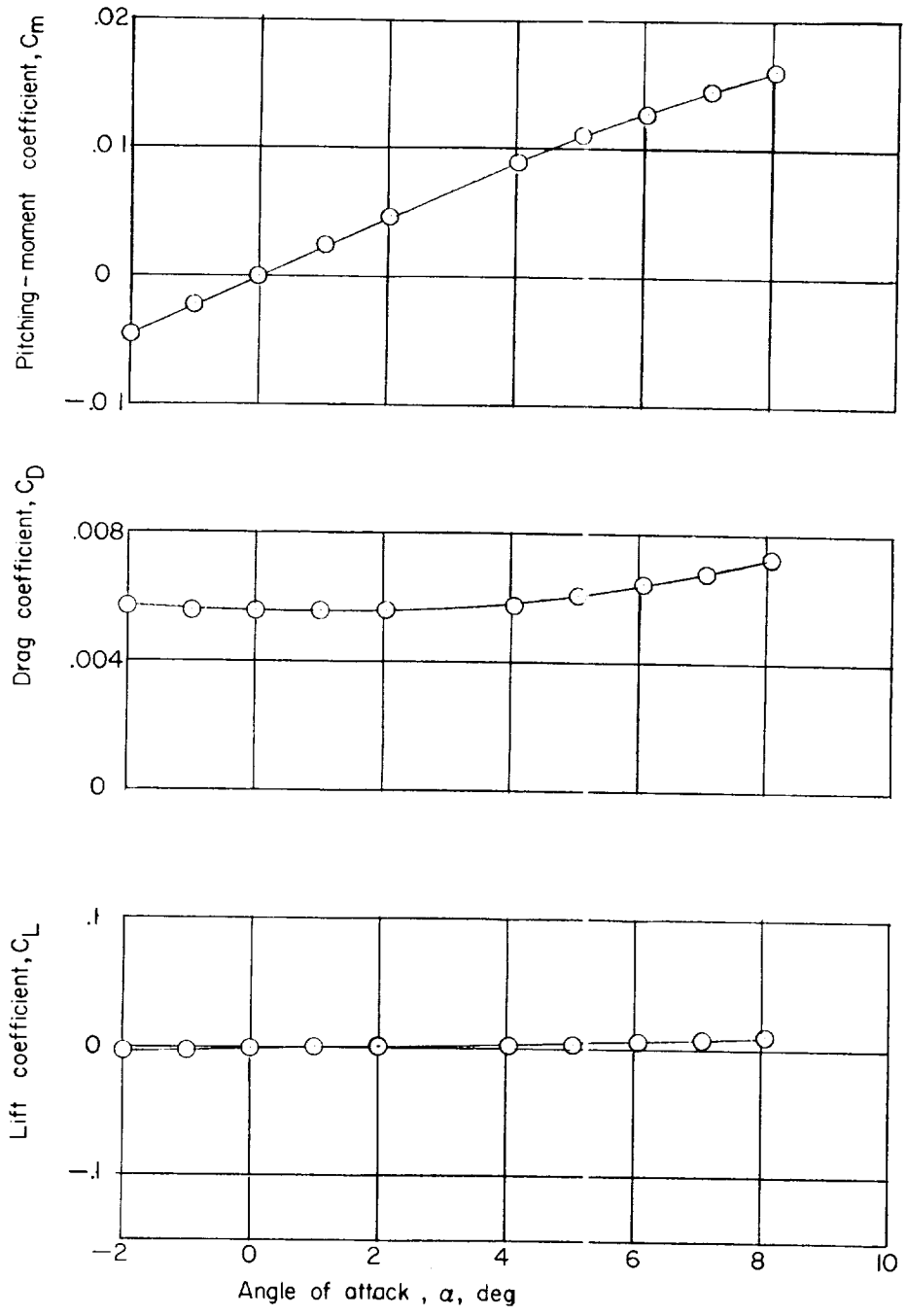

(a) M = 1.41; q ≈ 625 lb/sq ft abs.

Figure 10.- Variation with angle of attack of the longitudinal characteristics of body 1 alone with fixed transition.

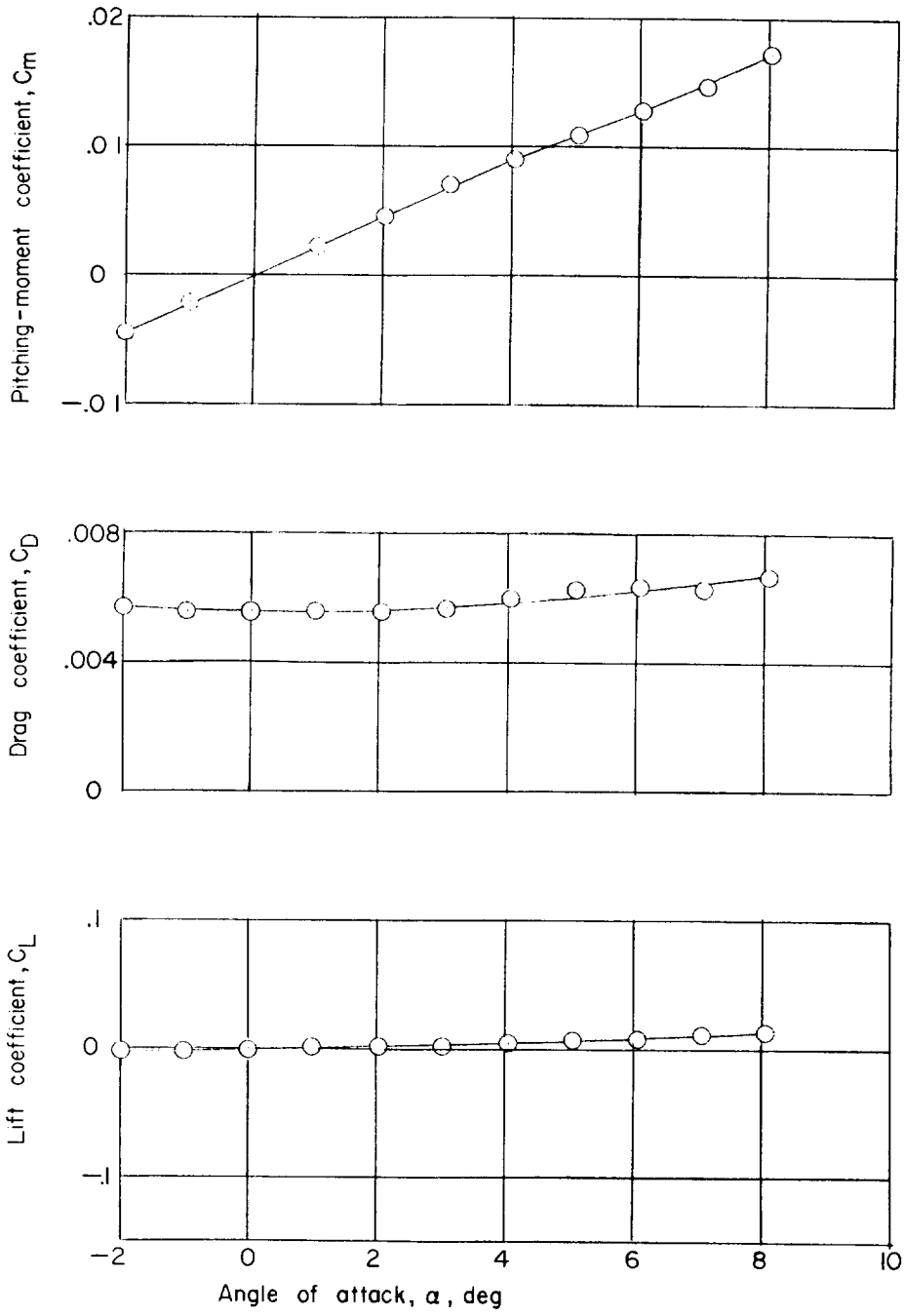

(b) M = 2.01; q ≈ 510 lb/sq ft abs.

Figure 10.- Concluded.

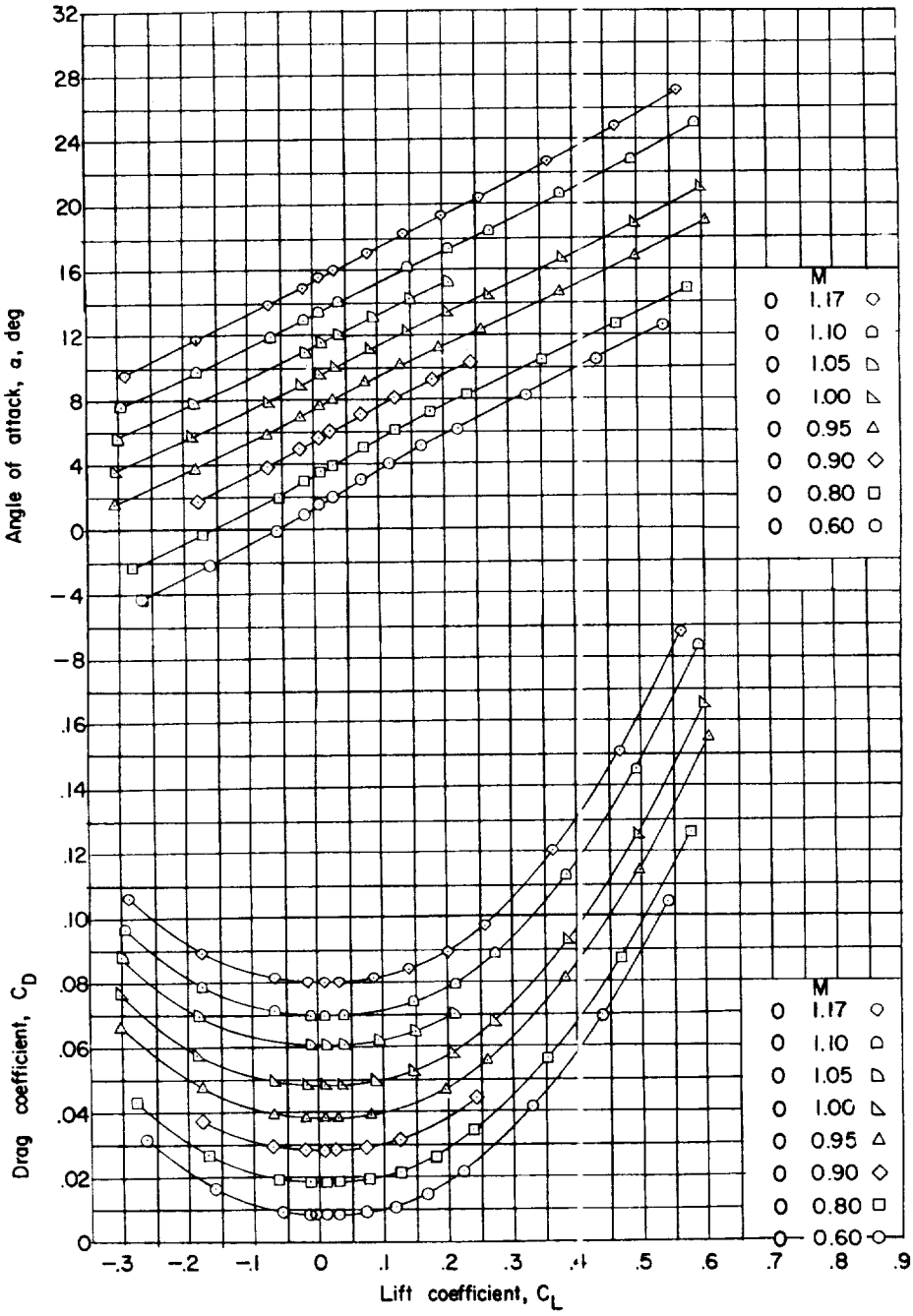

(a) Angle of attack and drag coefficient.

Figure 11.- Variation of aerodynamic parameters with lift coefficient. Transonic speeds; natural transition; body 2 - wing 2 configuration.

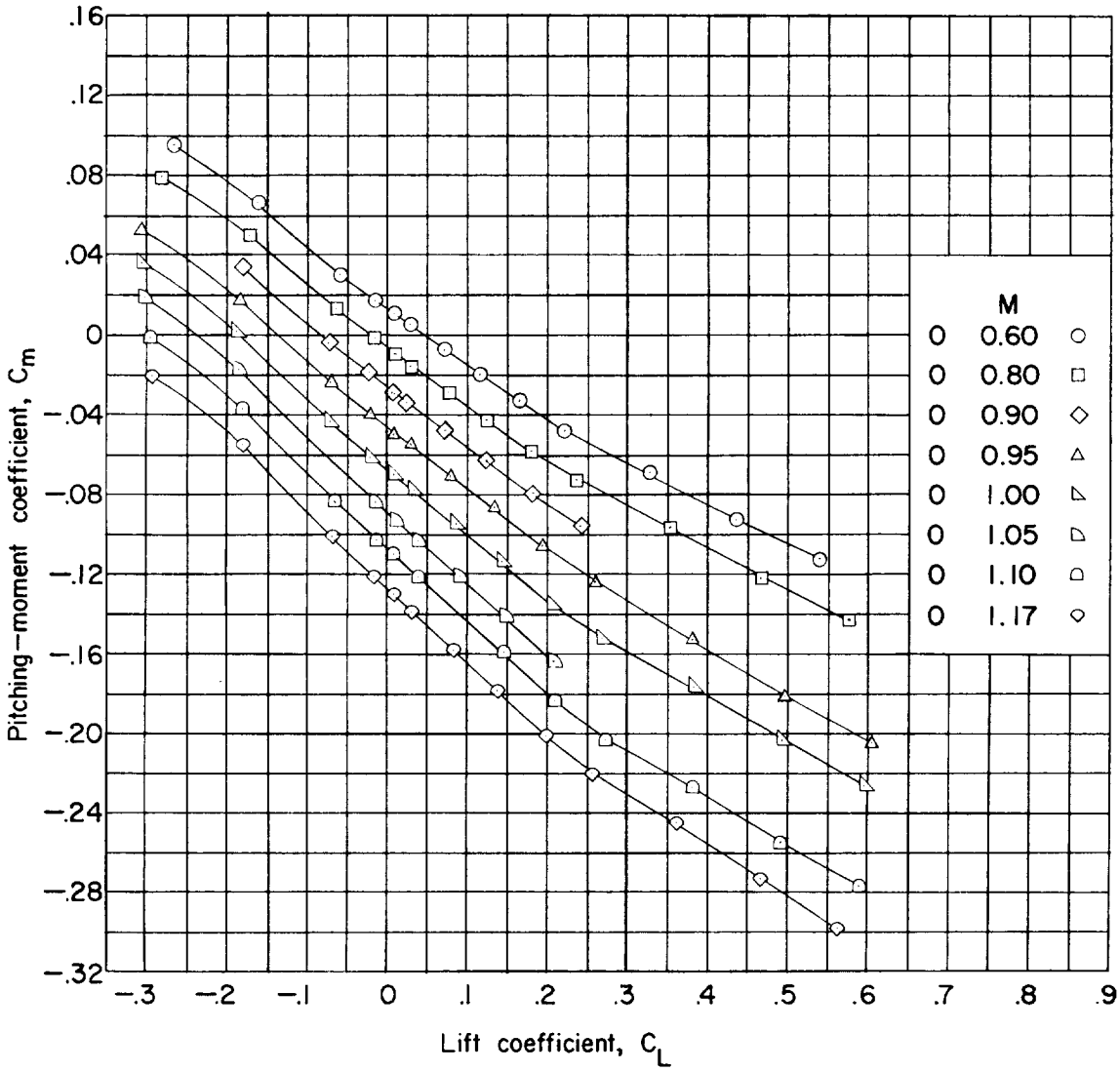

(b) Pitching-moment coefficient.

Figure 11.- Concluded.

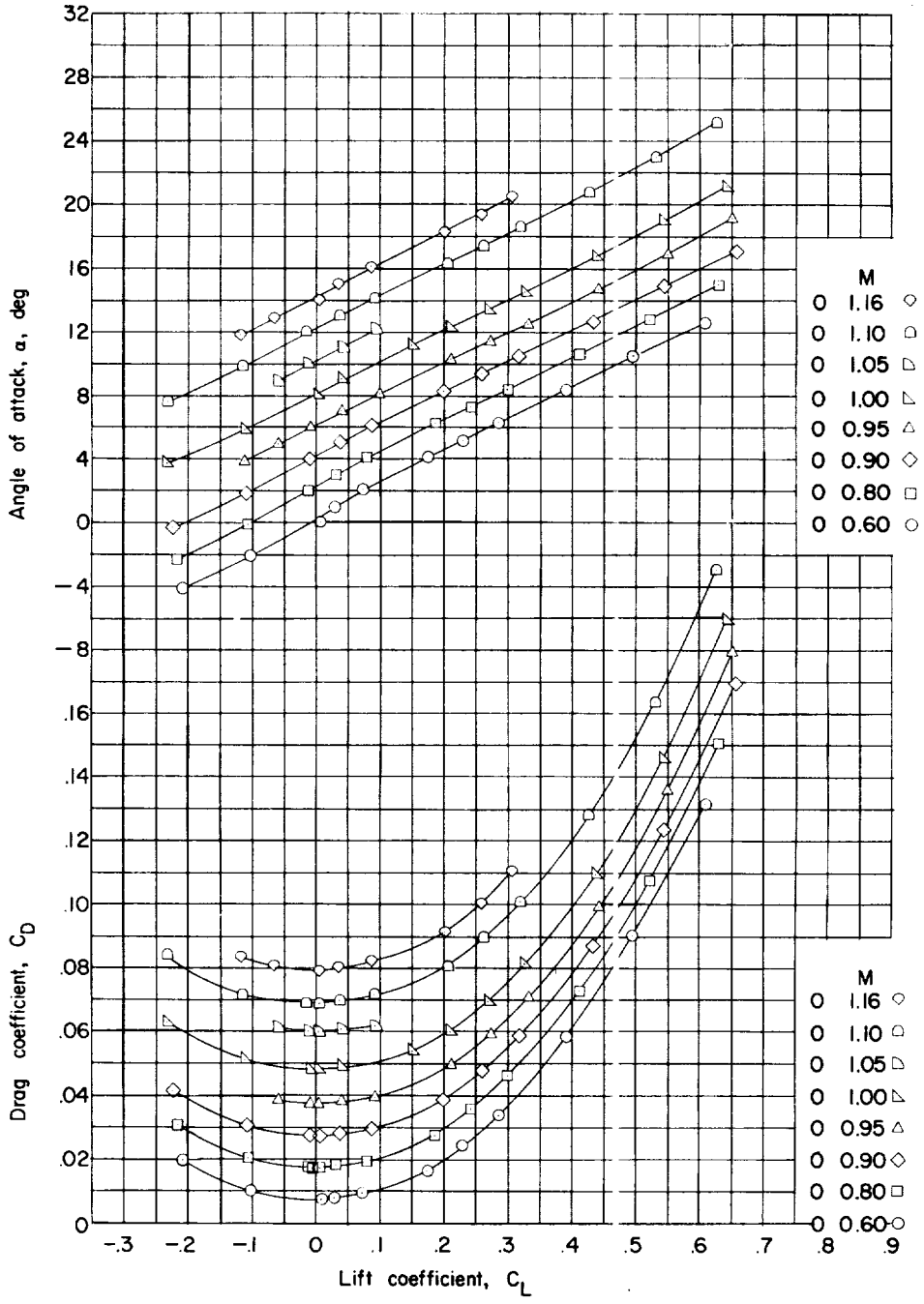

(a) Angle of attack and drag coefficient.

Figure 12.- Variation of aerodynamic parameters with lift coefficient. Transonic speeds; natural transition; body 5 - wing 1 configuration.

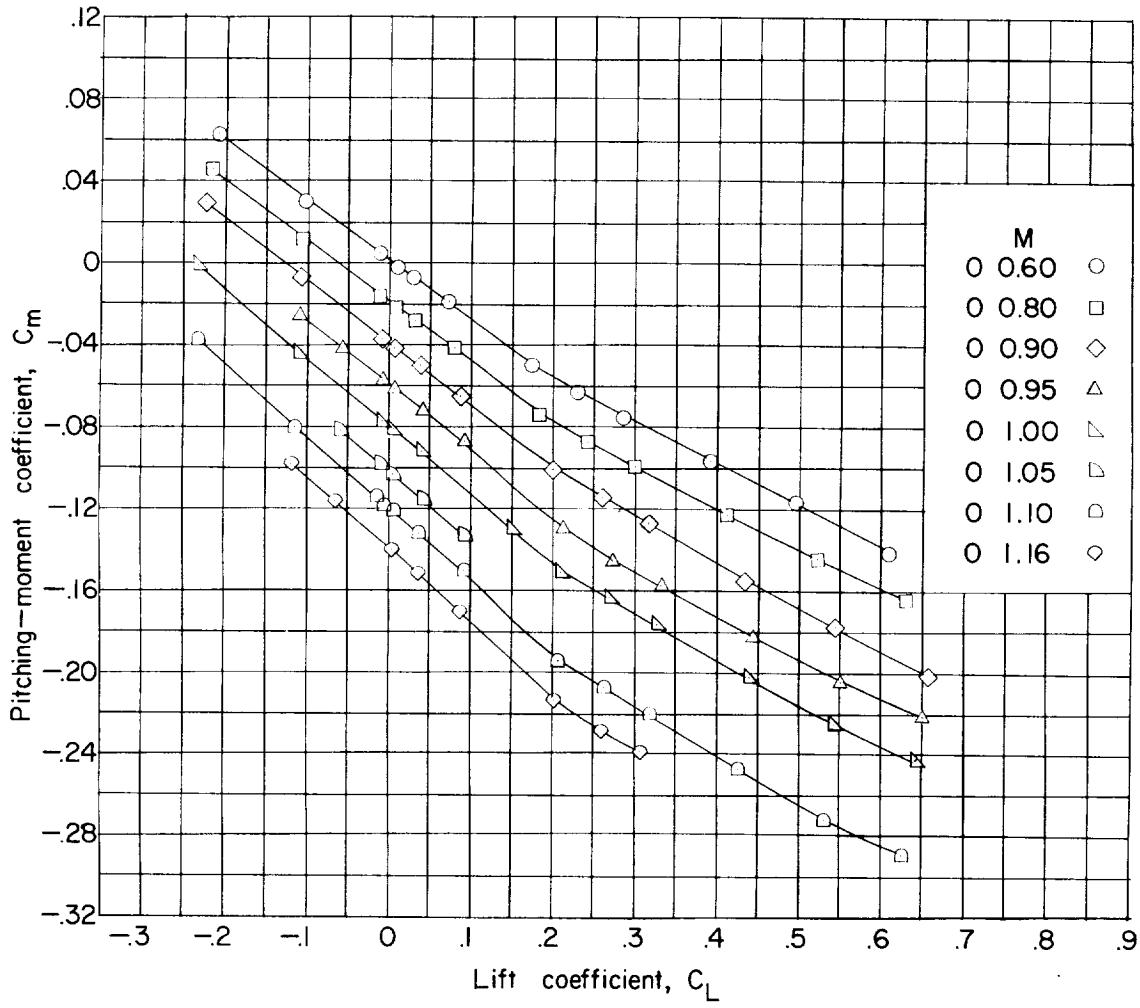

(b) Pitching-moment coefficient.

Figure 12.- Concluded.

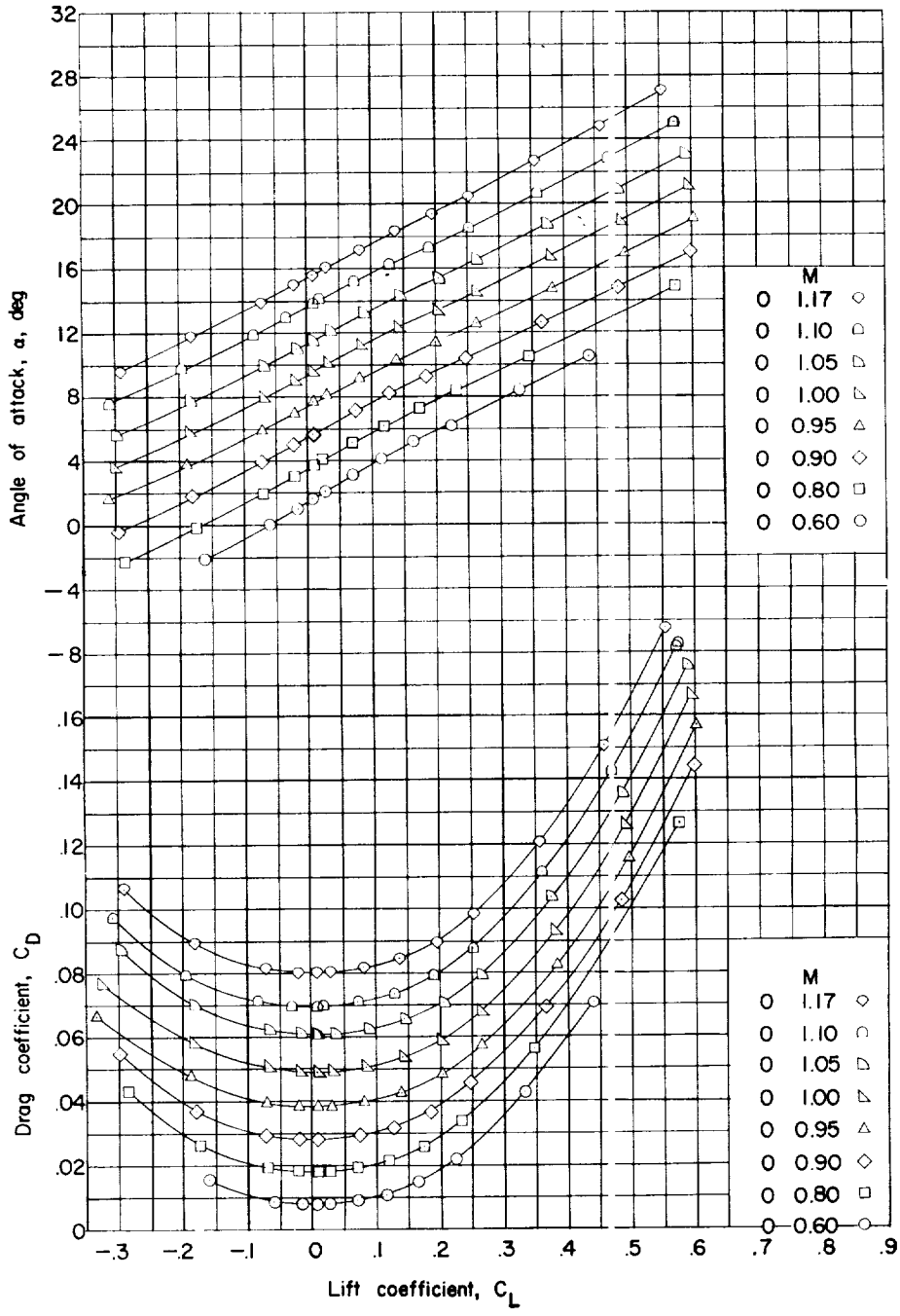

(a) Angle of attack and drag coefficient.

Figure 13.- Variation of aerodynamic parameters with lift coefficient. Transonic speeds; natural transition; body 5 - wing 2 configuration.

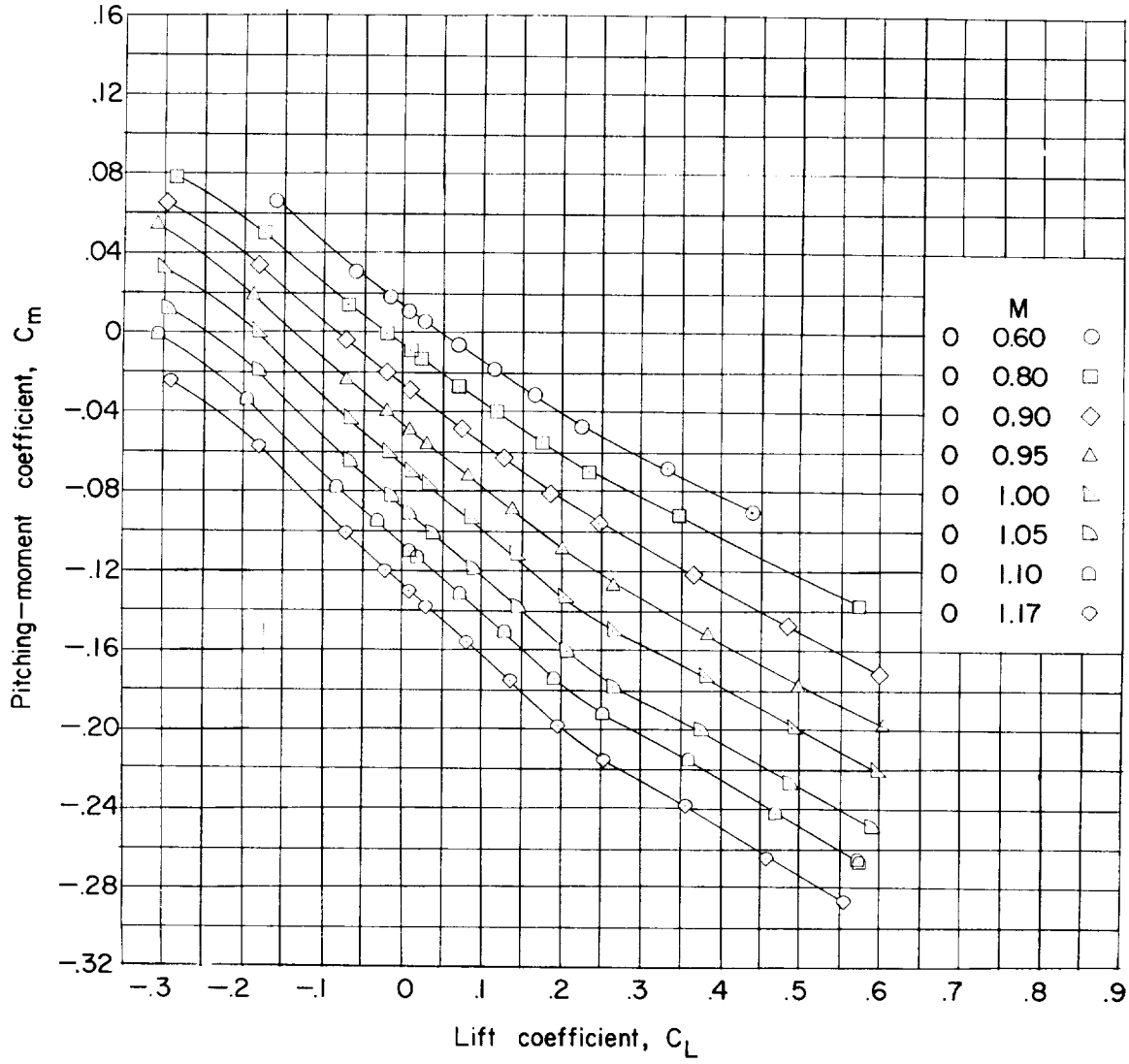

(b) Pitching-moment coefficient.

Figure 13.- Concluded.

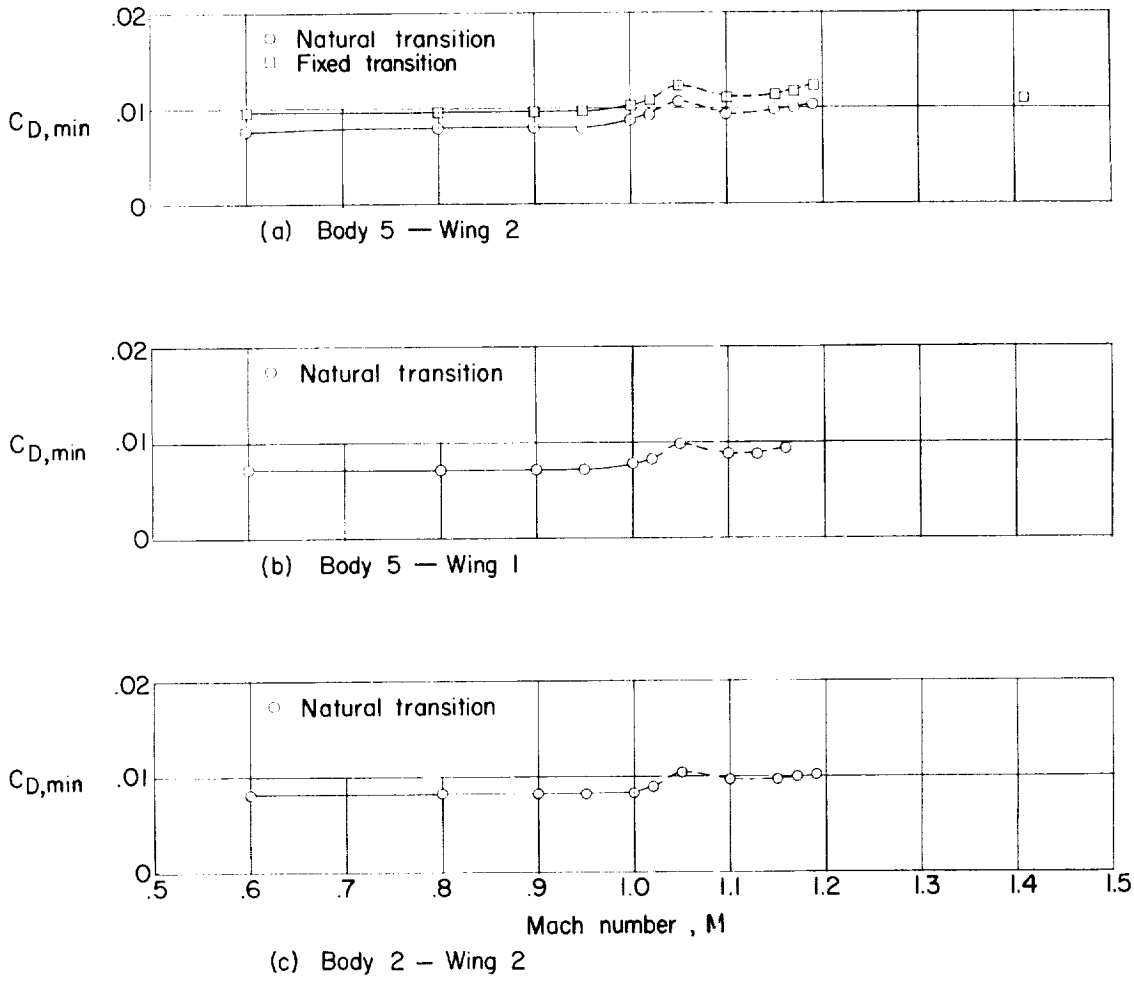

Figure 14.- Variation of minimum drag coefficient with Mach number.

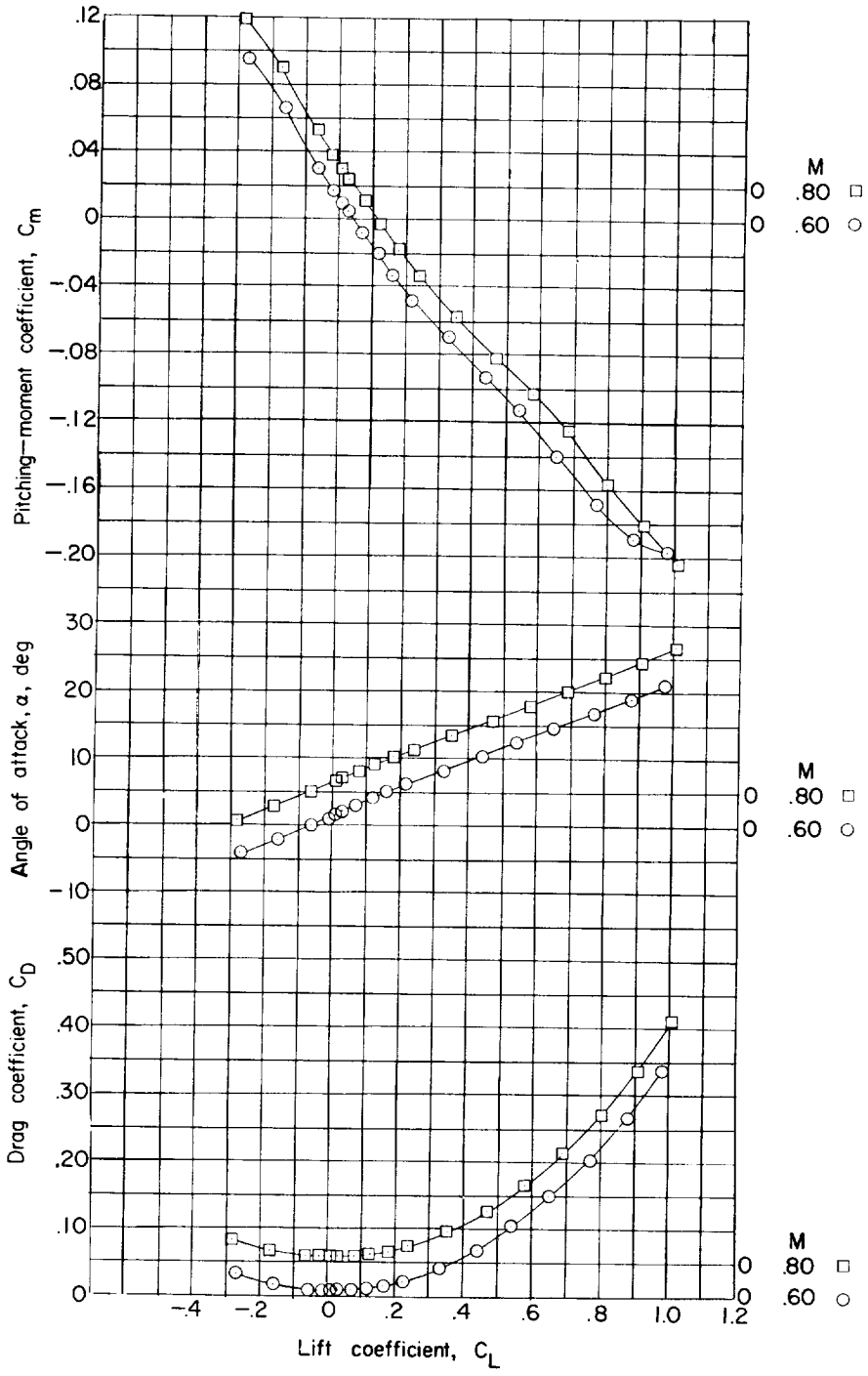

Figure 15.- Aerodynamic characteristics of the body 2 - wing 2 configuration at high lift coefficients.

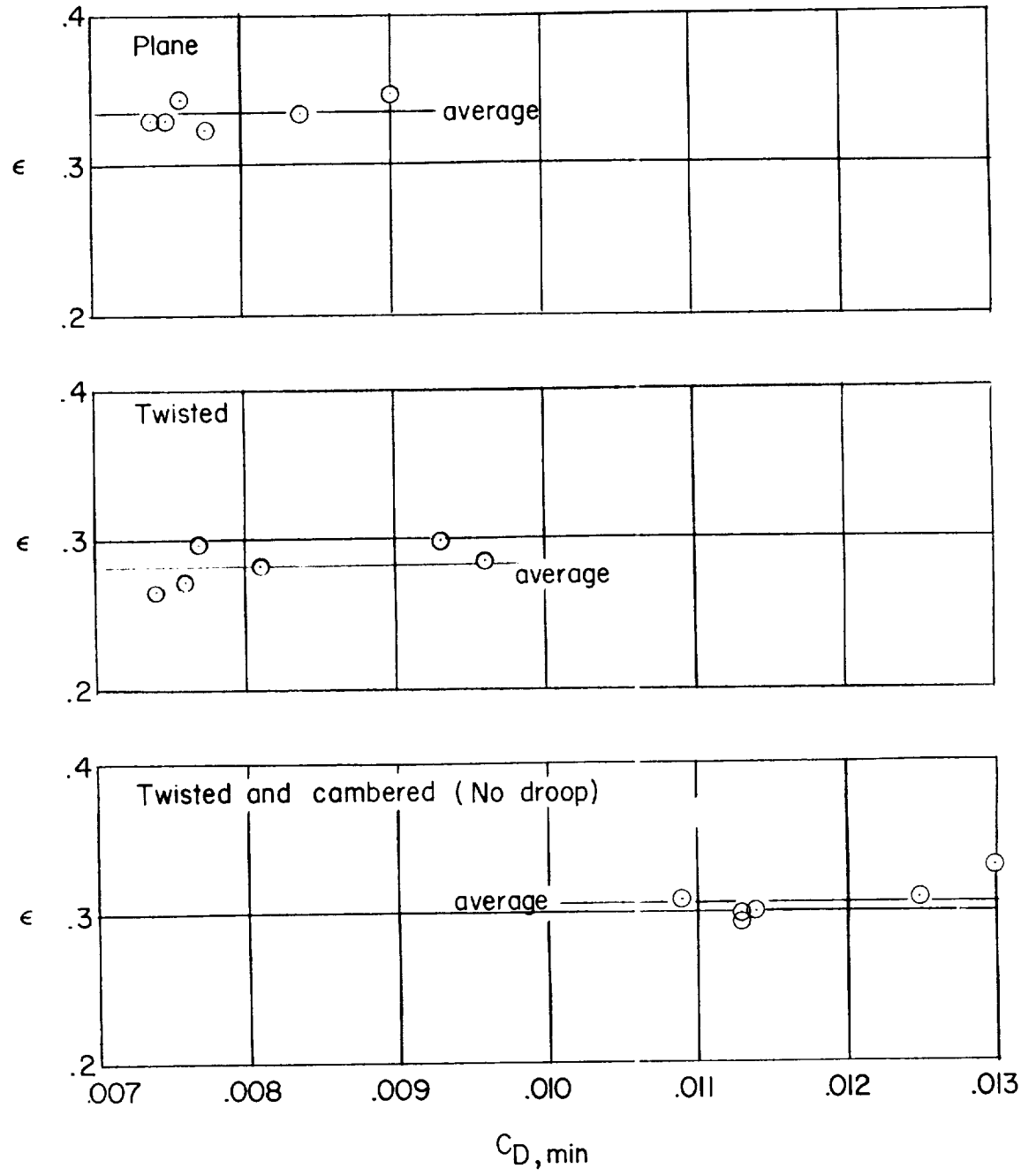

Figure 16.- Variation of drag-due-to-lift parameter with minimum drag coefficient for wings 1, 2, and 3 in combination with various bodies. Natural transition; M = 1.41; q ≈ 623 lb/sq ft abs.

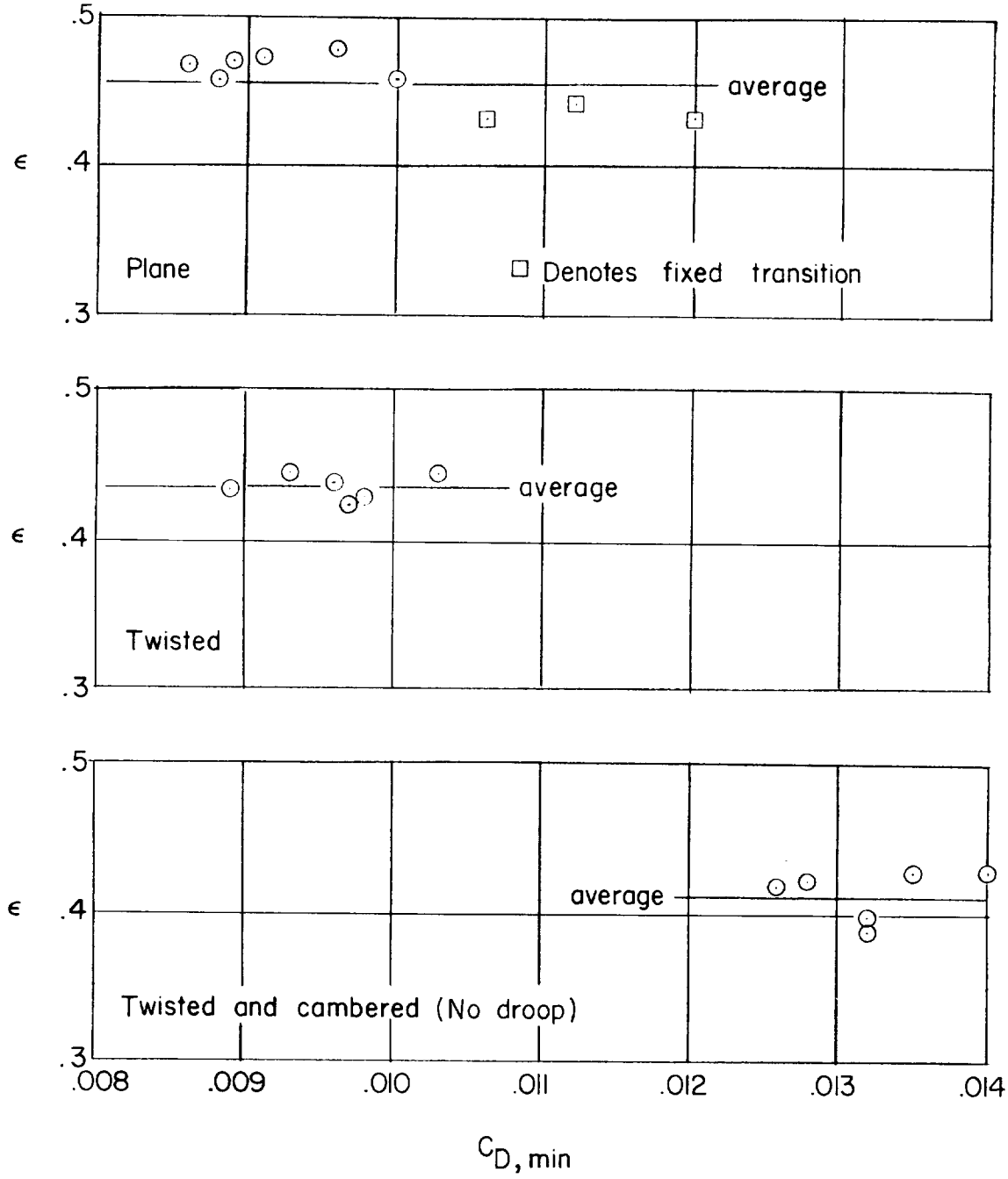

Figure 17.- Variation of drag-due-to-lift parameter with minimum drag coefficient for wings 1, 2, and 3 in combination with various bodies. Natural transition unless otherwise noted; M = 2.01; q ≈ 510 lb/sq ft abs.

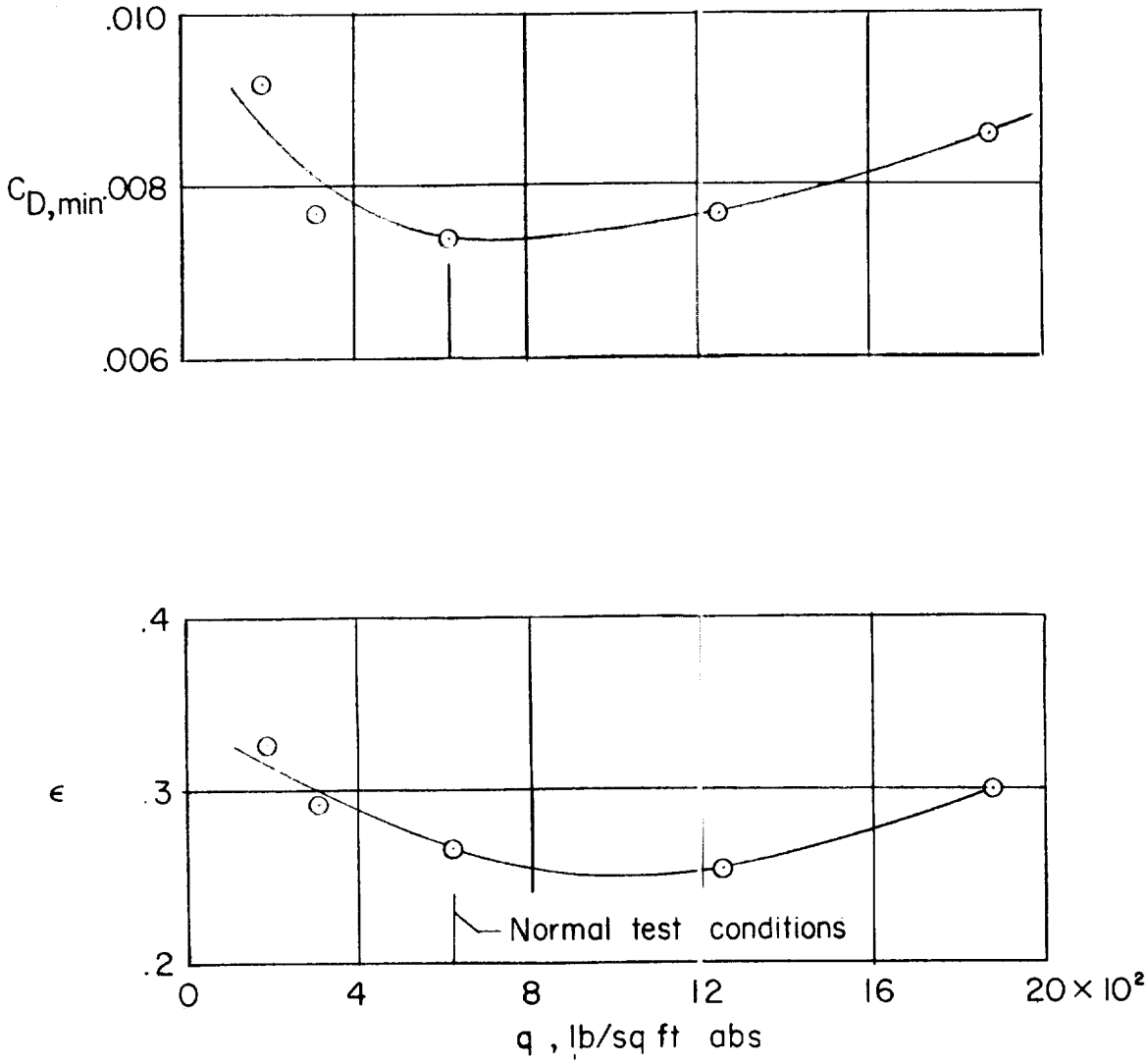

Figure 18.- Variation of minimum drag coefficient and drag-due-to-lift parameter with dynamic pressure for body 5 - wing 2 configuration. M = 1.41; natural transition.

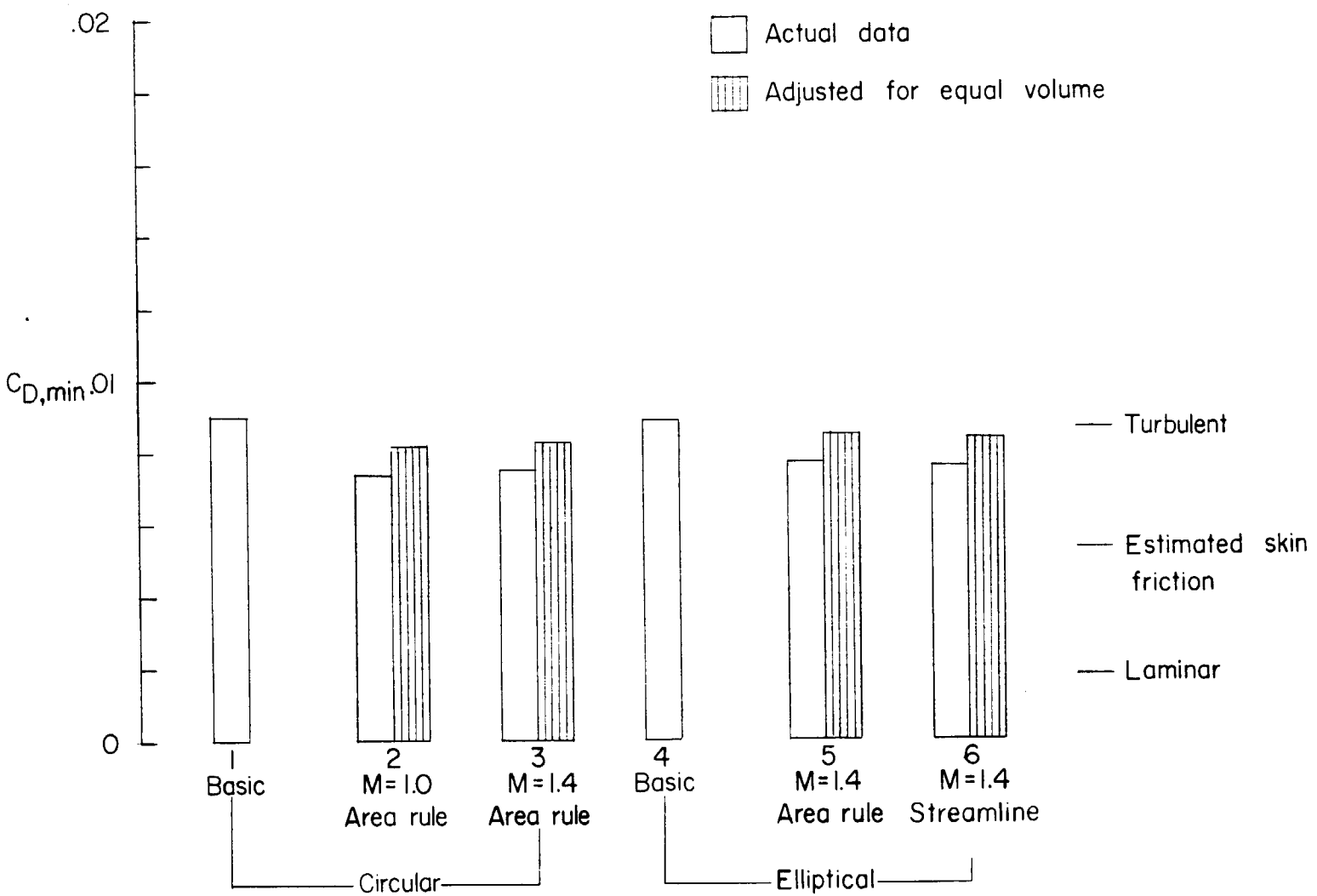

Figure 19.- Comparison of minimum drag coefficients for the various bodies in combination with the plane wing. Natural transition; M = 1.41; q ≈ 623 lb/sq ft abs.

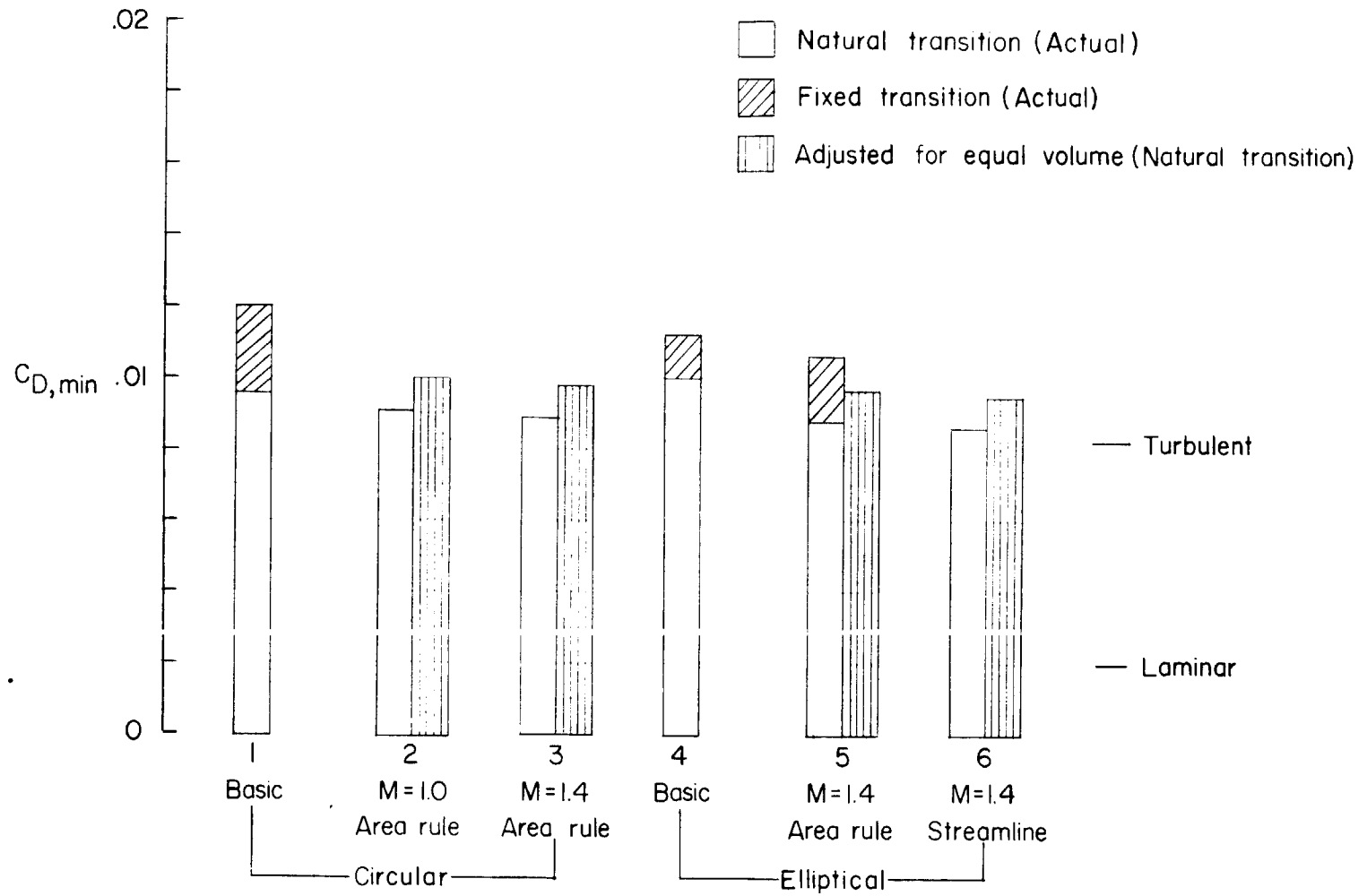

Figure 20.- Comparison of minimum drag coefficients for the various bodies in combination with the plane wing. M = 2.01; q ≈ 510 lb/sq ft abs.